

HF/UHF DUAL MODE RFID TRANSPONDER ANTENNA AND HF RANGE
EXTENSION VIA WIRELESS POWER TRANSMISSION

by
Selçuk AYDIN

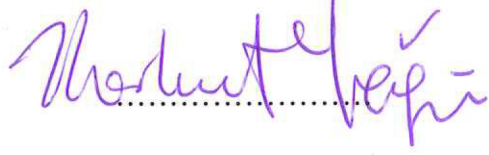
Submitted to the Institute of Graduate Studies in
Science and Engineering in partial fulfillment of
the requirements for the degree of
Master of Science
in
Electrical and Electronics Engineering

Yeditepe University
2010

**HF/UHF DUAL MODE RFID TRANSPONDER ANTENNA AND HF RANGE
EXTENSION VIA WIRELESS POWER TRANSMISSION**

APPROVED BY:

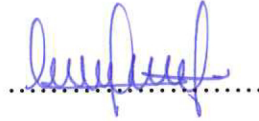
Assoc. Prof. Dr. Korkut Yeğin
(Thesis Supervisor)



Inst. Deniz Pazarıcı



Asst. Prof. Dr. Duygun Erol



DATE OF APPROVAL:

ACKNOWLEDGEMENTS

I'd like to thank to Assoc. Prof. Korkut Yeğın for his valuable interest on my graduate thesis. He always encouraged me to achieve success by simplest, correct way and sharing his own time. His own novel ideas and great experiences have helped me during design period of HF/UHF Compatible Passive RFID Transponder Antenna Design.

Additionally, I would like to sincere thank to Gökmen Işık, Murat Bilgiç and Salih Gülçimen for their great support and sharing their time with me on lab during performing measurements and preparing measurement setups.

I am also very thankful to my second home; Yeditepe University and the people who gave me chance to study Master of Science in Electrical and Electronics Engineering.

Finally, I'd like to thank to my family to share all your life with me and be with me all the time. Hence, I would like to dedicate this graduate thesis to my father, Mehmet AYDIN, my mother, Sever AYDIN and my sister, Fatma Sevcan AYDIN. It would really be difficult to complete this thesis without them.

ABSTRACT

HF/UHF DUAL MODE RFID TRANSPONDER ANTENNA AND HF RANGE EXTENSION VIA WIRELESS POWER TRANSMISSION

A novel HF/UHF compatible RFID transponder antenna is designed, simulated and measured for dual band operation and HF range increase. Dual mode compatible RFID transponder antenna enjoys the benefits of each mode and eliminates the disadvantages of single mode operation. The transponder antenna can easily be configured for either HF mode, or UHF mode only, or HF mode with UHF range extension mode.

Limited range of HF RFID systems can be overcome if more power can be delivered to the transponder antenna which could not be achieved in HF band due to near-field strength regulations set by the standards. However, using UHF band, wireless power can be delivered by the reader to the HF transponder. To achieve such operation, the transponder antenna must be dual band. The rectify circuit for wireless power transmission at UHF band must also be optimized for maximum efficiency and we obtained about 63% system efficiency when measured from end-to-end. The influence of coexistence of HF and UHF antennas on the same structure are well characterized and measured to corroborate simulation results.

Even though UHF RFID has benefit in having better read/write range capability, these tags can get easily affected by the surroundings or application environment such as on/near metal and plastics. When tags are placed in such environments, tag impedance can change and detune easily, and also radiation characteristics may change considerably, which, in turn, makes the UHF tag less reliable. Therefore, there is a need for an UHF RFID tag that is less sensitive to environment and is capable of preserving radiation characteristics in such environments. Although several studies which address this issue have been reported in the literature, they are all limited to dipole-like or slot dipole-like structures. We propose a microstrip antenna where its ground serves as isolation to its surroundings such that its main electrical performance metrics do not change drastically

when placed on or near metallic structures. The performance of the designed antenna has been compared to that of a Texas Instruments transponder antenna, which has widespread use for many UHF applications. We prove that our transponder antenna behaves much better than TI's antenna under a variety of typical RFID applications.

ÖZET

YÜKSEK FREKANS (YF) / PEK YÜKSEK FREKANS (PYF) İKİ MOD UYUMLU RFID ANTEN TASARIMI VE YÜKSEK FREKANSTAKİ OKUMA / YAZMA MESAFESİNİN KABLOSUZ GÜÇ AKTARIMI İLE GELİŞTİRİLMESİ

YF/PYF uyumlu RFID anten tasarlanmakta, iki bandta çalışacak şekilde ve YF frekansta okuma/yazma mesafesinin geliştirilmesi amaçlı simülasyonlar ve ölçümler yapılmaktadır. İki band uyumlu tasarlanan RFID anten her iki modun ayrı ayrı avantajlarını kullanarak, herbir bandın ayrı ayrı kullanılması sırasında meydana gelen dezavantajları ortadan kaldırmaktadır. Tasarlanan anten, istenildiğinde sadece YF’de, istenildiğinde PYF’de ya da tercih edildiği takdirde PYF kullanılarak YF’de okuma/yazma mesafesinde artış sağlayabilecek şekilde kullanılabilir.

YF’de standartlardaki belirlenen limitlerden dolayı ortaya çıkan kısıtlı okuma/yazma mesafesi problemi, yeterli miktarda güç aktarılabilirdiği takdirde ortadan kalkabilmektedir. PYF kullanarak okuyucu tarafından güç YF anten üzerine aktarılmaktadır. Bu tür bir uygulama için alıcı-verici anten iki bandda çalışacak şekilde olmalıdır. Kullanılması gereken doğrultucu devre maksimum verim verecek şekilde tasarlanmalıdır. Yapılan ölçümler sonucunda PYF’de çalışacak doğrultu devre verimliliği %63 olarak ölçülmüştür. YF ve PYF antenlerin aynı yapı üzerinde kullanılması düzgün bir şekilde sağlanmış ve simülasyon sonuçları ölçüm sonuçlarıyla desteklenmiştir.

PYF’de çalışan RFID sistemleri daha iyi okuma/yazma mesafeleri sağlamalarına rağmen, metal, plastik gibi maddeler içeren yüzeyler üzerindeki uygulamalarda çevre faktörlerinden kolaylıkla etkilendiklerinden ötürü gözle görülür performans kayıplarına maruz kalmaktadırlar. Bu yüzden PYF RFID sistemleri için çevreden en az şekilde etkilenmesi ve uygulanan her türlü ortama karşı performans kaybı yaşanmaması adına gereksinimler vardır. Geçmişte bu konuda çalışmalar yapılmasına rağmen, yapılan tüm çalışmalar dipol benzeri ya da yarıklı dipol benzeri yapılar üzerine olmuştur. Yapılmış olan bu çalışmada altta bulunan metalin oluşturmuş olduğu çevre etkenlerine karşı izolasyon

etkisinden dolayı yama anten kullanılmaktadır. Böylelikle metalik ve plastik içeren yüzeylerin tasarlanan anten üzerindeki olumsuz etkileri en aza indirilmektedir. Tasarlanan antenin performans metrikleri şu an kullanılmakta olan ve Texas Instruments tarafından geliştirilmiş alıcı-verici anten ile karşılaştırılmaktadır. Simulasyon ve ölçüm sonuçları tasarlanmış olduğumuz antenin, Texas Instruments tarafından geliştirilen alıcı-verici antene göre daha iyi anten kazancı değerleri verdiğini göstermektedir.

TABLE OF CONTENTS

| | |
|-------------------------------------------------------------|------|
| ACKNOWLEDGEMENTS | iii |
| ABSTRACT | iv |
| ÖZET | vi |
| TABLE OF CONTENTS..... | viii |
| LIST OF FIGURES..... | xi |
| LIST OF TABLES | xix |
| LIST OF SYMBOLS / ABBREVIATIONS..... | xx |
| 1. INTRODUCTION..... | 22 |
| 1.1. Radio Frequency Identification..... | 22 |
| 1.2. Frequency Ranges Used in RFID Systems | 25 |
| 1.3. Radio Licensing Regulations & Standards For RFID..... | 26 |
| 1.3.1. European Radio Licensing Regulations | 26 |
| 1.3.2. ISO Standards..... | 26 |
| 1.4. Dual Band or Dual Mode RFID Systems..... | 28 |
| 2. HF RFID DESIGN PRINCIPLES | 32 |
| 2.1. HF RFID Design | 32 |
| 2.1.1. Magnetic Field of A Small Loop | 32 |
| 2.1.2. Mutual Inductance Between Two Loops | 39 |
| 3. DUAL BAND PASSIVE RFID TAG ANTENNA DESIGN..... | 52 |
| 3.1. Design Specifications of Dual Band Design..... | 52 |
| 3.1.1. Design Specifications of HF antenna..... | 52 |
| 3.1.2. Design Specifications of UHF antenna..... | 53 |
| 3.2. Antenna Design and Modeling..... | 53 |
| 3.2.1. UHF Antenna Design and Modeling..... | 53 |
| 3.2.1.1. Calculation of patch antenna width..... | 54 |
| 3.2.1.2. Calculation of effective dielectric constant..... | 55 |
| 3.2.1.3. Calculation of effective length | 55 |
| 3.2.1.4. Calculation of length extension..... | 55 |
| 3.2.1.5. Calculation of actual length of patch antenna..... | 56 |
| 3.2.1.6. Calculation of ground plane dimensions..... | 56 |

| | |
|-------------------------------------------------------------------------|-----|
| 3.2.2. HF Antenna Design and Modeling | 58 |
| 3.2.3. Combination of HF and UHF antenna | 62 |
| 3.3. Effect of Environmental Changes on Tag Antenna | 70 |
| 3.3.1. Modeling and Design of Tag Antenna on Metallic Can | 70 |
| 3.3.2. Modeling and Design of Tag Antenna on Water Carboy | 79 |
| 3.3.3. Modeling and Design of Tag Antenna on Wooden Strip..... | 87 |
| 3.3.4. Modeling and Design of Tag Antenna on Paper Box | 95 |
| 3.4. Comparative Study of Dipole-Like Structures versus Our Design..... | 102 |
| 3.4.1. Free Space Analysis | 102 |
| 3.4.2. On Metallic Can Analysis | 103 |
| 3.4.3. On Water Carboy Analysis | 104 |
| 3.4.4. On Wooden Strip Analysis..... | 105 |
| 3.4.5. On Paper Box Analysis | 106 |
| 3.5. Measurements | 107 |
| 3.5.1. One-port (impedance) Measurements | 110 |
| 3.5.1.1. One-port Measurements for HF Antenna | 110 |
| 3.5.1.2. One-port Measurements for UHF Antenna in Free Space | 111 |
| 3.5.1.3. One-port Measurements for UHF Antenna on Metallic Can | 112 |
| 3.5.1.4. One-port Measurements for UHF Antenna on Water Carboy | 116 |
| 3.5.1.5. One-port Measurements for UHF Antenna on Wooden Strip | 120 |
| 3.5.1.6. One-port Measurements for UHF Antenna on Paper Box | 123 |
| 3.5.2. Two-port (gain) Measurements..... | 127 |
| 4. HF/UHF READER ANTENNA DESIGN, SIMULATION and MEASUREMENTS..... | 129 |
| 4.1. Design and Simulation of HF/UHF Reader Antenna..... | 129 |
| 4.1.1. Yagi UHF Reader Antenna Design and Simulations..... | 129 |
| 4.1.2. HF Reader Antenna Design and Simulations..... | 131 |
| 4.2. Measurements for HF/UHF Reader Antenna..... | 133 |
| 4.2.1. Measurements for UHF Yagi Reader Antenna | 133 |
| 4.2.2. Measurements for HF Reader Antenna..... | 136 |
| 5. IMPROVING READ/WRITE RANGE CAPABILITY OF HF TRANSPONDER..... | 138 |
| 5.1. Range Extension..... | 138 |
| 5.2. Rectifier circuit design, simulation and measurement | 148 |

6. CONCLUSIONS.....153
REFERENCES.....155

LIST OF FIGURES

| | |
|--------------------------------------------------------------------------------|----|
| Figure 1.1. Types of HF tags..... | 23 |
| Figure 1.2. RI-UHF-STRAP-08 tag designed by TI..... | 24 |
| Figure 1.3. Dual band tag designed and manufactured by Cobis Corporation | 24 |
| Figure 1.4. Frequency ranges used in RFID system | 25 |
| Figure 1.5. Dual band RFID designed by Leong | 28 |
| Figure 1.6. Dual operation tag designed by Mayer and Scholtz | 29 |
| Figure 1.7. Dual band tag designed by Iliev | 29 |
| Figure 2.1. Magnetic field of a small loop | 33 |
| Figure 2.2. Magnetic field on the axis of loop | 34 |
| Figure 2.3. Magnetic field strenght versus distance..... | 36 |
| Figure 2.4. Relative error for FEKO simulation and quasi-static analysis | 37 |
| Figure 2.5. Relative error for FEKO simulation and small loop analysis..... | 37 |
| Figure 2.6. Coupling between reader and tag | 39 |
| Figure 2.7. Mutual inductance between two loops | 40 |
| Figure 2.8. Circuit representation of two loops..... | 41 |
| Figure 2.9. Mutual inductance between reader and tag IC | 42 |
| Figure 2.10. Qauality factor of RLC circuit..... | 44 |
| Figure 2.11. Equivalent cirucit of a reader-tag system | 45 |
| Figure 2.12. Equivalent circuit of reader side | 45 |

| | |
|----------------------------------------------------------------------------------------------------------|----|
| Figure 2.13. Modulation of load impedance | 47 |
| Figure 2.14. Importance of tag orientation relative to H..... | 50 |
| Figure 3.1. Patch antenna | 54 |
| Figure 3.2. Dimensions of initial design..... | 57 |
| Figure 3.3. Cross slotted ground design for thickness 1.57 mm..... | 57 |
| Figure 3.4. Variables used in (3.7)..... | 59 |
| Figure 3.5. HF antenna model..... | 60 |
| Figure 3.6. Pure HF antenna designed in FEKO..... | 61 |
| Figure 3.7. Top and side views of latest design with dimensions..... | 63 |
| Figure 3.8. Bottom view of latest design with dimensions..... | 64 |
| Figure 3.9. Different views of FEKO..... | 65 |
| Figure 3.10.a. Real part of impedance versus frequency for designed antenna in free space | 66 |
| Figure 3.10.b. Imaginary part of impedance versus frequency for designed antenna in free space | 66 |
| Figure 3.11. Gain versus frequency for designed tag antenna in free space..... | 67 |
| Figure 3.12. Gain of designed tag in free space when $\theta=0$ changes with ϕ | 68 |
| Figure 3.13. FEKO model of RI UHF STRAP 08 | 68 |
| Figure 3.14.a. Real part of impedance versus frequency for the TI dipole antenna in free space..... | 69 |
| Figure 3.14.b. Imaginary part of impedance versus frequency for the TI dipole antenna in free space..... | 69 |

| | |
|----------------------------------------------------------------------------------------------------------------------|----|
| Figure 3.15. Gain versus frequency for TI dipole antenna in free space | 70 |
| Figure 3.16. FEKO model of tag antenna on metallic can..... | 71 |
| Figure 3.17.a. Real part of impedance for tag antenna on metallic can for different separations..... | 72 |
| Figure 3.17.b. Imaginary part of impedance for tag antenna on metallic can for different separations..... | 73 |
| Figure 3.18. Gain of the tag antenna on metallic can for different separations | 74 |
| Figure 3.19. Gain of the tag antenna in free space and on can | 75 |
| Figure 3.20. Gain of the tag antenna in free space and on can (larger can added) | 76 |
| Figure 3.21.a. Real part of the impedance for TI dipole antenna on metallic can for different separations | 77 |
| Figure 3.21.b. Imaginary part of the impedance for TI dipole antenna on metallic can for different separations | 77 |
| Figure 3.22. Gain of TI dipole antenna for different separations when it is on can | 78 |
| Figure 3.23. Gain of TI dipole antenna in free space and on can (larger can added) | 79 |
| Figure 3.24. FEKO model of tag antenna on water carboy | 80 |
| Figure 3.25.a. Real part of the impedance for tag antenna on water carboy for different separations..... | 81 |
| Figure 3.25.b. Imaginary part of the impedance for tag antenna on water carboy for different separations | 82 |
| Figure 3.26. Gain of the tag antenna on water carboy for different separations..... | 83 |
| Figure 3.27. Gain of designed antenna in free space and plastic water carboy | 83 |
| Figure 3.28. Gain of tag antenna in free space and on water carboy (larger carboy added)..... | 84 |

| | |
|------------------------------------------------------------------------------------------------------------------------------------------|----|
| Figure 3.29.a. Real part of the impedance for TI dipole on water carboy versus frequency for different separations | 85 |
| Figure 3.29.b. Imaginary part of the impedance for TI dipole on water carboy versus frequency for different separations | 86 |
| Figure 3.30. Gain of TI dipole on water carboy for different separations | 86 |
| Figure 3.31. Gain of TI dipole in free space and on water carboy (larger carboy added) ... | 87 |
| Figure 3.32. FEKO model of designed tag antenna placed on wooden strip | 88 |
| Figure 3.33.a. Real part of the impedance for designed tag antenna on wooden strip versus frequency for different separations | 89 |
| Figure 3.33.b. Imaginary part of the impedance for designed tag antenna on wooden strip versus frequency for different separations | 90 |
| Figure 3.34. Gain of designed tag antenna on wooden strip for different separations | 91 |
| Figure 3.35. Gain of tag antenna in free space and on wooden strip | 92 |
| Figure 3.36.a. Real part of the impedance for TI dipole on wooden strip versus frequency for different separations | 93 |
| Figure 3.36.b. Imaginary part of the impedance for TI dipole on wooden strip versus frequency for different separations | 93 |
| Figure 3.37. Gain of TI dipole antenna placed on wooden strip for different separations .. | 94 |
| Figure 3.38. Gain of TI dipole in free space and on wooden strip..... | 95 |
| Figure 3.39. FEKO model of tag antenna placed on paper box..... | 96 |
| Figure 3.40.a. Real part of the impedance for designed tag antenna on paper box versus frequency for different separations | 97 |
| Figure 3.40.b. Imaginary part of the impedance for designed tag antenna on paper box versus frequency for different separations | 97 |

| | |
|--------------------------------------------------------------------------------------------------------------------------------------------|-----|
| Figure 3.41. Gain of tag antenna when placed on paper box for different separations | 98 |
| Figure 3.42. Gain of tag antenna in free space and on paper box | 99 |
| Figure 3.43.a. Real part of the impedance for Ti dpole on paper box versus frequency for different separations | 100 |
| Figure 3.43.b. Imaginary part of the impedance for TI dipole on paper box versus frequency for different separations | 100 |
| Figure 3.44. Gain of TI dipole on paper box for different separations | 101 |
| Figure 3.45. Gain of TI dipole in free space and on paper box..... | 102 |
| Figure 3.46.a. Top view of the EAGLE drawing of patch antenna | 107 |
| Figure 3.46.b. Bottom view of the EAGLE drawing of patch antenna..... | 108 |
| Figure 3.47.a. Top view of latest prototype | 109 |
| Figure 3.47.b. Bottom view of latest prototype | 109 |
| Figure 3.48. Inductance versus frequency..... | 110 |
| Figure 3.49.a. Real part of impedance for simulation and measurement..... | 111 |
| Figure 3.49.b. Imaginary part of impedance for simulation and measurement | 112 |
| Figure 3.50. Designed tag antenna on metallic can | 113 |
| Figure 3.51.a. Measurement of real part of the impedance versus frequency when tag antenna is in free space and on metellic can | 114 |
| Figure 3.51.b. Measurement of imaginary part of the impedance versus frequency when tag antenna is in free space and on metellic can | 114 |
| Figure 3.52.a. Real part of the impedance versus frequency for measurement and simulation..... | 115 |

| | |
|-------------------------------------------------------------------------------------------------------------------------------------------|-----|
| Figure 3.52.b. Imaginary part of the impedance versus frequency for measurement and simulation..... | 116 |
| Figure 3.53. Designed tag on water carboy..... | 116 |
| Figure 3.54.a. Measurement of real part of the impedance versus frequency when tag antenna is in free space and on water carboy..... | 117 |
| Figure 3.54.b. Measurement of imaginary part of the impedance versus frequency when tag antenna is in free space and on water carboy..... | 118 |
| Figure 3.55.a. Real part of the impedance versus frequency for measurement and simulation..... | 119 |
| Figure 3.55.b. Imaginary part of the impedance versus frequency for measurement and simulation..... | 119 |
| Figure 3.56. Designed tag on wooden strip..... | 120 |
| Figure 3.57.a. Measurement of real part of the impedance versus frequency when tag antenna in free space and on wooden strip..... | 121 |
| Figure 3.57.b. Measurement of imaginary part of the impedance versus frequency when tag antenna in free space and on wooden strip..... | 121 |
| Figure 3.58.a. Real part of the impedance versus frequency for measurement and simulation..... | 122 |
| Figure 3.58.b. Imaginary part of the impedance versus frequency for measurement and simulation..... | 123 |
| Figure 3.59. Designed tag on paper box | 123 |
| Figure 3.60.a. Measurement of real part of the impedance for tag antenna in free space and on paper box..... | 124 |
| Figure 3.60.b. Measurement of imaginary part of the impedance for tag antenna in free space and on paper box | 125 |

| | |
|-------------------------------------------------------------------------------------------------------------------------------------|-----|
| Figure 3.61.a. Real part of the impedance versus frequency for measurement and simulation..... | 126 |
| Figure 3.61.b. Imaginary part of the impedance versus frequency for measurement and simulation..... | 126 |
| Figure 3.62. Dipole antenna with balun used during measurement as reference..... | 127 |
| Figure 3.63. Measurement setup for gain analysis: far side: dipole antenna, near side: designed antenna and separation: 4.55 m..... | 128 |
| Figure 4.1. Three-element Yagi antenna structure..... | 129 |
| Figure 4.2. FEKO model of designed Yagi antenna..... | 130 |
| Figure 4.3. Antenna gain characteristics of designed Yagi..... | 131 |
| Figure 4.4. HF reader antenna..... | 132 |
| Figure 4.5. FEKO model of designed HF reader antenna..... | 132 |
| Figure 4.6 Realized Yagi antenna..... | 134 |
| Figure 4.7. Impedance measurement for realized Yagi antenna..... | 135 |
| Figure 4.8. VSWR measurement for Yagi antenna..... | 135 |
| Figure 4.9. Realized HF reader antenna..... | 136 |
| Figure 4.10. Measurement setup used to measure inductance of HF reader coil..... | 137 |
| Figure 5.1. FEKO model of reader-tag system..... | 140 |
| Figure 5.2. FEKO model of Yagi transmitter and UHF tag system..... | 142 |
| Figure 5.3. FEKO model of UHF reader-tag system..... | 143 |
| Figure 5.4. Circuit scheme for the rectifier..... | 148 |
| Figure 5.5. Input-output characteristics of rectifier circuit..... | 149 |

| | |
|------------------------------------------------------------------------------------|-----|
| Figure 5.6. EAGLE drawing of rectifier circuit..... | 149 |
| Figure 5.7. Top view of rectifier circuit..... | 150 |
| Figure 5.8. Measurement setup when Yagi transmits and tag antenna receives..... | 150 |
| Figure 5.9. Measurement setup when Yagi transmits and dipole antenna receives..... | 151 |

LIST OF TABLES

| | |
|--------------------------------------------------------------------------------------------------------------------|-----|
| Table 1.1. Frequency ranges and allowed power limits..... | 26 |
| Table 3.1. HF design specifications of dual band | 52 |
| Table 3.2. UHF design specifications of dual band | 53 |
| Table 3.3. Comparative inductance values of HF antenna..... | 62 |
| Table 3.4. Effect of moving feed point | 64 |
| Table 3.5. Comparative results for designed patch and TI dipole in free space | 103 |
| Table 3.6. Comparative results for designed patch and TI dipole on metallic can | 104 |
| Table 3.7. Comparative results for designed patch and TI dipole on water carboy..... | 104 |
| Table 3.8. Comparative results for designed patch and TI dipole on wooden strip..... | 105 |
| Table 3.9. Comparative results for designed patch and TI dipole on paper box..... | 106 |
| Table 5.1. Comparative results for both theoretical and analytical analysis..... | 141 |
| Table 5.2. ΔV required to reach minimum operating voltage 2.5 V for HF tag | 143 |
| Table 5.3. Available source voltages for different distances when 0.5 W reader is used.. | 145 |
| Table 5.4. Available source voltages for different distances when 2 W reader is used..... | 146 |
| Table 5.5. Available source voltages for different distances when 4 W reader is used..... | 147 |
| Table 5.6. Induced voltage on the output of the rectifier circuit when different levels of power are applied | 152 |

LIST OF SYMBOLS / ABBREVIATIONS

| | |
|------------|-----------------------------------------|
| A | Area |
| a | Radius of a wire |
| B | Magnetic flux density |
| c | Speed of light in free space |
| cm | Centimeter |
| D | Directivity |
| dB_i | Decibel referenced to isotropic antenna |
| ΔL | Length Extension |
| f | Frequency |
| f_o | Resonance frequency |
| G | Gain |
| GHz | Gigahertz |
| h | Height of dielectric substrate |
| Hz | Hertz |
| I | Current |
| j | Unit imaginary number |
| KHz | Kilohertz |
| L | Inductance |
| L_{eff} | Effective Length |
| LF | Low Frequency |
| L_g | Minimum structure length |
| mm | Millimeter |
| mW | MiliWatt |
| μH | Micro Henry |
| MHz | Megahertz |
| N | Number of spiral turns |
| W | Width of Patch Antenna |
| W_g | Minimum structure width |

| | |
|-------------------------|------------------------------------------------|
| β | Phase constant of the medium |
| Γ | Reflection coefficient |
| ϵ | Dielectric permittivity of the medium |
| \vec{E} | Electric field strength |
| ϵ_{eff} | Effective dielectric constant |
| ϵ_0 | Absolute dielectric permittivity of free space |
| ϵ_r | Relative dielectric permittivity of the medium |
| \vec{H} | Magnetic field strength |
| λ | Wavelength |
| μ | Permeability of the medium |
| μ_0 | Permeability of free space |
| γ | Propagation constant of the medium |
| σ | Conductivity of the medium |
| Φ | Flux |
| Ω | Ohm |
| ω | Angular frequency |
| <i>A.C</i> | Alternating current |
| <i>Auto ID</i> | Automatic identification |
| <i>BW</i> | Bandwidth |
| <i>Corp</i> | Corporation |
| <i>FF</i> | Far field |
| <i>HF</i> | High Frequency |
| <i>ISO</i> | International Standard Organization |
| <i>ITU</i> | International Telecommunication Union |
| <i>NF</i> | Near Field |
| <i>RF</i> | Radio frequency |
| <i>RFID</i> | Radio frequency identification |
| <i>SRD</i> | Short Range Devices |
| <i>UHF</i> | Ultra-high frequency |
| <i>VSWR</i> | Voltage Standing Wave Ratio |

1. INTRODUCTION

Auto-identification (Auto ID) systems are important for many applications in logistics, industry, and manufacturing companies to provide information about the products, people and animals. Most popular Auto ID systems are optical character recognition and smart card based systems. For example, in smart card applications, the reader provides energy and clock pulse through a galvanic contact to establish data transfer between the card and the reader. Radio frequency identification (RFID) systems are in similar nature with smart-card systems, however, the energy and data-exchange are provided by using magnetic, electric or electromagnetic fields. The data carrying device is usually termed as the transponder or tag, and the reader, again sends power and clock to establish one-way or two-way communications. Compared to other Auto ID systems, RFID has a larger distance between the data-carrier and the reader, its response time is very fast (less than 1 second), and high data quantities can be exchanged, which, in turn, also enables a secure communication and precludes the unauthorized copying of the data-carrier [1].

1.1. RADIO FREQUENCY IDENTIFICATION

RFID gained widespread use with the evolution of low cost integrated circuit manufacturing in recent years. RFID systems are usually classified according to their operation bands. The most common bands are Low Frequency (LF) RFID, High Frequency (HF) RFID, Ultra High Frequency (UHF) and Microwave Frequency RFID. One of the most commonly used RFID system is HF RFID because it is cost effective, easy to realize and durable against harsh environments [1]. In HF RFID, printed coil antennas are used as a tag antenna and wound, spiral antennas are used for the reader antenna. In such systems, inductive coupling occurs. Inductive coupling causes energy transmission between interrogator antenna and the transponder (tag) antenna. Both antennas cause creation of magnetic field since both interrogator antenna and tag antenna behave like an air-core transformer [2]. HF RFID tags also work well in harsh environments such as on or near metallic and dielectric surfaces because magnetic field lines do not undergo significant

change in short distances. This can be regarded as the strongest side of HF RFID systems.

On the other hand, they have limited read/write range capability since magnetic field lines created between the interrogator antenna and the tag antenna decay with “ r^{-3} ”, where “ r ” is the distance from the source [3]. Due to this rapid decay, HF RFID tags should be close to the interrogator antenna for better read/write performance. Figure 1.1 shows different types of HF tags used in RFID systems;

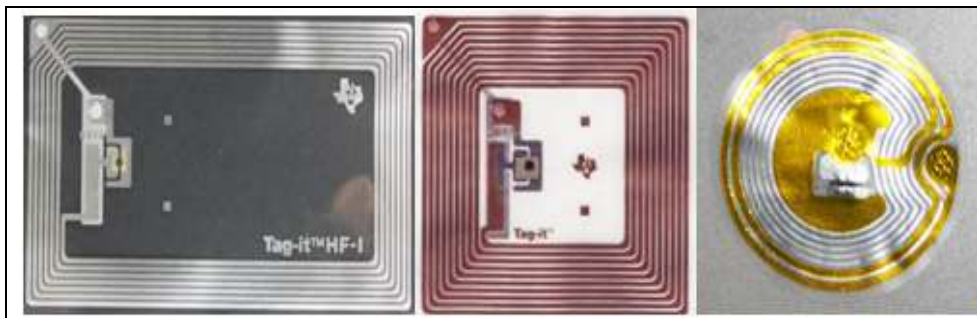


Figure 1.1. Types of HF tags

UHF RFID systems utilize UHF band where the operation wavelength is small compared to physical application distances [4]. Hence, the far field radiation pattern of the antenna plays an important role in two-way communications between the interrogator and the tag. In addition, UHF band presents much larger bandwidth which can be utilized for resolving security and authentication issues [4]. In UHF band, electromagnetic power in the far field decays with “ r^2 ” [5], [6]. Thus UHF RFID system provides more read/write range compared to HF RFID. Even though UHF RFID has benefit in having better read/write range capability, these tags can get easily affected by the surroundings or application environment such as on/near metal and plastics. When tags are placed in such environments, tag impedance can change and detune easily, and also radiation characteristics may change considerably, which, in turn, makes the UHF tag less reliable. Therefore, there is a need for an UHF RFID tag that is less sensitive to environment and is capable of preserving radiation characteristics in such environments. There has been considerable effort to improve the performance of UHF RFID tags on or near metallic surfaces [7]-[14]. However, if application requires long read/write range capability, UHF

tags should be chosen to have better performances. In Figure 1.2, UHF RFID tag antenna which is manufactured by Texas Instruments (TI) is given;

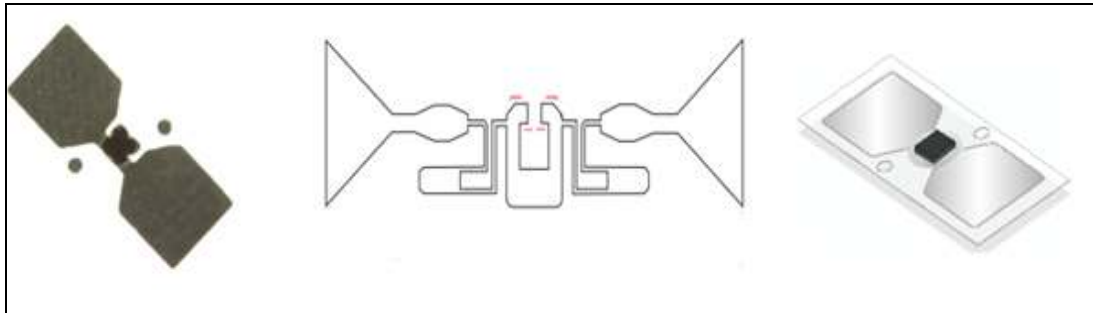


Figure 1.2. UHF RFID tag designed by TI (RI-UHF-STRAP-08)

There are also dual band RFID tags developed and manufactured by companies in order to use both HF and UHF in the same system. These types of tags are operational at both 13.56 MHz and 860-960 MHz. Dual band RFID tag which is designed and manufactured by Cobis Corporation is given in Figure 1.3;



Figure 1.3. Dual band tag designed and manufactured by Cobis Corporation

As mentioned previously, in addition to classification in terms of operation frequency, RFID tags are also classified according to functioning properties such as passive, active and semi-active tags. *Passive tags* are the tags which have no independent power source and get power from the reader directly. Read-only tags are typically passive tags. *Active tags* are the tags that are powered by an internal battery and are typically read/write tags. The battery supplied power of an active tag generally gives it a longer read

range. *Semi-active tags* are the tags which incorporate batteries but the battery is only used to power ICs.

1.2. FREQUENCY RANGES USED IN RFID SYSTEMS

100 KHz-5 GHz frequency ranges are used by RFID systems. Most common frequency bands used in RFID are 125/134 KHz, 13.56 MHz, 860-960 MHz and 2.45 GHz. RFID system which operates at 125/134 KHz frequency band is Low Frequency (LF) RFID system. LF RFID system has a bandwidth of 520 Hz. Systems which use 13.56 MHz band are named High Frequency (HF) RFID systems. These systems have bandwidth of 5 KHz of which 3 KHz is used for communications with 1 KHz guard band to minimize interference. RFID system which operates at 860-960 MHz band range is named as Ultra High Frequency (UHF) RFID system. UHF RFID system has bandwidth of 3 MHz

Frequency ranges used in RFID is given in Figure 1.4;

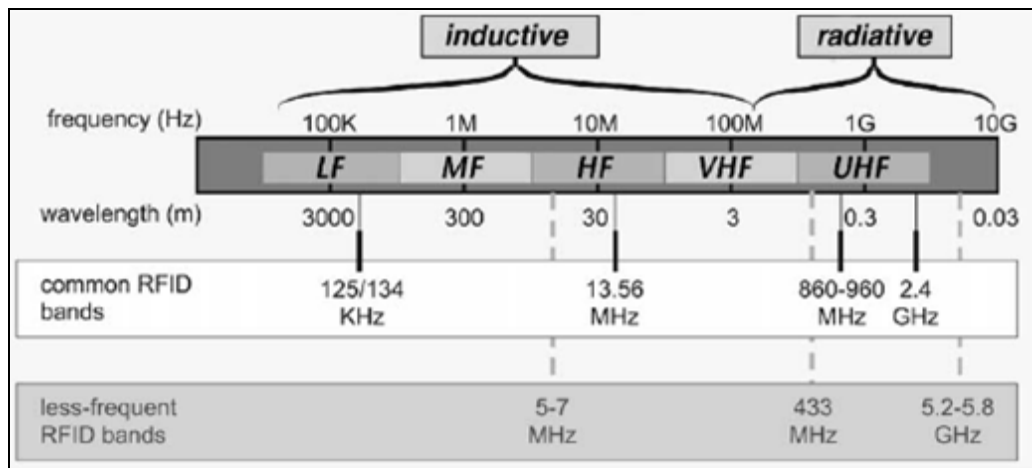


Figure 1.4. Frequency ranges used in RFID system [18]

1.3. RADIO LICENSING REGULATIONS & STANDARDS FOR RFID

1.3.1. European Radio Licensing Regulations

European Telecommunications Standards Institute (ETSI) aims to issue recommended standards for radio protocols, testing and operations within Europe. The standards determined by ETSI must be followed by all European countries. Two documents are presented for RFID in Europe;

CEPT/ ERC REC 70-03: This document generally covers spectrum allocations for a number of low-power applications, including RFID. There is still some consideration for 868 MHz RFID by European Research Council (ERC). However, 869.4-869.65 MHz frequency ranges are already introduced. Table 1.1 shows the frequency ranges with allowed power limits for Europe;

Table 1.1. Frequency ranges and allowed power limits

| <i>Frequency Range</i> | <i>Allowed Power Limits</i> |
|------------------------|-----------------------------|
| 865-868 MHz | 0.1 Watt |
| 865.6-867.6 MHz | 2.0 Watt |
| 865.6-868 MHz | 0.5 Watt |

ETSI 302-208: These are the regulations for RFID working within 865-868 MHz frequency ranges with maximum power usage of 2 Watt. According to this regulation, interrogators must have 200 KHz channel spacing and reader which is allowed to use power of 2 Watt must have sensitivity of -96 dBm.

1.3.2. ISO Standards

It is known that there are lots of standards introduced by International Standards Organization (ISO) about RFID and its applications. It is given information about the standards that are concerning 13.56 MHz HF and 868-869 MHz UHF RFID systems.

ISO/IEC 14443: This standard defines proximity cards used for identification and the transmission protocols for communication. It generally concerns frequency range 13.56 MHz +/- 7 MHz. It consists of 4 major parts and describes two types of cards such as type A and B, which both communicate at 13.56 MHz band. The main differences between these types are; usage of modulation techniques, coding schemes and protocol initialization procedures. According to this standard, maximum operational magnetic field strength at the transponder in terms of proximity is given as $137.5 \text{ dB}\mu\text{A} = 7.5 \text{ A/m}$.

ISO/IEC 15693: It is used generally for vicinity cards. These cards can be read from greater distances compared to proximity cards. Again system that is designed according to this standard works at 13.56 MHz frequency range and offers maximum read/write distance of 1-1.5 m. According to this standard vicinity is given as $134 \text{ dB}\mu\text{A} = 5 \text{ A/m}$.

ISO/IEC 18000-3: This is the main standard introduced for RFID systems. Especially part 3 of this standard is applicable for RFID system which operates at 13.56 MHz frequency band. This standard generally concerns air interface communications at 13.56 MHz. There are no standards defined EPC Global for this band.

ISO/IEC 18000-6A/6B/6C: It is the standard defined and introduced for RFID applications that can be used for item tracking and management. All ISO 18000 standards defined with part 1 defines the foundation for all air interface definitions. It concerns 860-960 MHz frequency bands. According to this standard bandwidth of a RFID system in Europe defined between 865.2–871.4 MHz.

ISO 18000-6 series standards concern RFID applications that can be applicable within 860-960 MHz frequency range. TYPE A and B, which are also named as ISO 18000-A and B are very similar to each other. The main difference between them is being the anti-collision algorithm used. Newly introduced standard ISO 18000-6C which is also known as EPC Global Class 1 Gen 2 concerns new designs and RFID systems to increase

usage range of the system causing bandwidth increase and flexibility in usage and most important part is compatibility of different brand chips, elements.

1.4. DUAL BAND OR DUAL MODE RFID SYSTEMS

It is also possible to design dual band, HF and UHF compatible RFID tag since they complement each other in many ways. For dual band operation, the tag can be either programmed for HF, or UHF, or both. The idea of dual band RFID has been first exploited in using a printed dipole and a multi-turn loop [15]. The printed dipole is intended for UHF and multi-turn loop is dedicated for HF. The design achieves an impedance of $24+j143 \Omega$ at UHF band with simulations and $56.26+j1134.5 \Omega$ with measurements. However, the UHF design still suffers degradation when the tag is placed on/near metallic surface. Actually, dipole-like UHF structures are prone to such degradation. In Figure 1.5, dual band RFID designed by Leong [15] is shown.

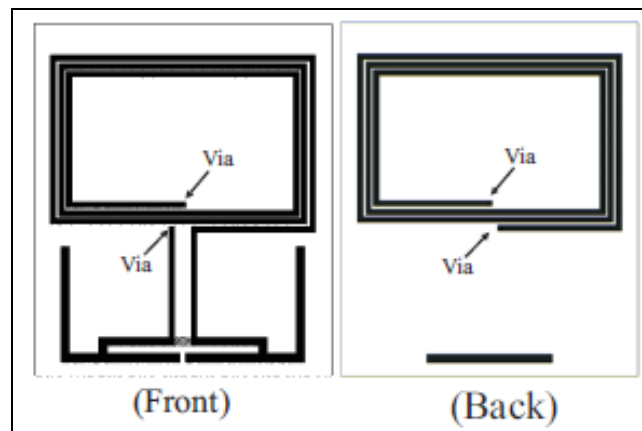


Figure 1.5. Dual band RFID designed by Leong [15]

Maybe the most notable study for dual band operation was carried out by Mayer and Scholtz [16]. The designed tag antenna and chip is capable of operating at 13.56 MHz and at 868 MHz. The antenna is a single feed for dual operation; hence it is different than previous dual band design. For HF band, spiral antenna is used as usual. The HF antenna is placed at outer side of the design to enlarge the diameter of the winding for collecting more magnetic flux. Capacitors are placed on several locations on the design to present short for

UHF operation while permit HF simultaneously. Slot loop antenna is used for UHF. The gain of the antenna at UHF band was stated as -4.69 dBi with dimensions 71×46 mm², considerably lower than dipole-like UHF tags. Dual band operation tag designed by Mayer and Scholtz is given in Figure 1.6;

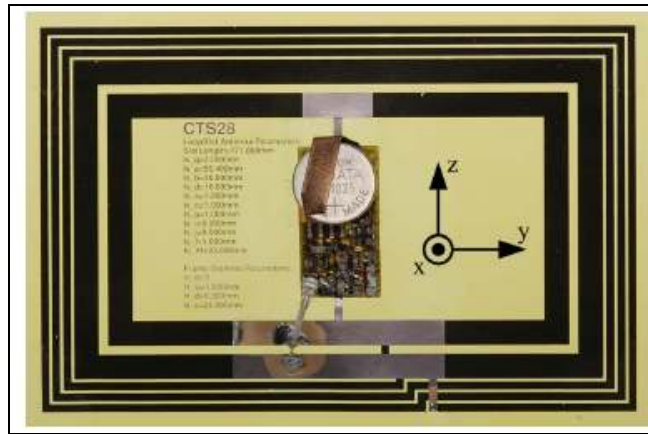


Figure 1.6. Dual operation tag designed by Mayer and Scholtz [16]

Third study on dual band tag design is reported by Iliev et al. [17]. The antenna is again a dipole-like structure with a gain of 2.3 dBi in free space. Resonance for HF part is achieved at 16.1 MHz with a quality factor of 10.1 . In Figure 1.7, tag designed by Iliev is shown;

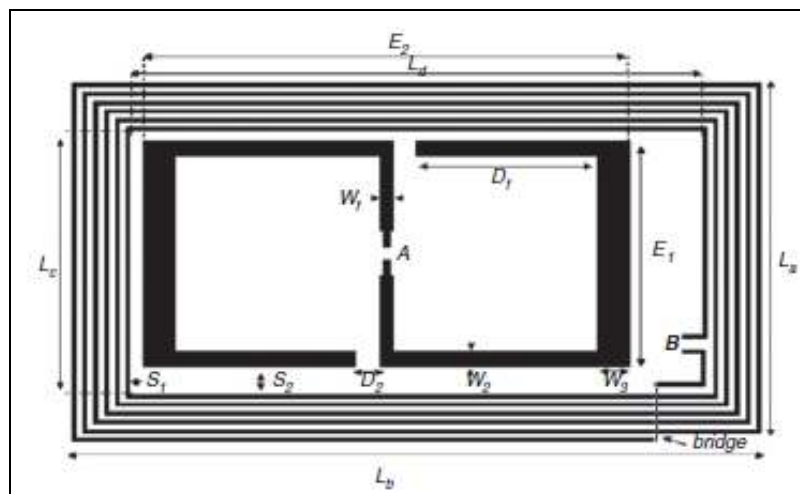


Figure 1.7. Dual band tag designed by Iliev [17]

Albeit previous dual band design attempts, there is still a need for dual band, HF and UHF compatible RFID tag that does not get affected from environment and yet still provide adequate gain for seamless operation. To achieve such high isolation from environment, we envisioned a microstrip patch antenna for UHF band and spiral, multi turn loop antenna for HF contrary to dipole-like structures in previous works. The existence of metallic plates for UHF band alters the inductance for HF antenna, however, careful design and placement of multi-turn loop alleviates this problem to a manageable level. Therefore, our work is different than previous dual band designs due to structurally different antenna shape, the use of an antenna ground that electromagnetically isolates the antenna from environment while preserving critical performance parameters such as gain and tag impedance. Our design is also unique in the sense that UHF patch antenna feed is specifically designed for this structure. The design can be easily realized using printed board technologies and simple vias. Therefore, the design can be considered low-cost for high volume manufacturing. The only disadvantage of using microstrip antenna is its rigid substrate that can not be bent or made conformal to the surface that the tag is attached to. Flexible substrates could have been used alternatively, however, to achieve the desired gain and physical size criteria, existing flexible substrates are deemed inappropriate for the current design.

In our design, we used 5 turns of printed coil for the HF antenna. One turn is on the top side which surrounds the upper electrode of the metallic patch antenna, Remaining 4 turns are placed on the bottom side that surround the lower electrode of the patch, that is the ground plane. Bottom and top spirals are connected using two vias. At 13.56 MHz band, our simulations achieve an inductance value of $3.37 \mu\text{H}$, and when measured, it is $2.54 \mu\text{H}$ at 13.56 MHz band. To increase the gain of the microstrip patch antenna and help to achieve target impedance value, a degenerated ground is used on the bottom electrode. A crossed slot is used as a form of degeneration. We also placed two notches two sides of the microstrip patch antenna for better impedance matching. During simulation at 868 MHz band, the design achieves a gain of 2.68 dBi with a radiation efficiency of 66%. Gain is measured as approximately 2.5 dBi using network analyzer with two port gain measurement. The design also has a complex impedance of $35.1219 + j161.871 \Omega$ at 868 MHz with simulations and $40.264 + j163.49 \Omega$ with measurements. Designed dual band

antenna has full dimensions of 94x94 mm². The proposed dual band antenna design is simulated and measured for tag being placed on metal, dielectric, wood, and paper box, typical applications of dual band tag.

Having a dual band design, we also propose a new method to increase the range of HF tag by sending wireless power through UHF band. Hence, additional power can be sent from the reader in UHF band, and that power can be utilized by the HF tag. In essence, this is similar to semi-active or fully active tags where there is additional energy source to operate the tag. Although, the maximum range for HF operation is 1.5 m and this range can not be considered true far-field for UHF operation, however, being outside the reactive zone of the UHF tag, it is possible to transmit power to the tag. Since tag is dual band, UHF portion of the tag rectifies the received RF power in UHF band and supplies to HF IC for an increased read range. The reader design for HF and UHF bands are also performed and simple experiments have been carried out to prove this new concept.

2. HF RFID DESIGN PRINCIPLES

2.1. HF RFID DESIGN

2.1.1. Magnetic Field of a Small Loop

The magnetic field of a small loop is given as (2.1), where μ shows the permeability of the medium, ε shows the dielectric constant of the medium, S shows area of the small loop, ω shows angular frequency, I shows the current on loop, β shows propagation constant, R is the distance and θ shows the angle from broadside.

$$\begin{aligned}
 \vec{E} &= -\frac{j\omega\mu IS}{4\pi} j\beta \left(1 + \frac{1}{j\beta R}\right) e^{-j\beta R} \sin\theta \hat{a}_\phi \\
 \vec{H} &= \frac{j\omega\mu IS}{4\pi} j\omega\varepsilon \left(1 + \frac{1}{j\beta R} + \frac{1}{(j\beta R)^2}\right) \frac{e^{-j\beta R}}{R} \sin\theta \hat{a}_\theta \\
 &+ \frac{j\omega\mu IS}{4\pi} j\omega\varepsilon \left(\frac{1}{j\beta R} + \frac{1}{(j\beta R)^2}\right) \frac{e^{-j\beta R}}{R} \cos\theta \hat{a}_R
 \end{aligned} \tag{2.1}$$

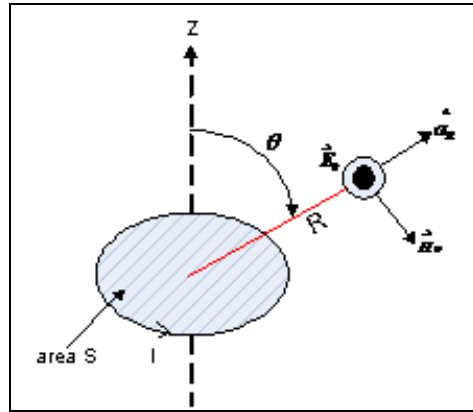


Figure 2.1. Magnetic field of a small loop

Spherical coordinate unit vectors are given with \hat{a}_θ , \hat{a}_ϕ and \hat{a}_r . The magnitudes of magnetic field components are;

$$\begin{aligned} |H_\theta| &= \frac{\omega^2 \mu \epsilon I S}{4\pi R} \sin \theta \left| 1 + \frac{1}{j\beta R} + \frac{1}{(j\beta R)^2} \right| \\ |H_r| &= \frac{\omega^2 \mu \epsilon I S}{4\pi R} \cos \theta \left| 1 + \frac{1}{j\beta R} + \frac{1}{(j\beta R)^2} \right| \end{aligned} \quad (2.2)$$

where,

$$\beta^2 = \omega^2 \mu \epsilon \quad \text{and,} \quad \vec{B} = \mu_0 \vec{H}.$$

Above derivations assume a small loop, i.e. $IS \ll 1$. Although they provide good idea about the fields, they are not exact for finite loops.

On the other hand, one can use quasi-stationary approximation of magnetic field created by a loop. The current is assumed steady-current (DC) and Biot-Savart law is used to find field expressions.

On the axis of the loop the magnetic field is given as;

$$B_z = \frac{\mu_0 I a^2}{2(R^2 + a^2)^{3/2}} \quad (2.3)$$

As shown in Figure 2.2 and in (2.3), “ a ” shows the radius of the loop and μ_0 shows the permeability of the free space.

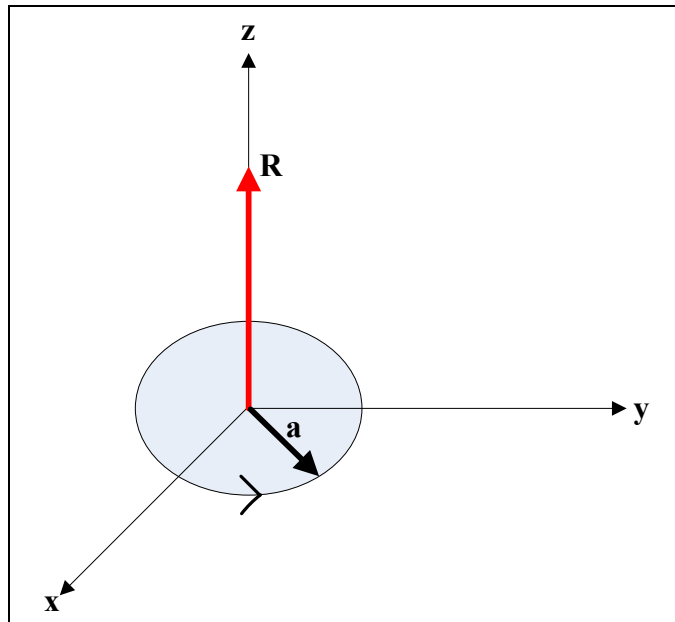


Figure 2.2. Magnetic field on the axis of loop

At the center of the loop $R=0$ and (2.3) is simplified as;

$$B_z = \frac{\mu_0 I}{2a} \quad (2.4)$$

Also, on the axis of the loop, magnetic field is,

$$B_z = \frac{\mu_0 I a^2}{2(R^2 + a^2)^{3/2}} = \frac{\mu_0 I a^2}{2R^3 (1 + a^2 / R^2)^{3/2}} \quad (2.5)$$

For $R \gg a$ condition, (2.5) reduces to,

$$B_z = \frac{\mu_0 I a^2}{2R^3} \quad (2.6)$$

Hence, it can be said that $B_z \propto \frac{1}{R^3}$.

If a rectangular conductor with edge lengths “ a ”, “ b ” is used; the magnetic field is expressed as,

$$B_z = \frac{\mu_0 I a b}{4\pi \sqrt{\left(\frac{a}{2}\right)^2 + \left(\frac{b}{2}\right)^2 + R^2}} \left[\frac{1}{\left(\frac{a}{2}\right)^2 + R^2} + \frac{1}{\left(\frac{b}{2}\right)^2 + R^2} \right] \quad (2.7)$$

In (2.5), choosing coil radius “ a ” large does not guarantee maximum field strength. Even at $R=0$, it is small. For $R \gg a$, field decreases with $1/R^3$. Given a distance “ R ”, taking derivative of “ B ” with respect to “ a ” gives the optimal coil radius.

$$\begin{aligned} \frac{dB}{da} &= \frac{\mu_0 I a}{(R^2 + a^2)^{3/2}} + \left(\frac{\mu_0 I a^2}{2} \right) \left(-\frac{3}{2} \right) \frac{1}{(R^2 + a^2)^{5/2}} (2a) \\ &= \frac{\mu_0 I a}{(R^2 + a^2)^{3/2}} \left[1 - \frac{3a^2}{2(R^2 + a^2)} \right] \end{aligned} \quad (2.8)$$

When $\frac{dB}{da} = 0$, optimal coil radius is found as $a = \sqrt{2}R$.

Obviously, quasi-static and small loop time harmonic expressions are the approximations to the real magnetic field of a coil. Hence, one needs to simulate the structure for accurate values of “ H ”.

If we assume 50 mm radius loop and compare the magnetic field intensity using both approaches and 3D EM simulator FEKO, we obtain the results shown in Figure 2.3.

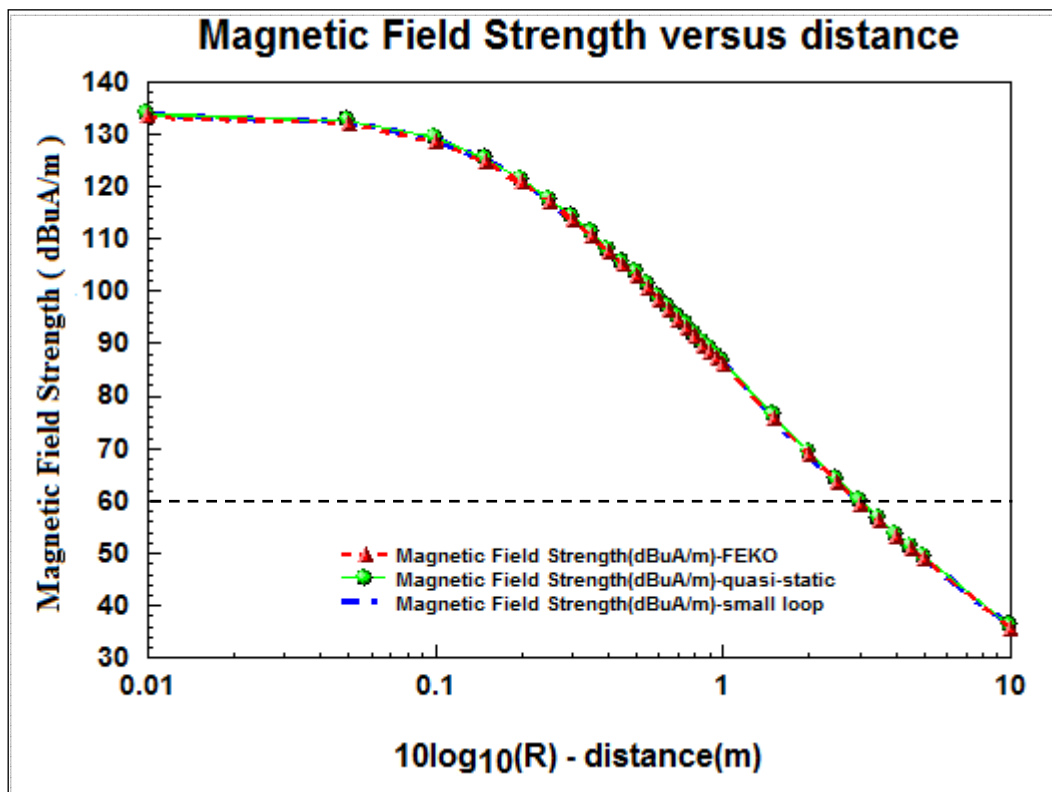


Figure 2.3. Magnetic Field strength versus distance

We also examined a small loop which has dimensions of 35x25 cm². In Figure 2.4, relative error for FEKO simulation and Quasi-static analysis and in Figure 2.5 relative error for FEKO simulation and small loop are given.

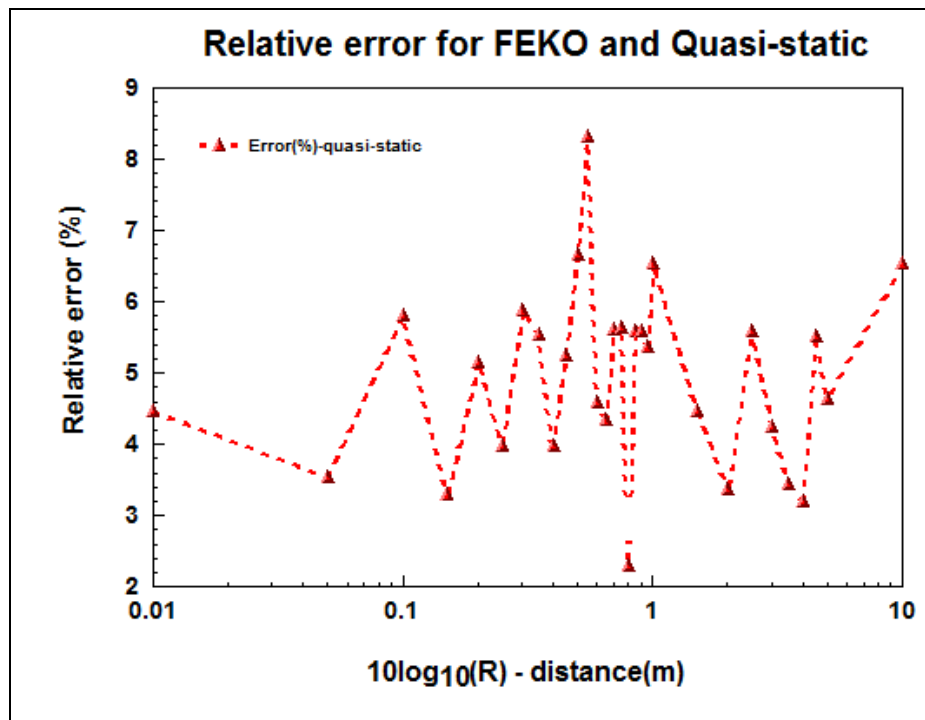


Figure 2.4. Relative error for FEKO simulation and quasi-static analysis

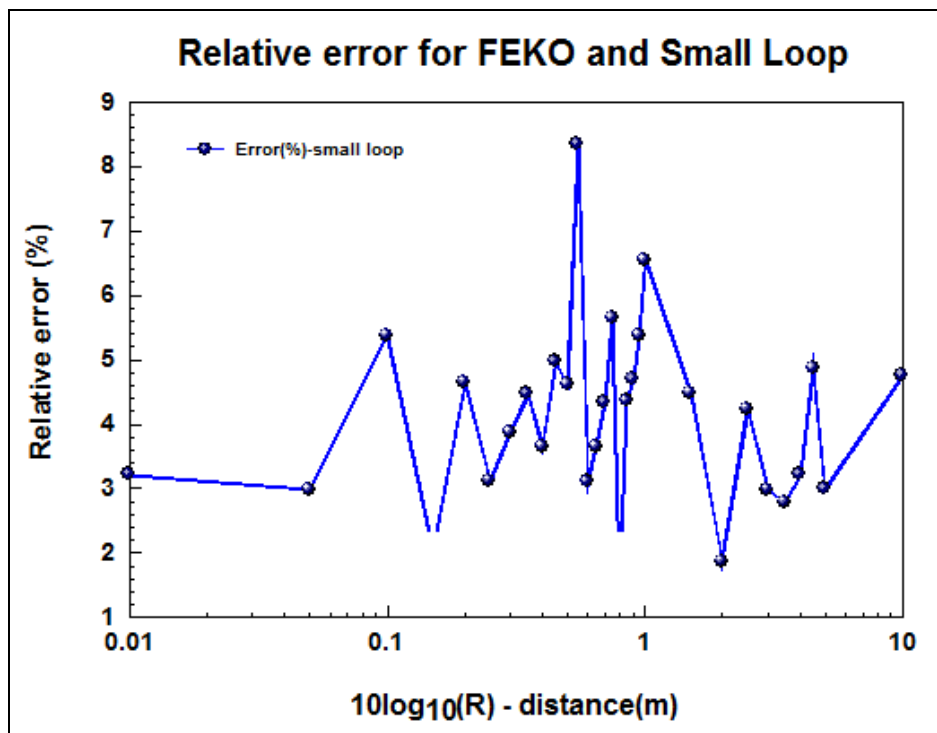


Figure 2.5. Relative error for FEKO simulation and small loop analysis

Inductance of the circular loop is defined as;

$$L_{CIRCULAR\ LOOP} = \frac{\psi}{I} = \frac{N\Phi}{I} \quad (2.9)$$

where magnetic flux is defined as,

$$\Phi = \int \vec{B} \cdot d\vec{s} \quad (2.10)$$

In (2.9), ψ is the total flux and N is the total turns. While doing calculations, of course not only on-axis B_z but also off-axis expression must be known to get the inductance. The inductance of a small loop is given as;

$$L_{LOOP} = \mu_0 N^2 a \ln\left(\frac{2a}{d}\right) \quad (2.11)$$

In (2.11), “ a ” is the optimal coil radius and “ d ” is the diameter of the loop.

2.1.2. Mutual Inductance between Two Loops

The coupling between reader and tag coil is illustrated in Figure 2.6;

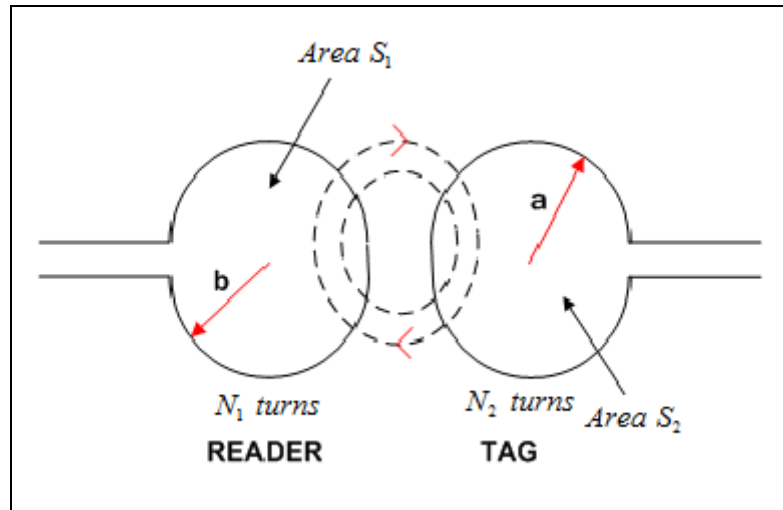


Figure 2.6. Coupling between reader and tag

The mutual coupling can be expressed as,

$$M_{21} = \frac{B(I_1)N_2A_2}{I_1} = \frac{\mu_0 N_1 b^2}{2(R^2 + b^2)^{3/2}} (N_2 \pi a^2) \quad (2.12)$$

In (2.12), “ A ” is the cross sectional area, I_1 is the current in reader side, “ R ” is the distance between reader and HF tag and “ b ” is the optimal coil radius.

The coupling can also be expressed as;

$$k = \frac{M}{\sqrt{L_1 L_2}} \quad \text{where } 0 \leq k \leq 1 \quad (2.13)$$

In (2.13), if $k=0$ there is no magnetic coupling and $k=1$ perfect coupling occurs. At a given distance R , k can be defined as,

$$k(R) \approx \frac{a^2 b^2}{\sqrt{ab}} \frac{1}{(R^2 + b^2)^{3/2}} \quad \text{for } b \geq a \quad (2.14)$$

The mutual inductance M between two loops is,

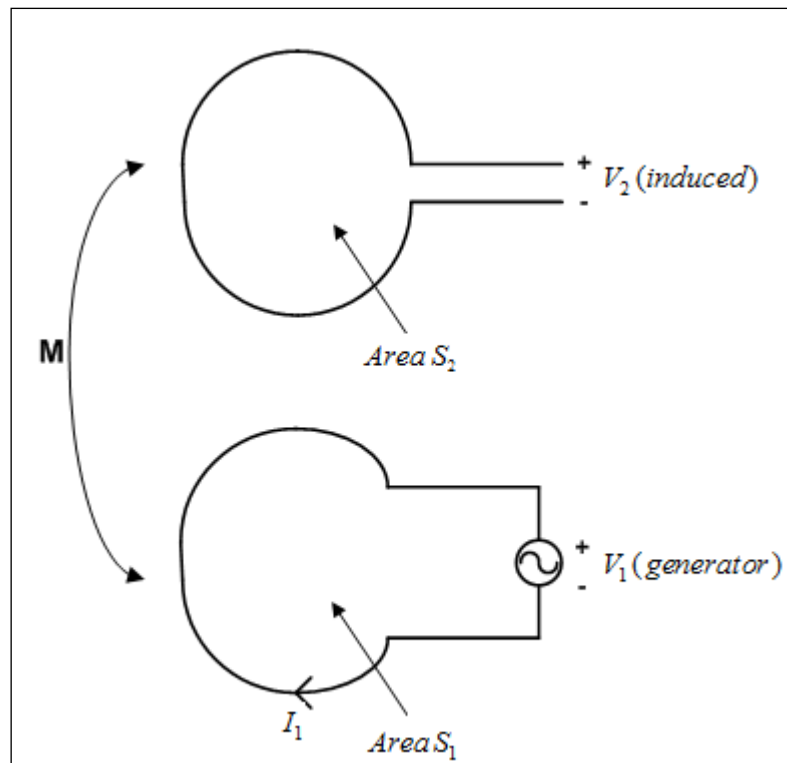


Figure 2.7. Mutual inductance between two loops

$$V_2 = -\frac{d\Psi_2}{dt} = -\frac{d}{dt} \int B(I_1) ds_2 \quad (2.15)$$

Circuit representation of mutual coupling is shown in Figure 2.8;

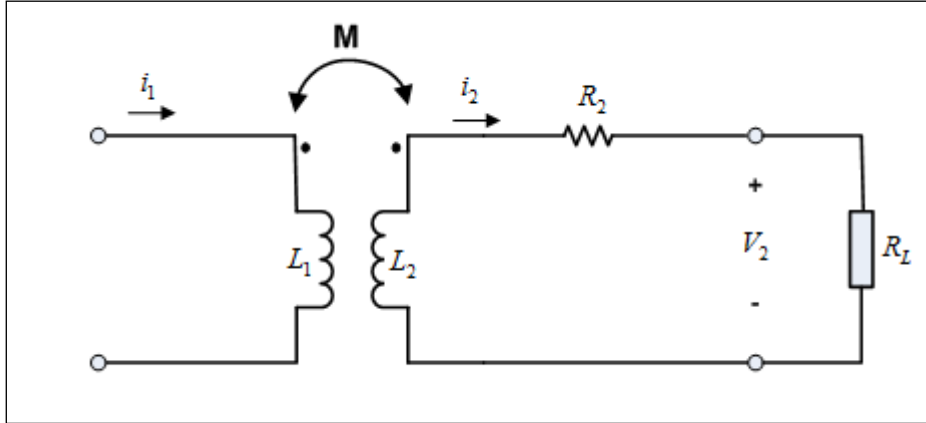


Figure 2.8. Circuit representation of two loops

$$V_2 = \frac{d\Psi_2}{dt} = M \frac{di_1}{dt} - L_2 \frac{di_2}{dt} - i_2 R_2 \quad (2.16)$$

In phasor representation;

$$\mathbf{V}_2 = j\omega M i_1 - j\omega L_2 i_2 - i_2 R_2 \quad (2.17)$$

$$\mathbf{V}_2 = \frac{j\omega M i_1}{1 + \frac{j\omega L_2 + R_2}{R_L}} \quad (2.18)$$

In (2.18), when R_L goes to ∞ , which is open circuit situation, $\mathbf{V}_2 = j\omega M i_1$ and when R_L goes to 0, which is short circuit situation, $\mathbf{V}_2 = 0$.

Hence, by changing R_L it is possible to change impedance seen at coil 1. Circuit representation with R_L being replaced by tag-IC impedance is shown in Figure 2.9;

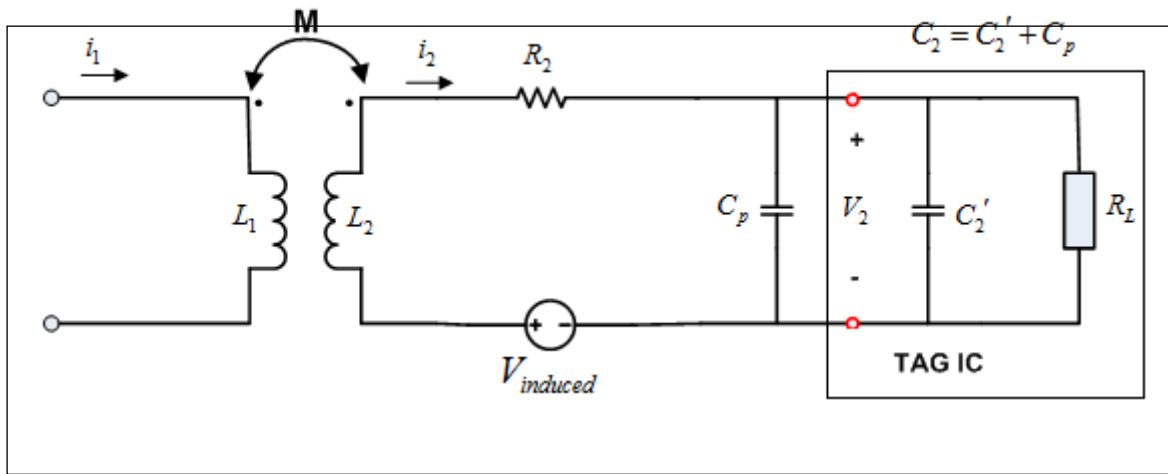


Figure 2.9. Mutual inductance between reader and tag IC

If $f_0 = \frac{1}{2\pi\sqrt{L_2 C_2}}$, which is the resonant case, required tag voltage is calculated as;

$$C_2' = \frac{1}{(2\pi f_0)^2 L_2} - C_p \quad (2.19)$$

$$\mathbf{V}_2 = \frac{\mathbf{V}_{\text{ind}}}{1 + (j\omega L_2 + R_2) \left(\frac{1}{R_L} + j\omega C_2 \right)} \quad (2.20)$$

$$\mathbf{V}_{\text{ind}} = j\omega M i_1 = j\omega k \sqrt{L_1 L_2} i_1 \quad (2.21)$$

$$\mathbf{V}_2 = \frac{j\omega M i_1}{1 + (j\omega L_2 + R_2) \left(\frac{1}{R_L} + j\omega C_2 \right)} \quad (2.22)$$

$$|\mathbf{V}_2| = \frac{\omega k \sqrt{L_1 L_2} i_1}{\left[\left(\frac{\omega L_2}{R_L} + \omega R_2 C_2 \right)^2 + \left(1 - \omega^2 L_2 C_2 + \frac{R_2}{R_L} \right)^2 \right]^{1/2}} \quad (2.23)$$

Quality factor is;

$$Q = \frac{1}{R_2 \sqrt{\frac{C_2}{L_2} + \frac{1}{R_L} \sqrt{\frac{L_2}{C_2}}}} = \frac{1}{\frac{R_2}{\omega L_2} + \frac{\omega L_2}{R_L}} \quad (2.24)$$

A closer look to the quality factor will help choosing L_2 ;

$$\frac{dQ}{dL_2} = \frac{d}{dL_2} \left(\frac{\omega R_L L_2}{R_2 R_L + \omega^2 L_2^2} \right) = 0 \quad (2.25)$$

$$= \frac{\omega R_L}{R_2 R_L + (\omega L_2)^2} - \frac{\omega R_L L_2 2(\omega L_2) \omega}{(R_2 R_L + (\omega L_2)^2)^2} = 0 \quad (2.26)$$

$$R_2 R_L + (\omega L_2)^2 - 2\omega^2 L_2^2 = 0 \quad (2.27)$$

$$(\omega L_2^2) = \frac{R_2 R_L}{3} \rightarrow L_2 = \frac{1}{\omega} \sqrt{\frac{R_2 R_L}{3}} \quad (2.28)$$

Thus, for every (R_L and R_2) there is a L_2 value which would maximize Q . Usually R_2 is fixed, therefore, R_L determines the energy transfer.

If we have L_2 constant, what the optimal value of R_L for maximum Q can also be found. Let's look at quality factor, Q . We consider the circuit in Figure 2.10;

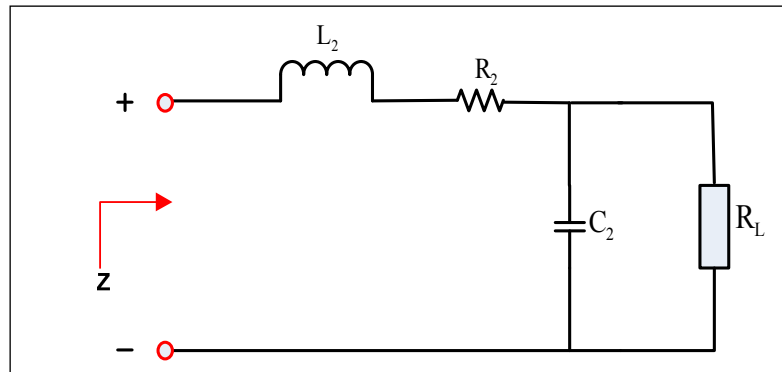


Figure 2.10. Quality factor of RLC circuit

Since $\omega = \frac{1}{\sqrt{L_2 C_2}}$, (2.24) can also be written as;

$$Q = \frac{1}{\frac{R_2}{\omega L_2} + \frac{\omega L_2}{R_L}} = \frac{\omega R_L R_2}{R_L R_2 + \omega^2 L_2^2} \quad (2.29)$$

It is observed that, Q is linear in R_L . When R_L goes to ∞ , $Q = \omega / R_2$ and when R_L goes zero, Q becomes zero.

In Figure 2.11, reader-tag system equivalent circuit and in Figure 2.12 equivalent circuits of a reader antenna are shown;

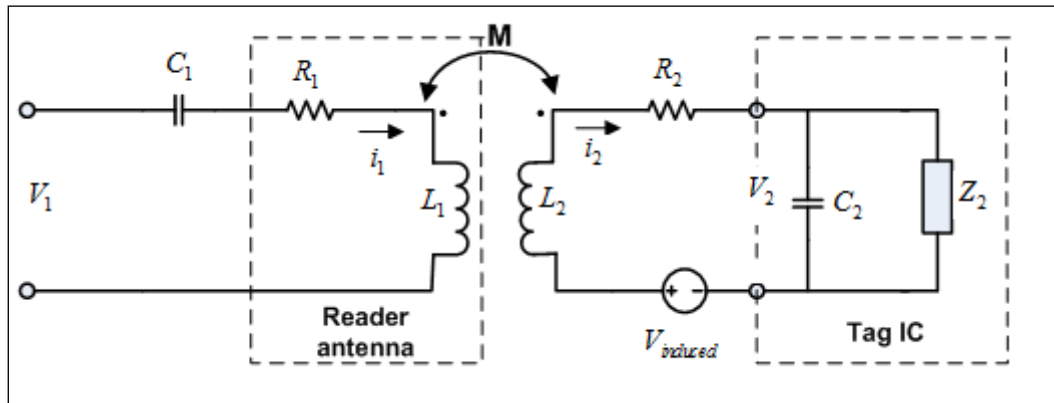


Figure 2.11. Equivalent circuit of a reader-tag system

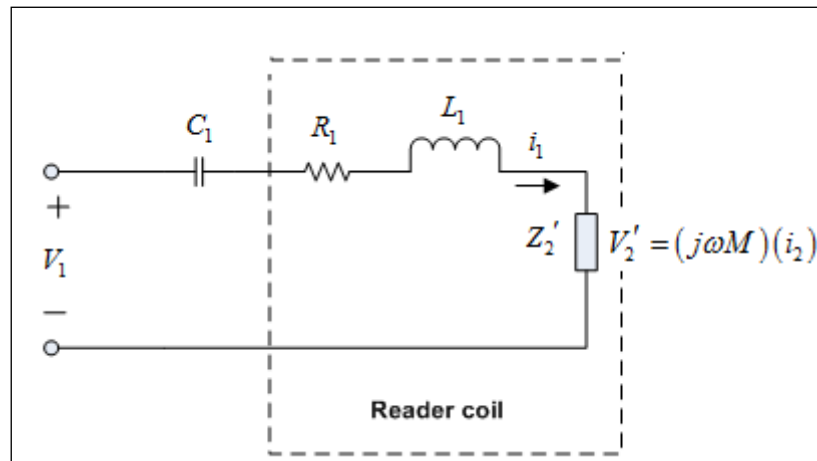


Figure 2.12. Equivalent circuit of reader side

If we want to find the value for V_1 ;

$$V_1 = \frac{i_1}{j\omega C_1} + i_1 R_1 + j\omega L_1 i_1 - j\omega M i_2 \quad (2.30)$$

If the system is at resonant at reader side,

$$V_1 = i_1 R_1 - j\omega M i_2 \quad (2.31)$$

$$i_2 = \frac{V_{\text{ind}}}{R_2 + j\omega L_2 + Z_2} \quad \text{and } V_{\text{ind}} = j\omega M i_1 \quad (2.32)$$

$$i_2 = \frac{j\omega M i_1}{R_2 + j\omega L_2 + Z_2} \quad (2.33)$$

$$V_1 = i_1 R_1 - j\omega M \frac{j\omega M i_1}{R_2 + j\omega L_2 + Z_2} = i_1 R_1 + \frac{\omega^2 k^2 L_1 L_2}{R_2 + j\omega L_2 + Z_2} i_1 \quad (2.34)$$

So Z_2' can be given as;

$$Z_2' = \frac{\omega^2 k^2 L_1 L_2}{R_2 + j\omega L_2 + Z_2} = \frac{\omega^2 k^2 L_1 L_2}{R_2 + j\omega L_2 + \frac{R_L}{1 + j\omega R_L C_2}} \quad (2.35)$$

Increasing R_L causes a decrease on load current and increases Z_2' . Also when R_L increases, Q increases.

Let's consider two situations:

a.) When R_L goes to 0,

$$Z_2' = \frac{\omega^2 k^2 L_1 L_2}{R_2 + j\omega L_2} \quad (2.36)$$

b.) When R_L goes to ∞ ,

$$Z_2' = \frac{\omega^2 k^2 L_1 L_2}{R_2 + j\omega L_2 + \frac{1}{j\omega C_2}} \quad (2.37)$$

To modulate Z_2' , one can either need to change R_L or change C_2 as shown in Figure 2.13;

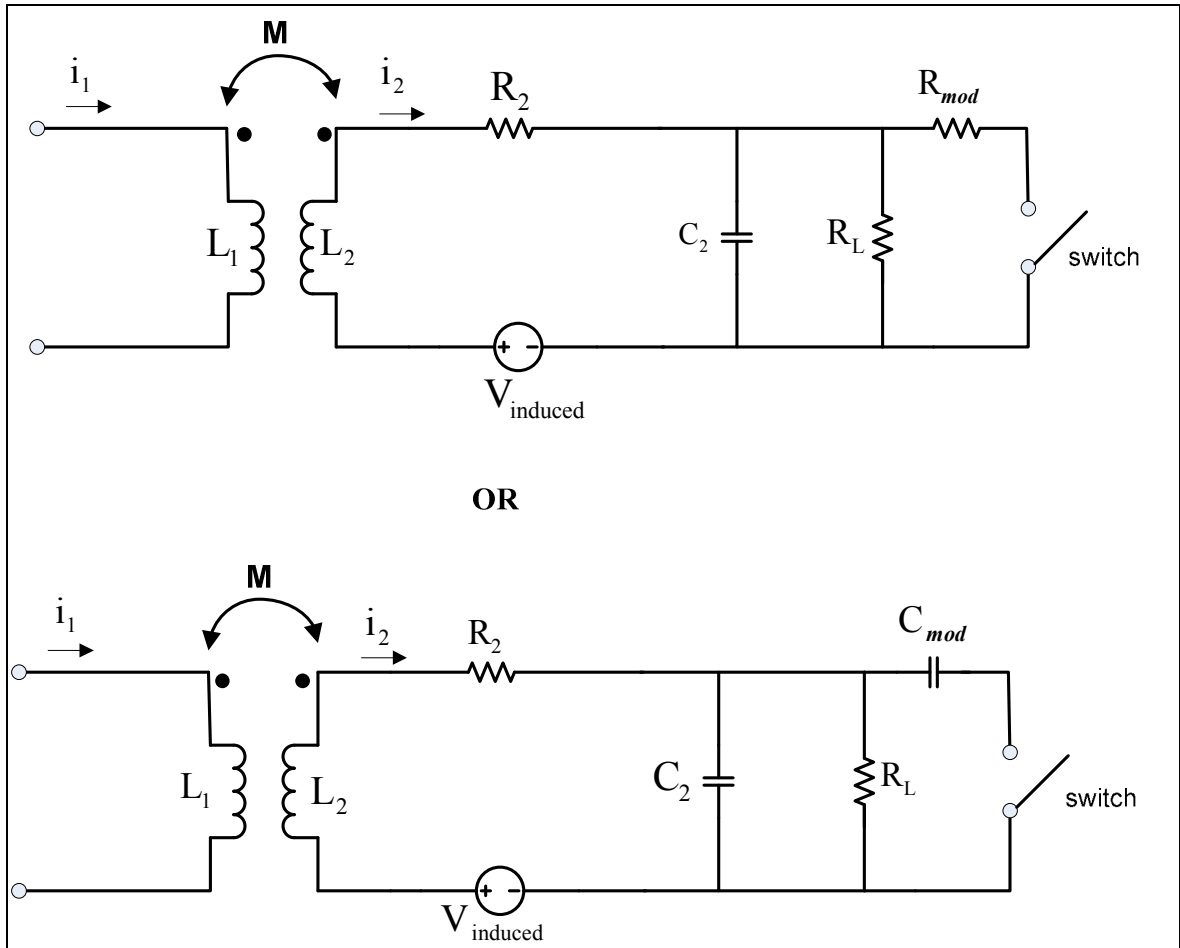


Figure 2.13. Modulation of load impedance

Changing R_L ; also called *ohmic load modulation* produces $Z_2'(R_L)$ and $Z_2'(R_L // R_{mod})$ switching between C_2 and $C_2 + C_{mod}$ creates two resonant frequencies at the transponder and at the reader side.

Load modulation can also be controlled by a subcarrier frequency which is normally 842 KHz or 423 KHz or 212 KHz away from the resonant frequency.

The magnetic field intensity can be expressed in terms of V_2 , N_2 , and S_2 (tag coil area) as;

$$|H_0| = \frac{V_2 \left[\left(\frac{\omega L_2}{R_L} + \omega R_2 C_2 \right)^2 + \left(1 - \omega^2 L_2 C_2 + \frac{R_2}{R_L} \right)^2 \right]^{1/2}}{\omega \mu_0 S_2 N_2} \quad (2.38)$$

Or using $\frac{1}{\omega_0^2} = L_2 C_2$ which is resonant case,

$$|H_0| = \frac{V_2 \left[\omega^2 \left(\frac{L_2}{R_L} + \frac{R_2}{\omega_0 L_2} \right)^2 + \left(\frac{\omega_0^2 - \omega^2}{\omega_0^2} + \frac{R_2}{R_L} \right)^2 \right]^{1/2}}{\omega \mu_0 S_2 N_2} \quad (2.39)$$

Therefore, V_2 can be expressed as,

$$V_2 = \omega \mu_0 |H_0| S_2 N_2 Q \quad (2.40)$$

where, the quality factor Q is given as,

$$Q = \frac{1}{R_2 \sqrt{\frac{C_2}{L_2} + \frac{1}{R_L} \sqrt{\frac{L_2}{C_2}}} = \frac{1}{\frac{R_2}{\omega L_2} + \frac{\omega L_2}{R_L}} \quad (2.41)$$

If $R_2=0$ at $\omega=\omega_0$, Q becomes,

$$\frac{1}{Q} = \frac{\omega_0 L_2}{R_L} \text{ and } Q = \frac{R_L}{\omega_0 L_2} = R_L \sqrt{\frac{C}{L_2}} \quad (2.42)$$

and V_2 can be expressed as,

$$V_2 = \omega \mu_0 |H_0| S_2 N_2 \left(R_L \sqrt{\frac{C}{L_2}} \right) \quad (2.43)$$

Hence, it can be said that if minimum operating voltage is known, then H_0 can be specified. In the example below, V_2 shows the minimum tag IC voltage, H_0 shows the required magnetic field intensity, N_2 shows the numbers of turns needed, S_2 shows the area of the tag, Q shows the quality factor, ω shows angular frequency and μ_0 shows permeability of free space.

We assume that the tag size is given as $86 \times 60 \text{ mm} = 5.16 \times 10^{-3} \text{ m}^2$

$$\omega = 2\pi f_0 = 2\pi(13.56 \times 10^6) \quad (\text{rad} / \text{s})$$

$$N_2 = 4 \text{ turns}$$

$$Q \cong 40$$

$$V_2 \cong 2V$$

$$|H_0| = 22.6 \text{ mA} / \text{m}$$

Another important criterion for HF system is the tag orientation relative to the incoming magnetic field intensity, H . Figure 2.14 shows a typical tag orientation;

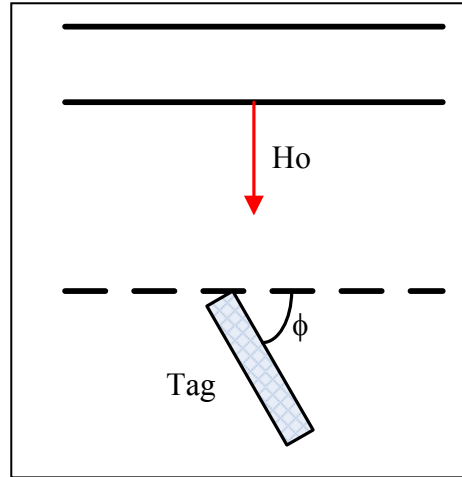


Figure 2.14. Importance of tag orientation relative to H

In the Figure 2.14, it is obvious that only $H_0 \cos \phi$ is able to induce voltage at the tag. So, ampere-turns can be defined according to $H_0 \cos \phi$;

$$N_1 I_1 = \frac{2H_0 \cos \phi (b^2 + R^2)^{3/2}}{a^2} \quad (2.44)$$

Hence, steps for the design can be summarized as follow;

- 1.) Determine the minimum required tag IC voltage V_2 .
- 2.) From V_2 determine the required magnetic field intensity H_0 for given V_2 , S_2 , N_2 , Q and ω .
- 3.) From minimum H_0 , determine N_1, I_1 for given distance R . Use 3D EM solver such as FEKO to get exact field quantity.

4.) Check the magnetic field created by the reader if it satisfies the regulatory limits at $R=0$ (should not exceed $42 \text{ dB}\mu\text{A}/\text{m}$) and at $R=10\text{m}$ (should not exceed $134 \text{ dB}\mu\text{A}/\text{m}$). This completes the design of HF tag reader system.

3. DUAL BAND (HF/UHF) PASSIVE RFID TAG ANTENNA DESIGN

In the previous sections; basic system information, frequency ranges and limitations for RFID and HF/UHF RFID system design principles are discussed. In this section, design specifications of HF and UHF antennas, then, design steps of Dual Band Passive RFID Tag is given with; a) antenna design and modeling, b) prototyping which includes realization steps and lastly c) measurement results

3.1. DESIGN SPECIFICATIONS OF DUAL BAND DESIGN

3.1.1. Design Specifications of HF antenna

Table 3.1. HF Design Specifications of dual-band tag

| Quantity | Typical | Target |
|------------------------|----------------------------------------|---------------------------------------------------------|
| Inductance | $2-3 \mu H$ | $2-3 \mu H$ |
| Communication standard | ISO 15693, ISO 14443 | ISO 15693 |
| Dimensions | $75 \times 85 \text{ mm} (L \times W)$ | $94 \times 94 \text{ mm} (L \times W)$ due to dual band |
| Operating Frequency | 13.56 MHz | 13.56 MHz |
| Structure | rectangular, square and round | Rectangular or square |

3.1.2. Design Specifications of UHF antenna

Table 3.2. UHF Design Specifications of dual-band tag

| Quantity | Typical | Required |
|---------------------|-------------------------------------------------|------------------------------|
| Input impedance | $(20 - 100) + j(100 - 250) \Omega$ | $35 + j165\Omega$ |
| Structure | rectangular, square | square |
| Gain Performance | $0 - 2.5 \text{ dBi}$ | 3 dBi |
| Efficiency | $55 - 70 \%$ | $\geq 60 \%$ |
| Operating frequency | 865 - 871 MHz in Europe and 918 - 925 MHz in US | 861 - 871 MHz with 10 MHz BW |

3.2. ANTENNA DESIGN AND MODELING

This section covers the antenna design and modeling. First, steps in the design and modeling UHF part of the dual band passive tag antenna are presented. Then, design and modeling steps of HF part are detailed. Last, dual band passive RFID is presented.

3.2.1. UHF Antenna Design and Modeling

Dual band passive RFID tag design starts with the design of UHF antenna since it is more difficult to design UHF part compared to HF part.

Dipole-like structures get easily affected from environment. There is no isolation between antenna structure and the environment. Thus, we used microstrip patch antenna with antenna ground which electromagnetically isolates the antenna itself from the environment while preserving critical performance parameters such as gain and tag impedance.

Designed UHF antenna should operate at 868 MHz frequency band that is the frequency band used by UHF RFID Tags within Europe. Before achieving the latest design, thickness of 1.57 mm is used for the dielectric substrate with a dielectric constant of 6.15 to design the tag antenna. After performing measurements, we observed that gain performance for the initial design was not adequate. We used Taconic RF 43 dielectric material which has dielectric constant of 4.3 with having loss factor of 0.0033. Taconic RF 43 dielectric material has a much less loss factor compared to FR4, which is typically used for PCB construction. In our design, a thickness of 3.18 mm is chosen to achieve high radiation efficiency.

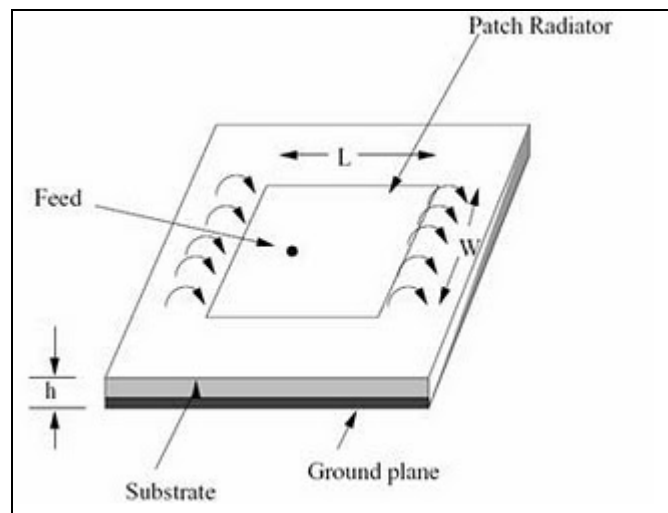


Figure 3.1. Patch antenna [19]

3.2.1.1. Calculation of Patch antenna width

First step for designing UHF antenna is to calculate the width of the patch antenna as shown in Figure 3.1. The width of patch is calculated as [19];

$$W = \frac{c}{2f_0 \sqrt{\left(\frac{\epsilon_r + 1}{2}\right)}} \quad (3.1)$$

In (3.1), c is the speed of light, f_0 is the frequency of operation for designed antenna and ϵ_r is the dielectric constant of the substrate.

3.2.1.2. Calculation of effective dielectric constant

Effective dielectric constant is calculated as [19] ;

$$\epsilon_{effective} = \frac{\epsilon_r + 1}{2} + \frac{\epsilon_r - 1}{2} \left[1 + 12 \frac{h}{W} \right]^{-\frac{1}{2}} \quad (3.2)$$

In (3.2), h is the height of dielectric substrate and W is the width of the patch. If all variables are substituted in (3.2), effective dielectric constant for initial design is found as 5.921.

3.2.1.3. Calculation of effective length

After calculating both effective dielectric constant and width of patch, we calculate effective length of the patch as [19].

$$L_{effective} = \frac{c}{2f_0 \sqrt{\epsilon_{effective}}} \quad (3.3)$$

If all variables are substituted to (3.3), effective length is found as 71.03 mm.

3.2.1.4. Calculation of length extension

The fringing fields along the width are modeled as radiating slots. This fringing field effect causes microstrip antenna look greater than its physical size. This length difference is called “length extension” and denoted by ΔL . The length extension can be calculated as [19]

$$\Delta L = 0.412h \frac{(\epsilon_{effective} + 0.3) \left(\frac{W}{h} + 0.264 \right)}{(\epsilon_{effective} - 0.258) \left(\frac{W}{h} + 0.8 \right)} \quad (3.4)$$

Using (3.4), length extension is calculated as 0.701 mm.

3.2.1.5. Calculation of actual length of the patch antenna

The actual length of the patch (L) is calculated as [19] ;

$$L=L_{\text{effective}}-2\Delta L \quad (3.5)$$

If all variables are substituted in (3.5), actual patch length is found as 70.329 mm.

3.2.1.6. Calculation of the ground plane dimensions

All the expressions given previously are used to calculate dimensions for the patch antenna itself. But to achieve full antenna structure ground plane size should be defined. The ground plane dimension, which is required for the whole structure is given as [19];

$$\begin{aligned} L_{\text{ground}} &= 6h + L \\ W_{\text{ground}} &= 6h + W \end{aligned} \quad (3.6)$$

L_{ground} is calculated as 79.75 mm and W_{ground} is calculated 100.81 mm. All the dimensions calculated here are used as a starting point for the design. After some modifications, the size of the antenna is achieved. At the end, tag antenna which has dimensions of 84x84 mm² is formed with substrate thickness 1.57 mm. Figure 3.2 shows the dimensions of initial design;

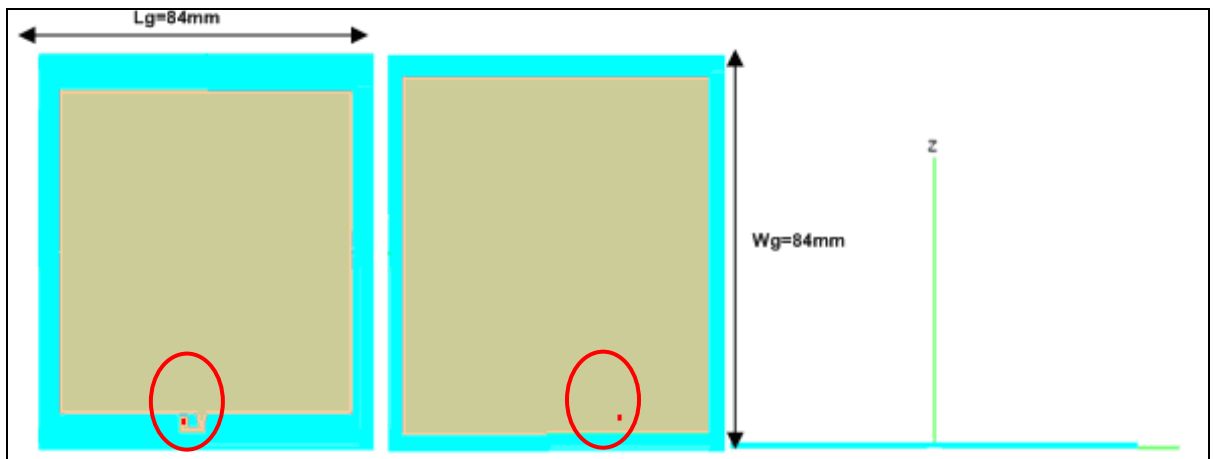


Figure 3.2. Dimensions of initial design

With simulations, we achieved to have a complex impedance of $9+j85 \Omega$ and gain of 0.82 dBi with a radiation efficiency of 38%.

As it is seen that the initial design might be acceptable in terms of input impedance, but it fails gain and radiation efficiency specifications. To improve the gain, we used crossed slot in the ground [24]. Cross slot is also used to reduce patch dimensions.

In our design, cross slot is used in right hand side of the center of the ground. This point is achieved via simulations. Figure 3.3 shows the cross slot grounded tag design for thickness of 1.57 mm.

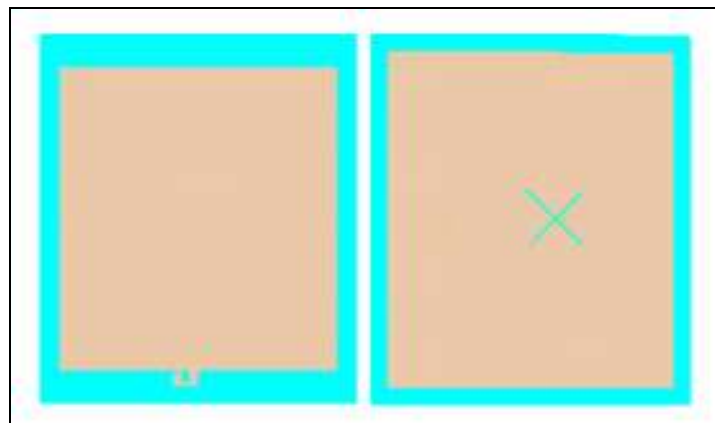


Figure 3.3. Cross slotted ground design for thickness 1.57mm

We observed that we did not meet the radiation efficiency specifications with $h=1.57$ mm thickness. Therefore, we decided to use a thicker substrate Taconic RF 43 dielectric material, which has dielectric constant of 4.3 with dielectric loss of 0.0033 for the new design. The thickness of the substrate is increased to 3.175 mm.

Width of the patch (W) is calculated as 106.15 mm, $L_{effective}$ is calculated as 85.712 mm, and the actual length of the patch (L) is found to be 82.759 mm through simulations with substrate thickness of 3.175 mm. Using (3.6), L_{ground} is calculated as 101.809 mm and W_{ground} is found to be 125.2 mm. After performing several modifications and optimizations, latest dimensions are found as 94×94 mm² ($L \times W$) with 3.175 mm thickness.

After UHF antenna design, we added multiturn spirals to the design to achieve HF operation.

3.2.2. HF Antenna design and modeling

As a starting point, HF antenna is designed in free space. We used 5 turns of spirals in the design to meet design specifications. The approximate inductance value of 5 turns of spiral can be calculated analytically. The approximate inductance of a spiral with rectangular shape is given as [20];

$$L \cong N^2 \frac{\mu_0 \mu_r}{\pi} \left[-2(W+L) + 2\sqrt{L^2 + W^2} - L \ln \left(\frac{L + \sqrt{L^2 + W^2}}{W} \right) - W \ln \left(\frac{W + \sqrt{L^2 + W^2}}{L} \right) + L \ln \left(\frac{2W}{a} \right) + W \ln \left(\frac{2L}{a} \right) \right] \quad (3.7)$$

In (3.7), “ N ” is the number of spiral turns, “ W ” is the width of spiral, L indicates the length of spiral, “ a ” is the wire radius, μ_0 is permeability of free space and μ_r is the relative permeability of the medium. Figure 3.4 shows the design parameters.

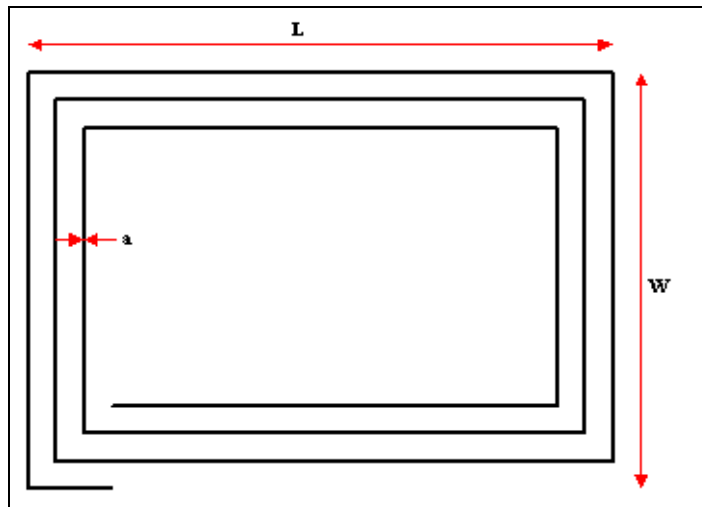


Figure 3.4. Variables used in (3.7)

Inductance value of pure rectangular shape 5-turns spiral is theoretically calculated as $7.76 \mu\text{H}$ using (3.7). Figure 3.5 shows the HF antenna that is implemented on upper and lower parts of the dielectric substrate.

In Figure 3.5, there are total 5 turns of spirals. The spiral on top side is shown with red line and the other remaining four spirals that are located on bottom are shown with black lines. In the same figure, separation between lines is given as 0.3 mm, and the width of each spiral used in model is given 0.5 mm. Two vias are used to connect top spiral to bottom spiral which are given with black circles in the same figure. One of the vias, the one which is close to "+" side of the Tag IC is used to feed HF antenna, HF antenna feed direction is given from "-" to "+".

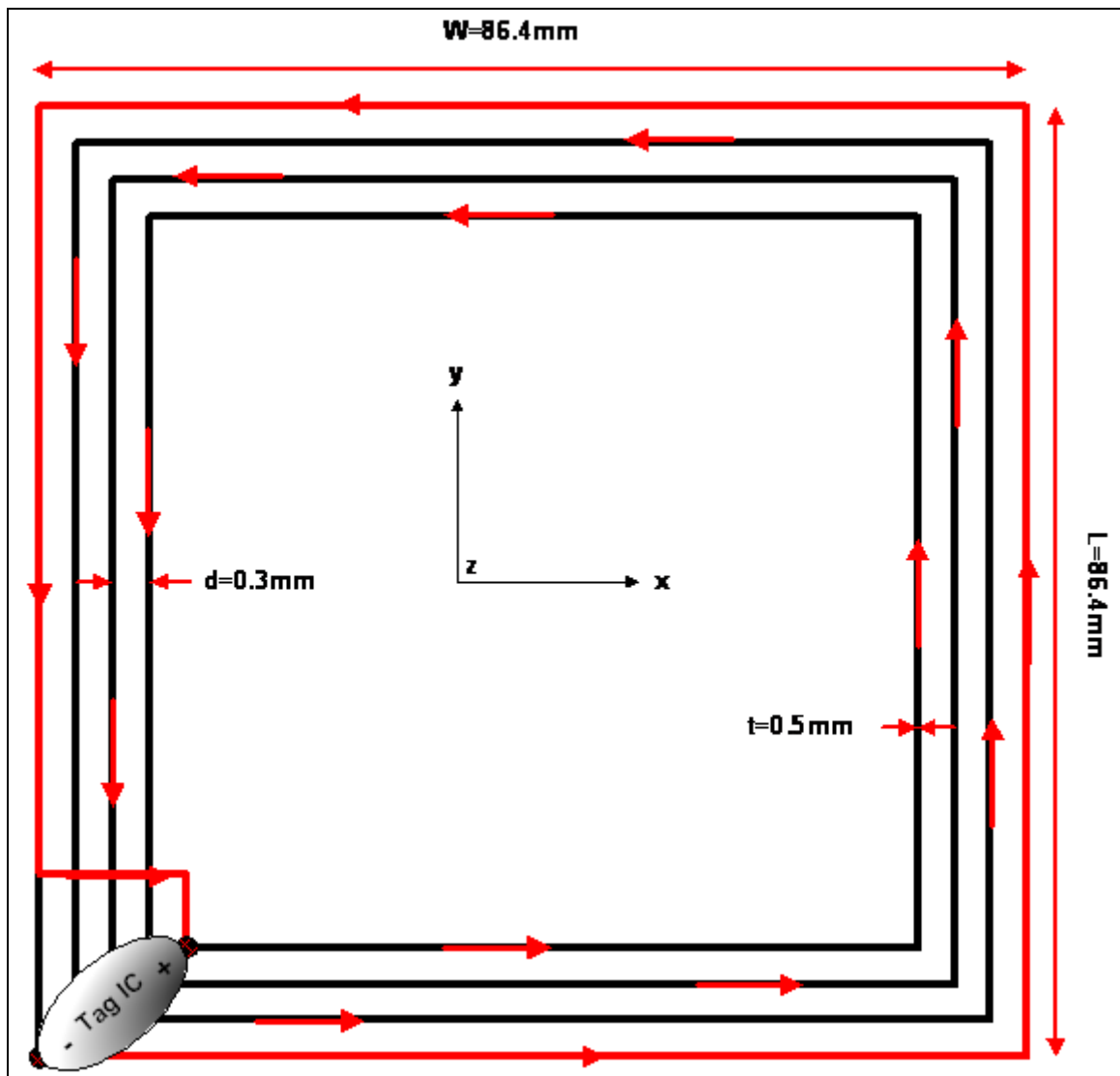


Figure 3.5. HF antenna model

HF antenna is modeled using FEKO. Firstly, HF antenna in free space is modeled, and then, HF antenna on dielectric substrate is simulated. Figure 3.6 shows the FEKO figure for the HF antenna in free space;

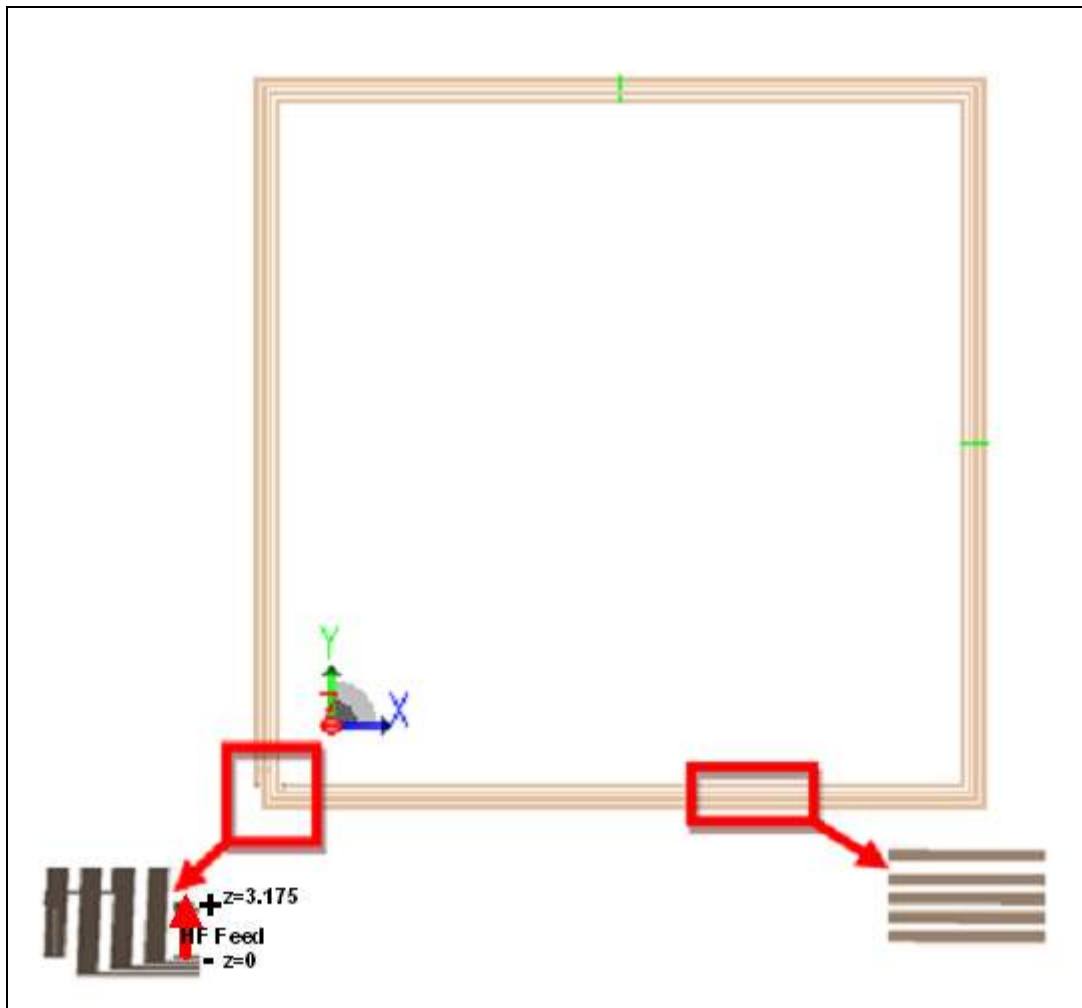


Figure 3.6. Pure HF antenna designed in FEKO

Inductance value of $7.73 \mu\text{H}$ is obtained for pure HF antenna in free space at 13.56 MHz with simulation. The inductance value for a pure HF antenna in free space was theoretically calculated as $7.76 \mu\text{H}$ using (3.7). Before performing final HF tag design, HF antenna with degenerated ground plane on bottom side and patch antenna on top side is designed. Comparative results for HF inductance are given in Table 3.3;

Table 3.3. Comparative inductance values of HF antenna

| Theoretical | HF antenna in air (FEKO) | HF antenna with ground plane added (FEKO) | HF antenna with upper and bottom metalizations (FEKO) | HF antenna with substrate (FEKO) |
|--------------------|--------------------------|-------------------------------------------|-------------------------------------------------------|----------------------------------|
| 7.76 μH | 7.73 μH | 6.78 μH | 6.76 μH | 3.37 μH |

3.2.3. Combination of HF and UHF Antenna

The design is given in Figures 3.7 and 3.8. Figure 3.7 shows the top and side views, and Figure 3.8 shows the bottom view of the latest design;

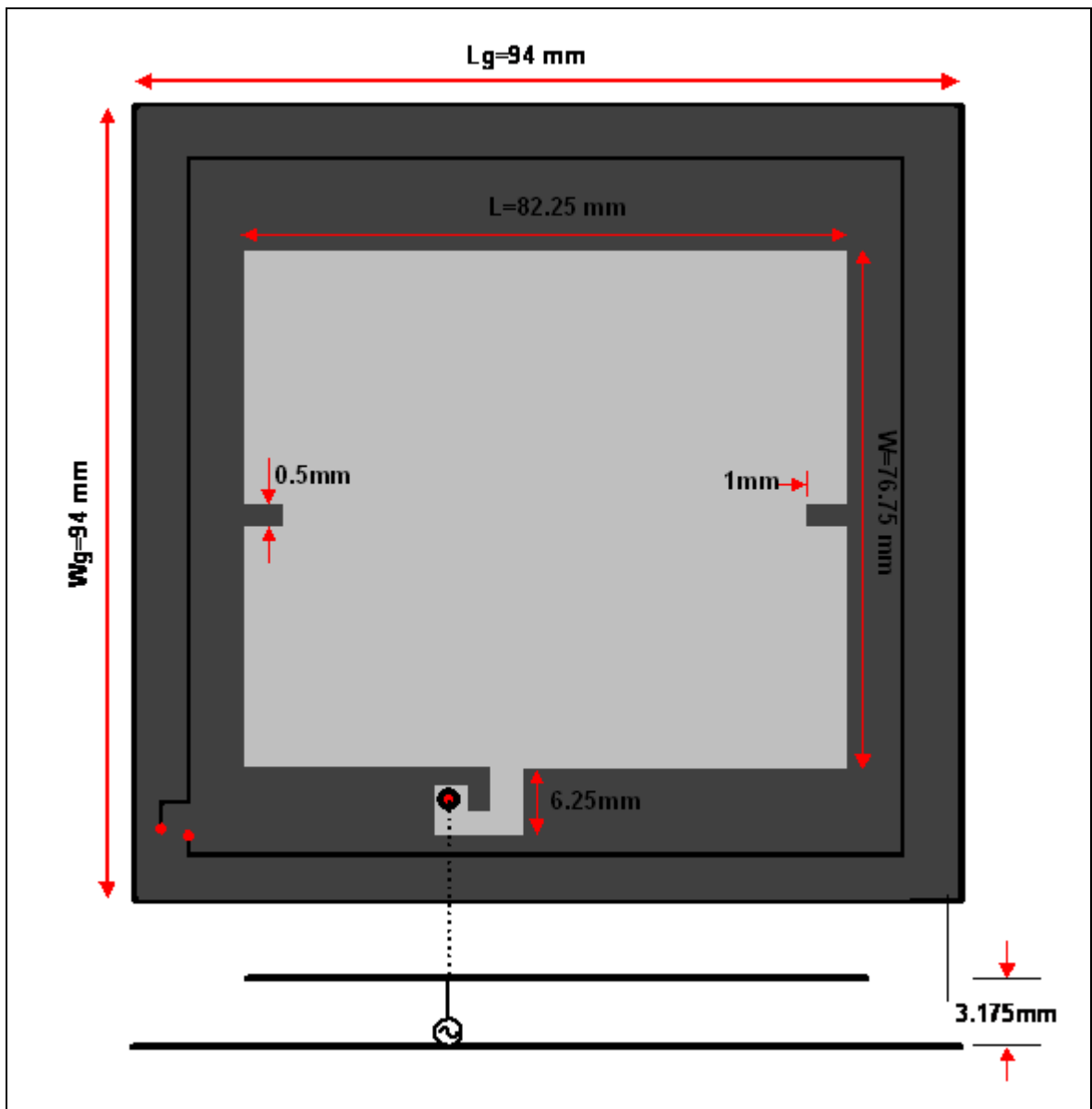


Figure 3.7. Top and side views of latest design with dimensions

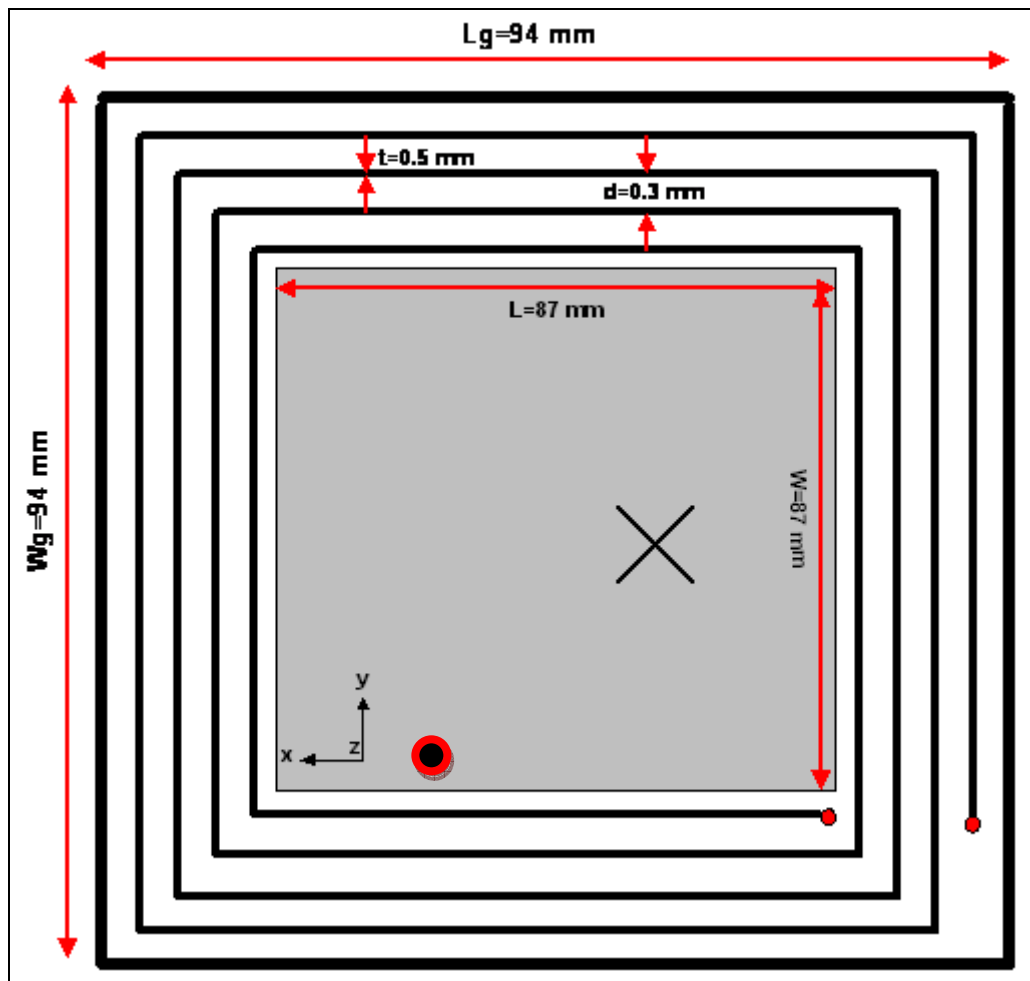


Figure 3.8. Bottom view of latest design with dimensions

Another critical point for the design is choosing appropriate point for the feed. In Figure 3.8, UHF feed is shown with red circle. The mid-edge of the ground plane is taken as the starting point for feed point. The feed point is varied in simulations to meet the target impedance. Table 3.4 shows the effect of moving feed point for the design;

Table 3.4. Effect of moving feed point

| Feed point at center of the edge | Feed is moved right | Feed is moved left |
|----------------------------------|---------------------|--------------------|
| $17+j126 \Omega$ | $8+j97 \Omega$ | $30+j159 \Omega$ |

Feed point which is already set to left-side of the mid-edge is moved towards, inwards to increase the gain. On the bottom side, degenerated ground is used. Degenerated ground is achieved via adding a cross slot.

Patch antenna dimensions are given as 82.25 mm along x-axis and 76.75 mm along y-axis as shown in Figure 3.7. Three vias used for the design; one of them is used to the feed UHF and one of them is used to feed HF part, whereas, third via helps to connect upper spirals to bottom spirals. On the right and left side of the patch antenna as shown also in Figure 3.7, two notches with length of 1 mm along x-direction and width of 0.5 mm along y-direction are to achieve better antenna and impedance performance, in addition to reduced antenna size. Figure 3.9 shows the different views of FEKO model;

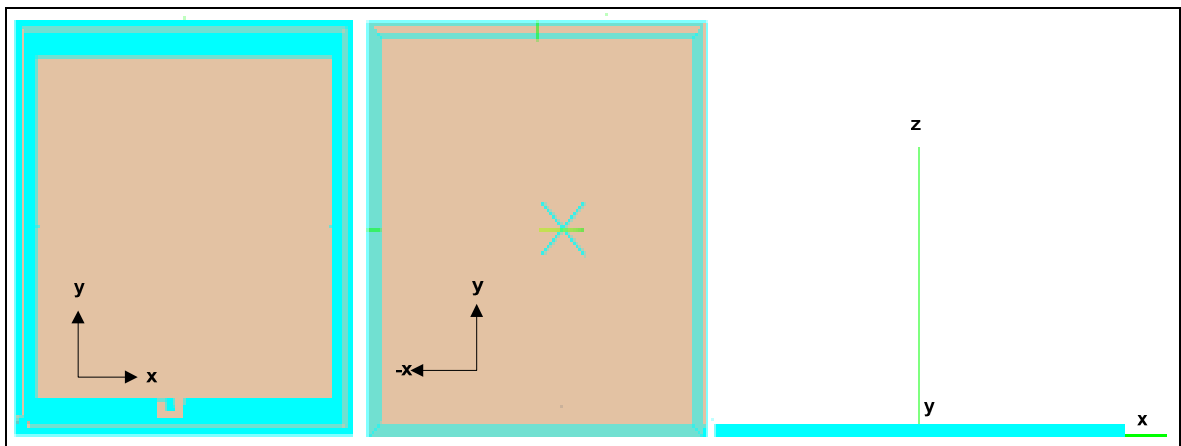


Figure 3.9. Different views of FEKO model

Simulations are performed on impedance and gain. The design achieves a impedance of $35.12 + j161.87 \Omega$ at 868 MHz, UHF Band. Figure 3.10 (a) and (b) shows the real and imaginary part of the impedance with frequency;

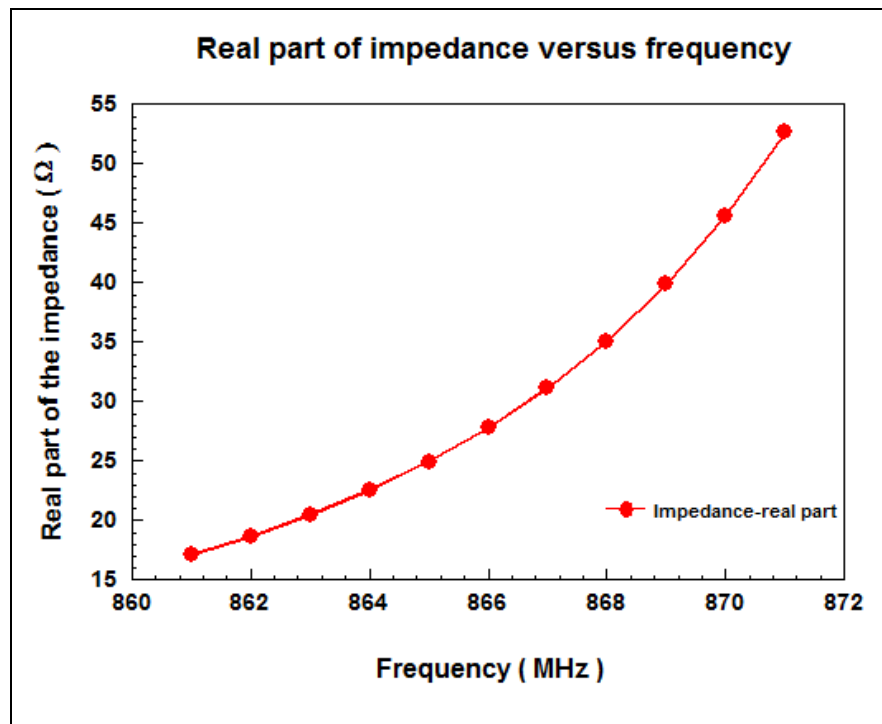


Figure 3.10.a) Real part of impedance versus frequency for designed antenna in free space

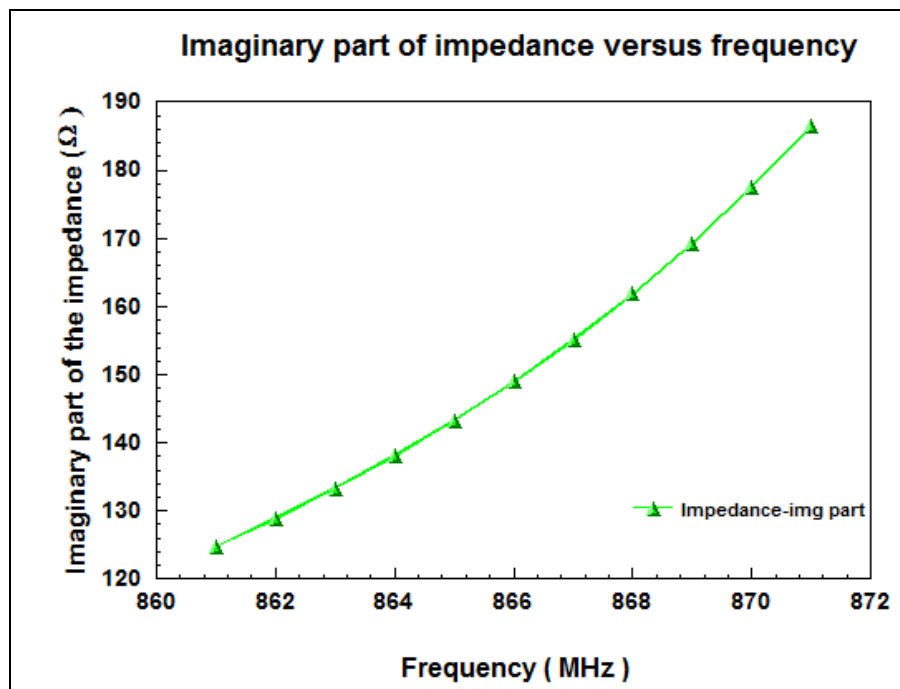


Figure 3.10.b) Imaginary part of the impedance versus frequency for designed antenna in free space

In Figure 3.10 (a), it is seen that real part of the impedance increases from 861-871 MHz band. It is aimed to match this impedance to tag IC impedance. Simulation of real part impedance shows that modeled antenna fits the real part of the tag IC impedance which is between $25\text{-}50\ \Omega$, depending on the manufacturer of the IC. As it is known that the chip impedance has negative imaginary part. Hence it is necessary to have positive imaginary part for the input impedance of the tag antenna.

The imaginary part of impedance versus frequency is given in Figure 3.10 (b). Our target chip impedance has imaginary part between $-j125\ \Omega$ to $-j165\ \Omega$. Our design achieves an imaginary part of $j161.87\ \Omega$.

In our simulations, we obtained 2.68 dBi gain with a radiation efficiency of 66.41% at 868 MHz. Gain change with frequency is given in Figure 3.11.

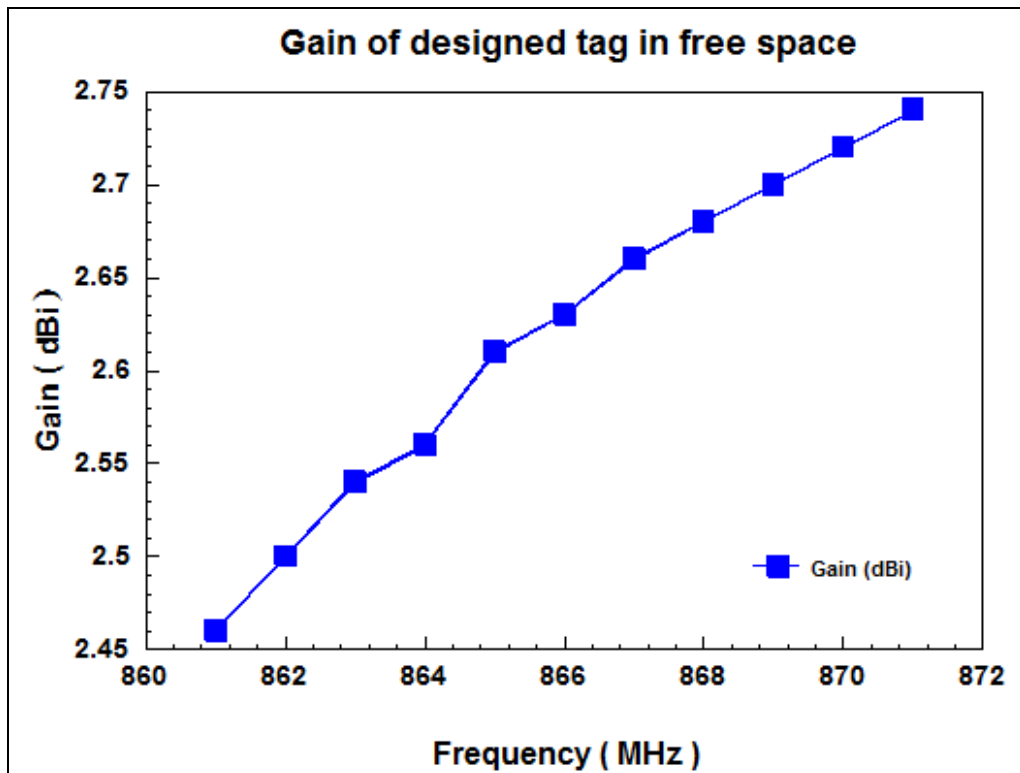


Figure 3.11. Gain versus frequency for designed tag antenna in free space

Figure 3.12 shows the azimuth gain at $\theta=0^\circ$, where θ refers to angle from broadside.

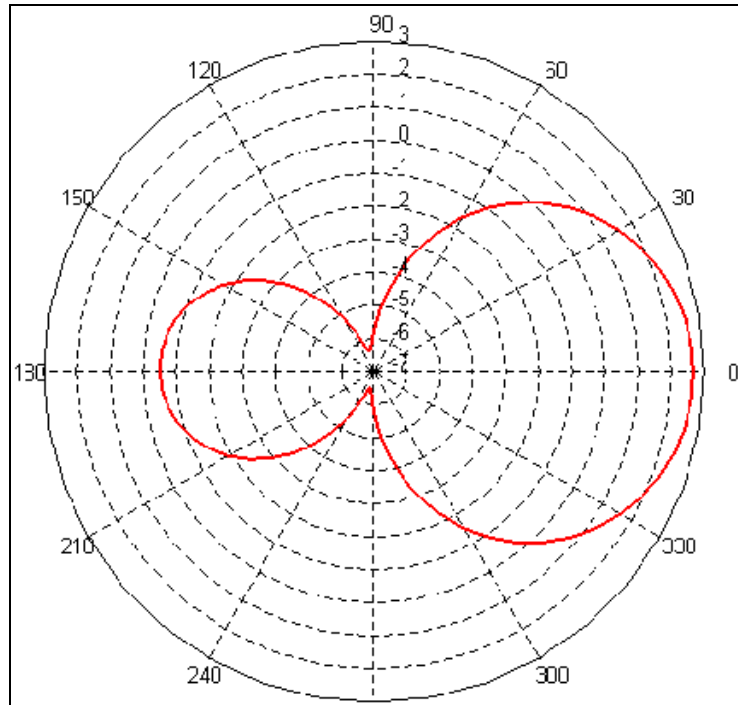


Figure 3.12. Gain of designed tag in free space when $\theta = 0$ changes with ϕ

Texas Instruments has a tag antenna design which operates between 860-960 MHz band. Texas Instrument's RI-UHF-STRAP 08 is taken as a benchmark to compare the performances of the designed tag antenna. Figure 3.13 shows the FEKO model of RI UHF STRAP 08. In free space, TI dipole antenna has input impedance of $28.81+j46.44 \Omega$ and gain of 1.89 dBi. Figure 3.14 (a) and (b) show how real and imaginary part of input impedance for TI dipole change with frequency;

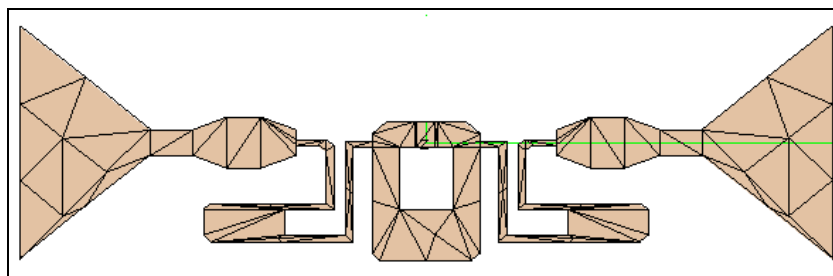


Figure 3.13 FEKO model of RI UHF STRAP 08

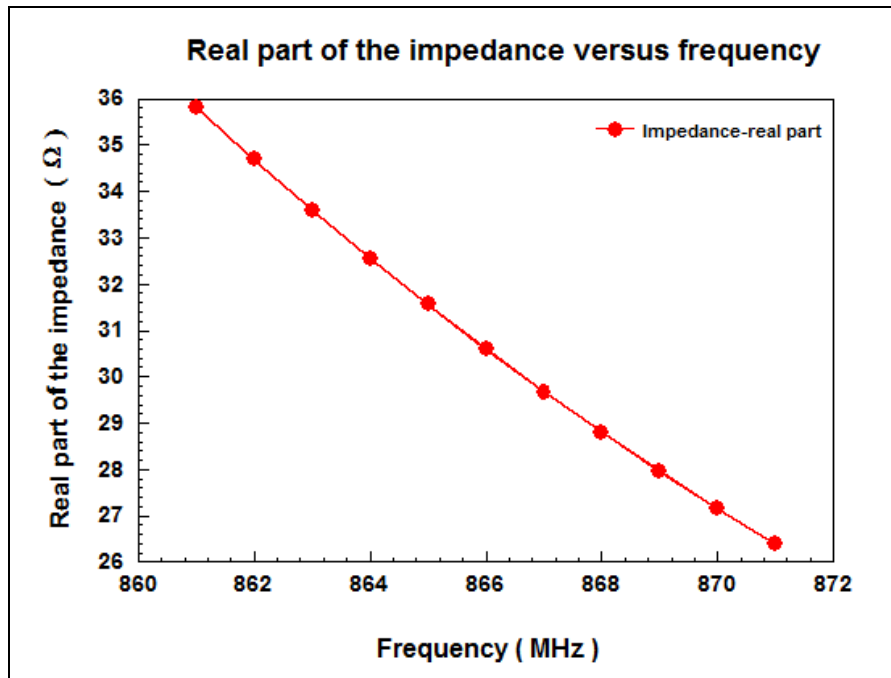


Figure 3.14.a) Real part of impedance versus frequency for the TI dipole antenna in free space

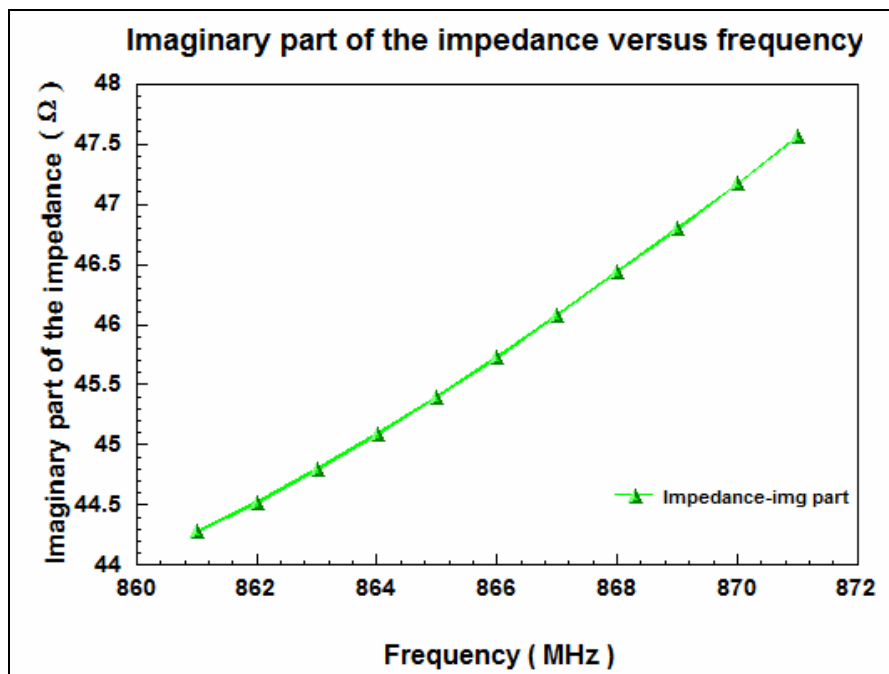


Figure 3.14.b) Imaginary part of the impedance versus frequency for the TI dipole antenna in free space

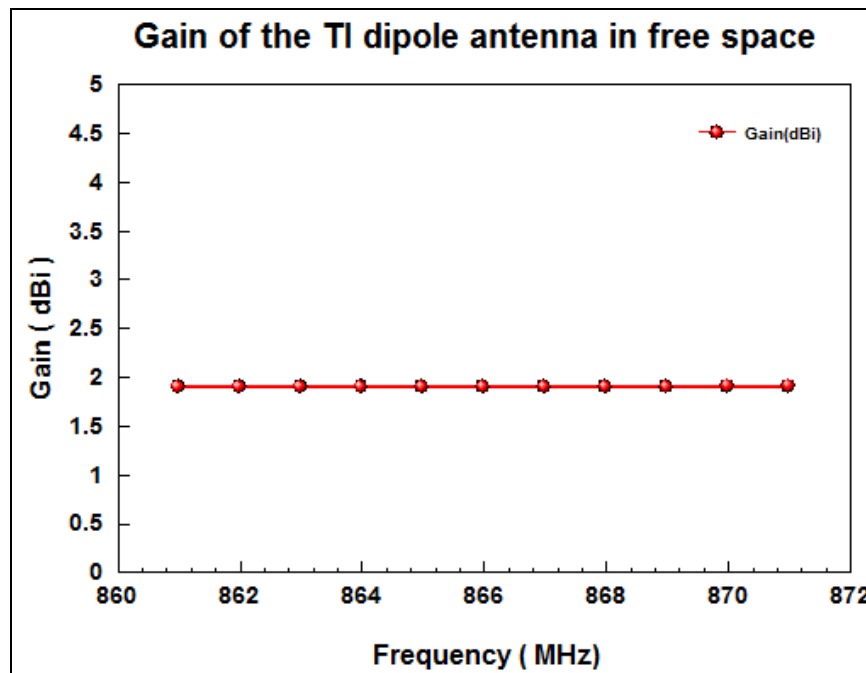


Figure 3.15. Gain versus frequency for TI dipole antenna in free space

3.3. EFFECT OF ENVIRONMENTAL CHANGES ON TAG ANTENNA

The antenna is modeled on metallic can to investigate the effects of on-metal performance. Then, the tag antenna is modeled on water carboy to investigate the effect of plastics, on antenna performance. In addition to the effects of metal and plastics, tag antenna is placed on wooden strip, and card box. In this section, results are compared to those of free space.

3.3.1. Modeling and Design of Tag Antenna on Metallic Can

Metallic can has a height of 35 cm and radius of 10 cm. In the Figure 3.16, there is a separation of 0.75 mm between the top of the can and the designed tag antenna. Figure 3.16 shows the tag antenna modeled on metallic can;

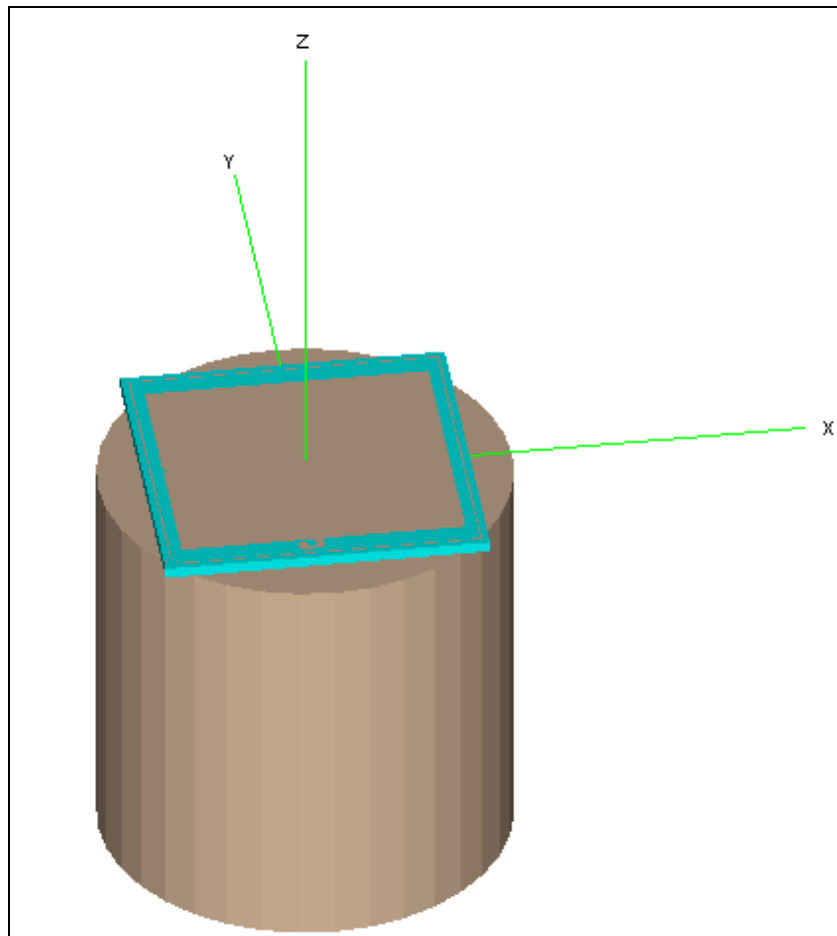


Figure 3.16. FEKO model of tag antenna on metallic can

Our designed antenna has an impedance of $35.73+j163.78 \Omega$ and gain 2.75 dBi when it is on metallic can. Figure 3.17 (a) and (b) shows the variation of real and imaginary parts of the impedance with different tag-to-metal separations;

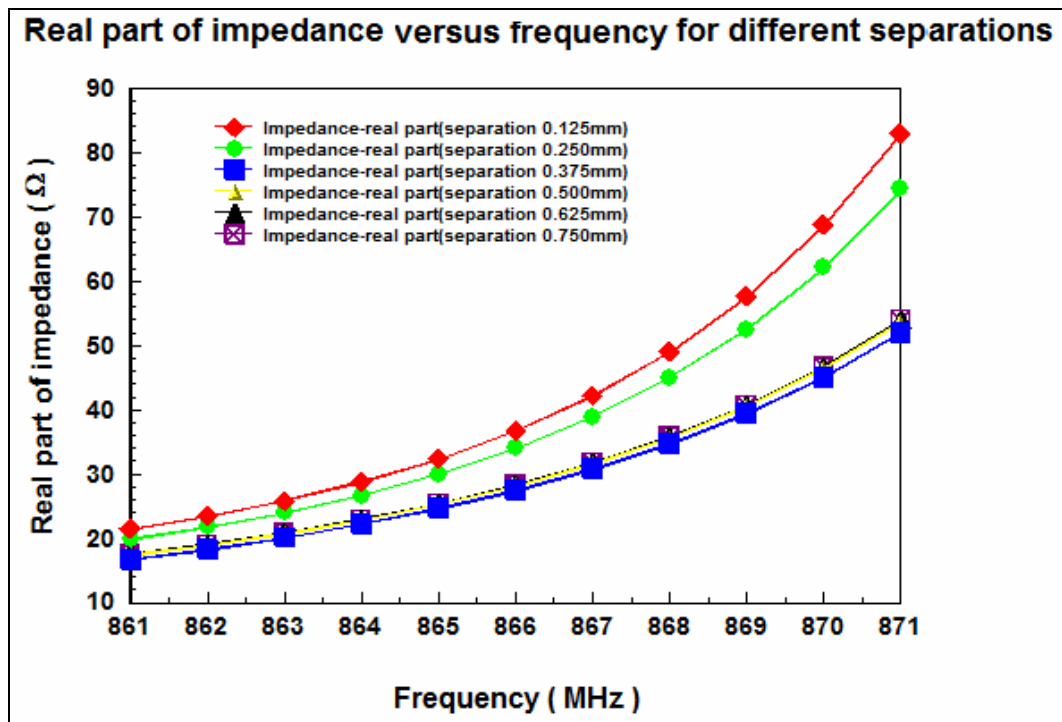


Figure 3.17.a) Real part of the impedance for tag antenna on metallic can for different separations (separation between designed tag and top of can)

In Figure 3.17 (a), it is seen that real part of the impedance decreases as separation increases up to 0.375 mm, after this separation all values are really close to each other. Figure 3.17 (b) shows how imaginary part of the impedance behaves for different separations;

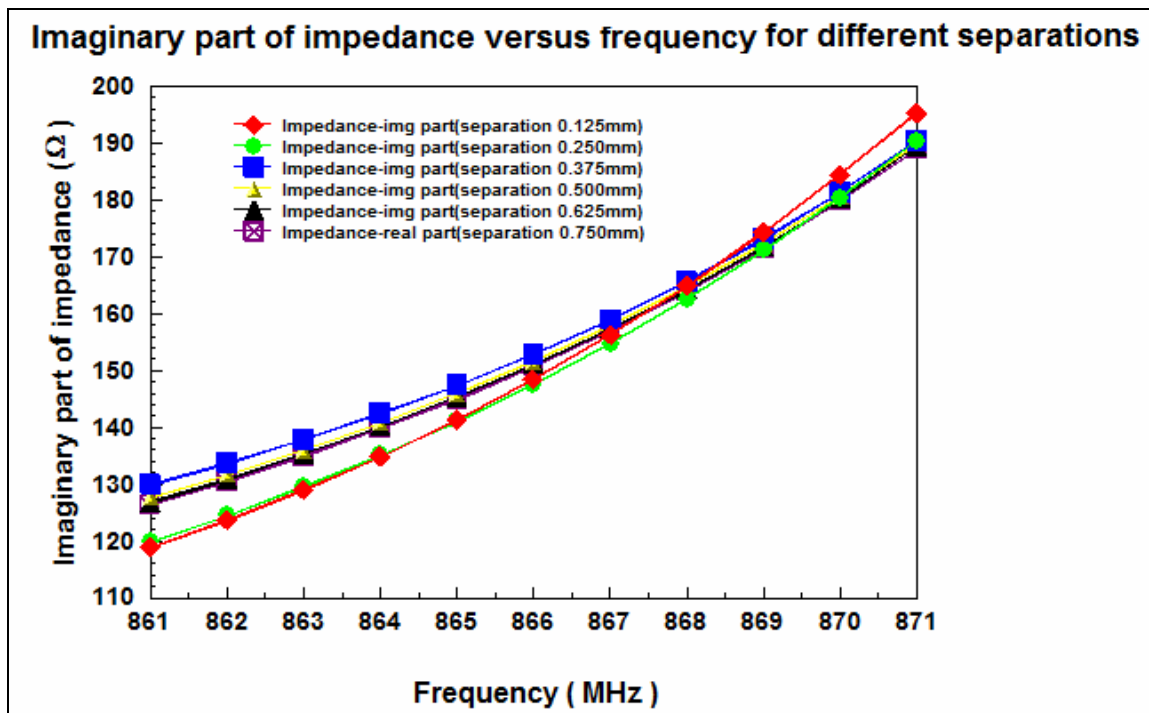


Figure 3.17.b) Imaginary part of the impedance for tag antenna on metallic can for different separations (separation between designed tag and top of can)

Figure 3.17 (b) verifies that imaginary part of the designed tag antenna is not much affected with the separation values when it is placed on metallic can. Figure 3.17 (b) also shows that imaginary part of the impedance does not change considerably as separation changes.

We also studied how the separation affects gain for as shown in Figure 3.18. It is found that separation up to 0.375 mm affects the gain of the tag antenna.

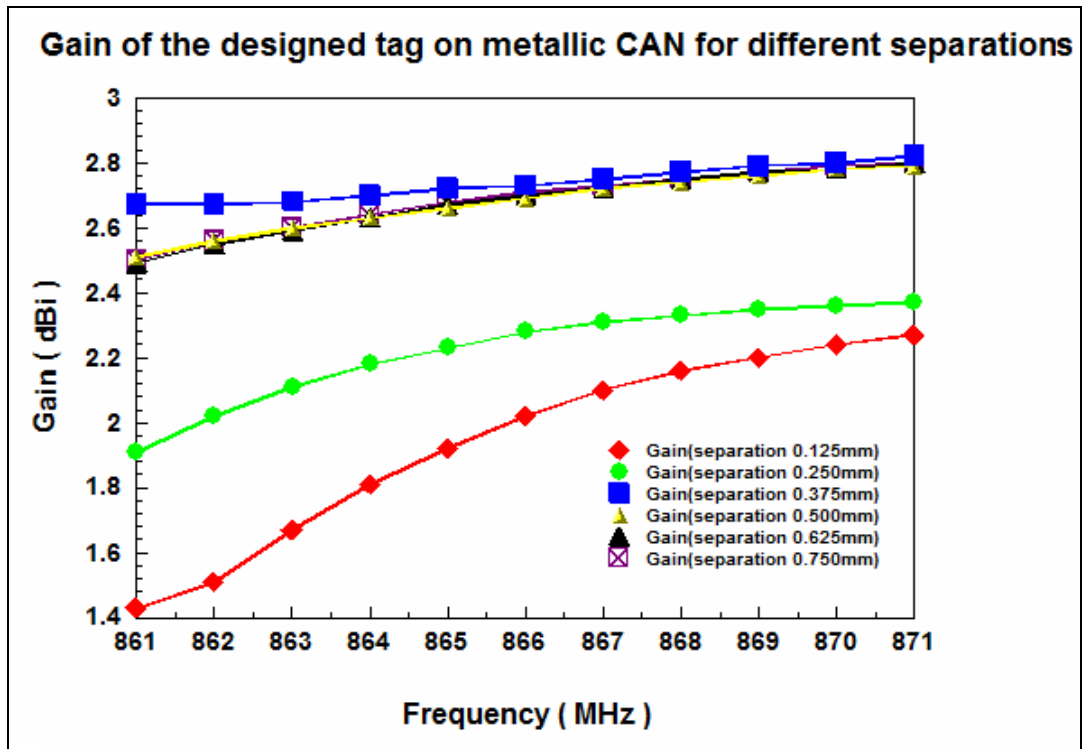


Figure 3.18. Gain of the tag antenna on metallic can for different separations

It is clear that gain values remain almost unchanged for separations greater than 0.375 mm.

We also compared the free space gain of designed tag antenna and tag antenna on metallic can. All the gain analysis are done at $\theta = 0^\circ$. Figure 3.19 shows the gain of the tag antenna when it is on metallic can compared to tag antenna in free space (separation between tag antenna and can is taken as 0.75 mm);

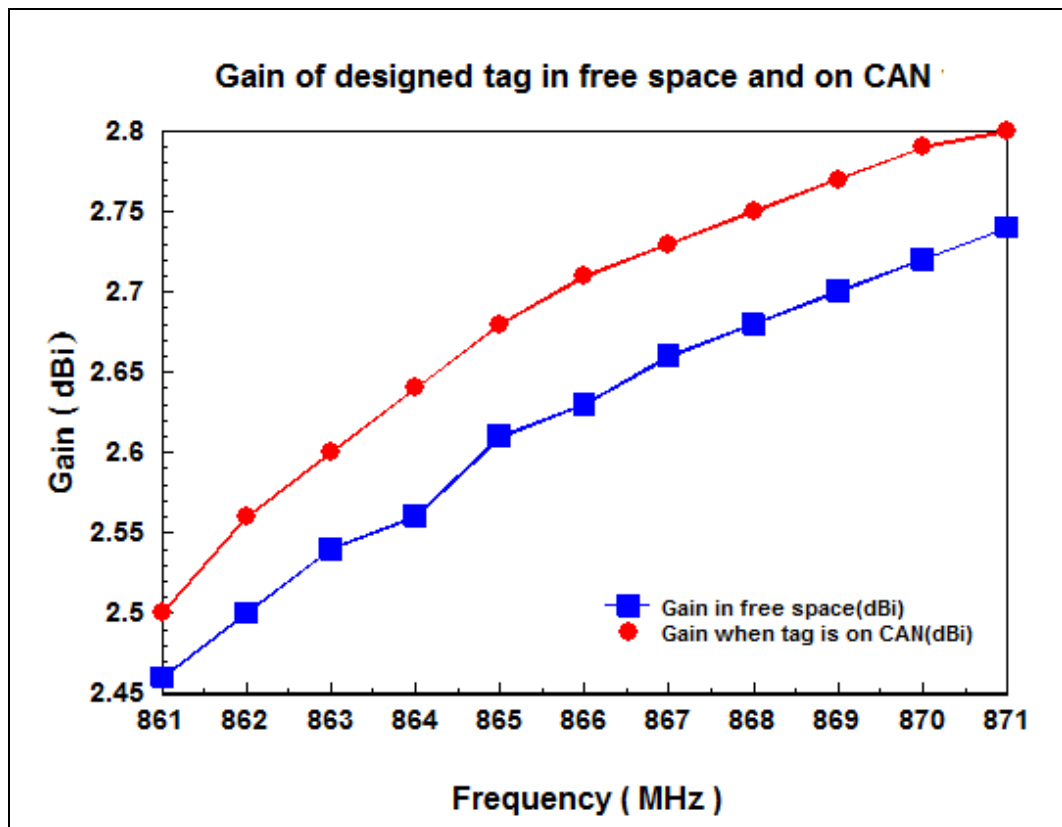


Figure 3.19. Gain of tag antenna in free space and on can (separation is taken as 0.75 mm)

If the height of the can is increased to 55 cm from 35 cm and radius to 20 cm from 10 cm, the results do not change considerably. We observed an impedance of $32.60+j158.10 \Omega$ with gain of 2.87 dBi at 868 MHz. It is seen that there is less decrease in impedance, but there is an increase in gain. So, it can be said that the metal effect on ground plane increases gain but decreases in impedance. Figure 3.20 shows the effect of increasing metallic can dimensions compared free space result and previous metallic can result;

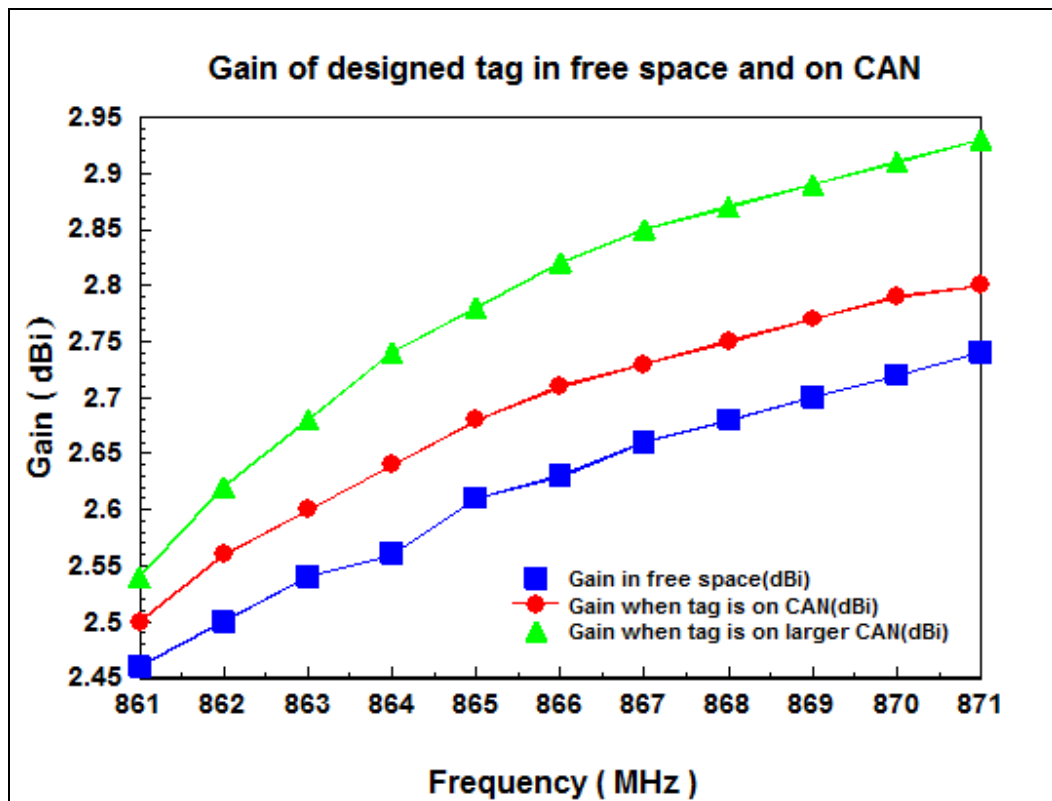


Figure 3.20. Gain of tag antenna in free space and on can (larger can added)

Figure 3.21 (a) and (b) shows how TI dipole real and imaginary part of the impedance change with separation. It is shown in Figure 3.21 (a) that TI dipole has very small real part of impedances for different separations when it is on metallic can. These values are not adequate for good impedance matching. When separation increases for the TI dipole, real part of the impedance decreases. We can say that TI dipole antenna is affected from metal significantly.

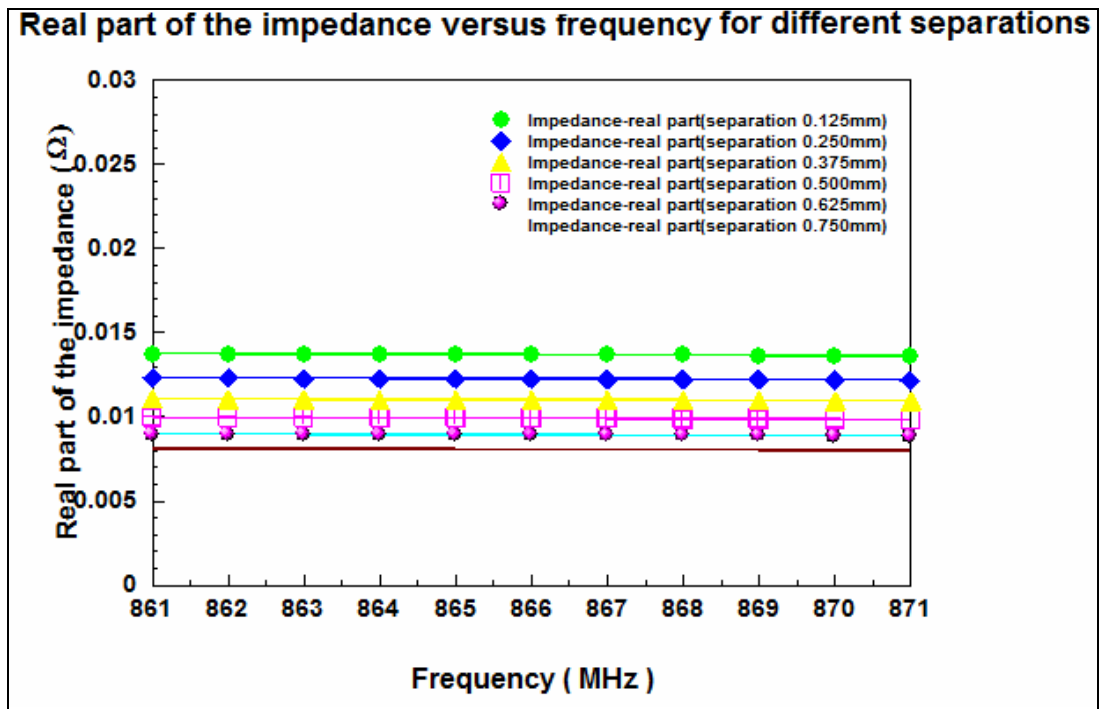


Figure 3.21.a) Real part of the impedance for TI dipole antenna on metallic can for different separations

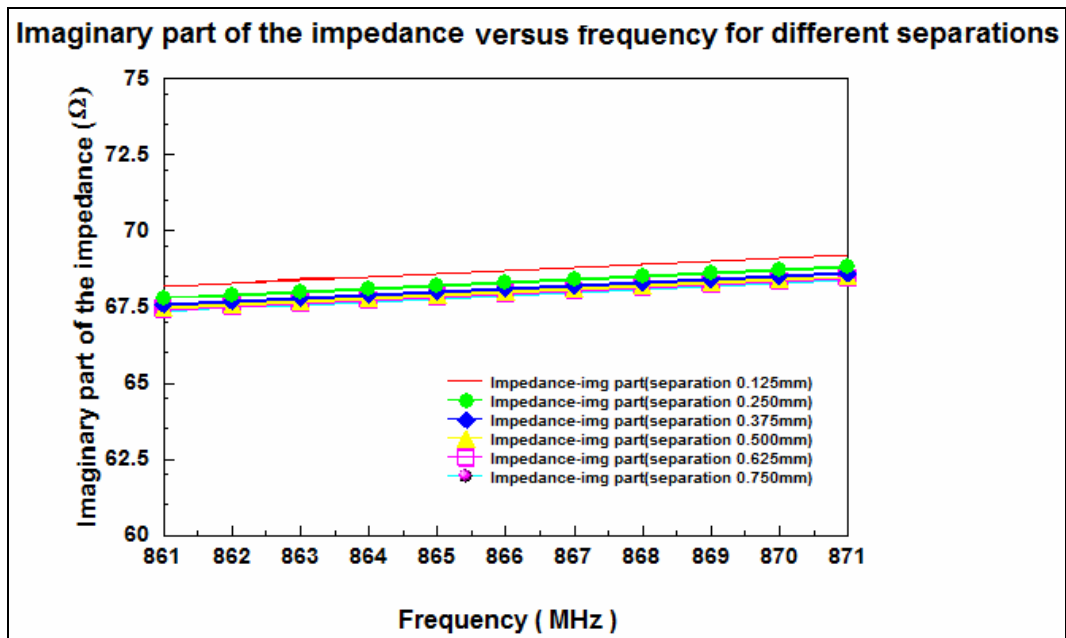


Figure 3.21.b) Imaginary part of the impedance for TI dipole antenna on metallic can for different separations

As it is seen in Figure 3.21 (b), that as separation decreases, imaginary part of the impedance increases when TI dipole antenna is on metallic can. Figure 3.22 shows the change of gain with different separations;

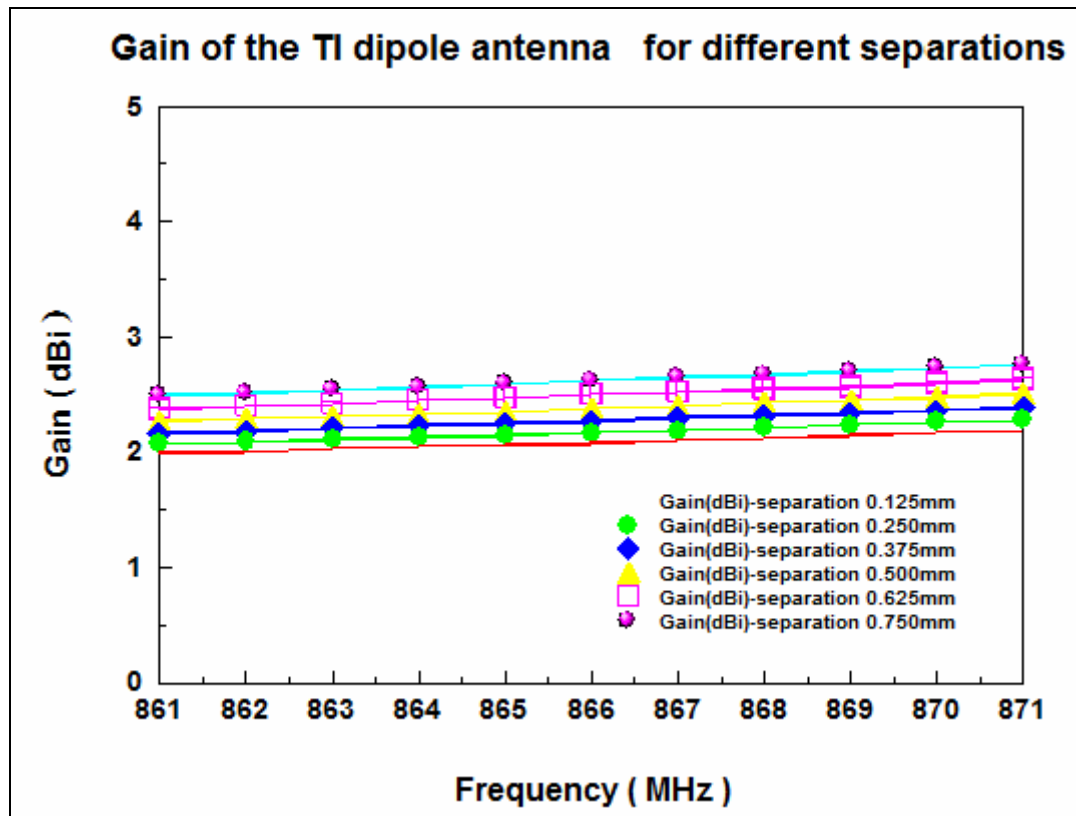


Figure 3.22. Gain of TI dipole antenna for different separations when it is on metallic can

Figure 3.23 shows the effect of increasing metallic can sizes on TI dipole antenna. Results are compared with free space analysis. It is seen that increasing metallic can sizes causes the same effect as it did for our antenna.

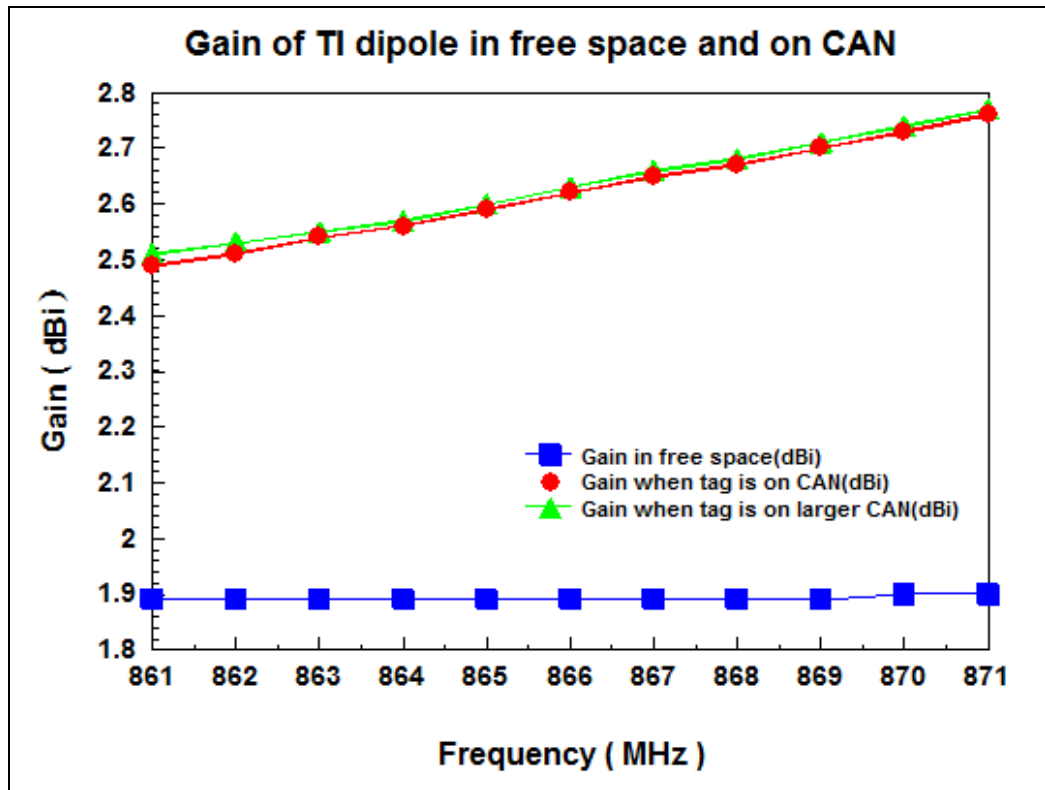


Figure 3.23. Gain of TI dipole antenna in free space and on can (larger can added)

3.3.2. Modeling and Design of Tag Antenna on Water Carboy

Plastic empty water carboy is modeled for this purpose. Dielectric constant of 4.1 with a loss of 0.012 is given for plastic carboy. Height of the water carboy is taken as 45 cm and radius 15 cm. There is separation of 0.75 mm between top of the water carboy and the tag antenna.

Figure 3.24 shows the FEKO model of the antenna placed on water carboy;

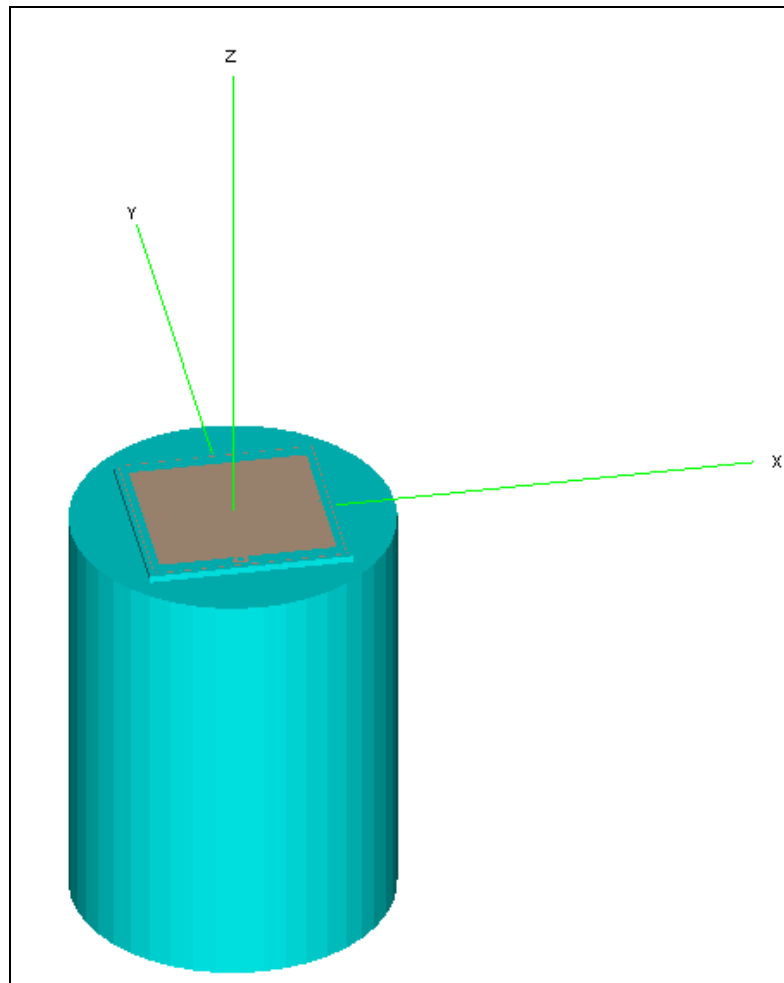


Figure 3.24. FEKO model of tag antenna on water carboy

At 868 MHz, it has an impedance of $40.99 + j170.16 \Omega$ with a gain of 2.59 dBi when tag antenna is on plastic water carboy.

Figure 3.25 (a) and (b) show the real and imaginary part of the impedance for different separations.

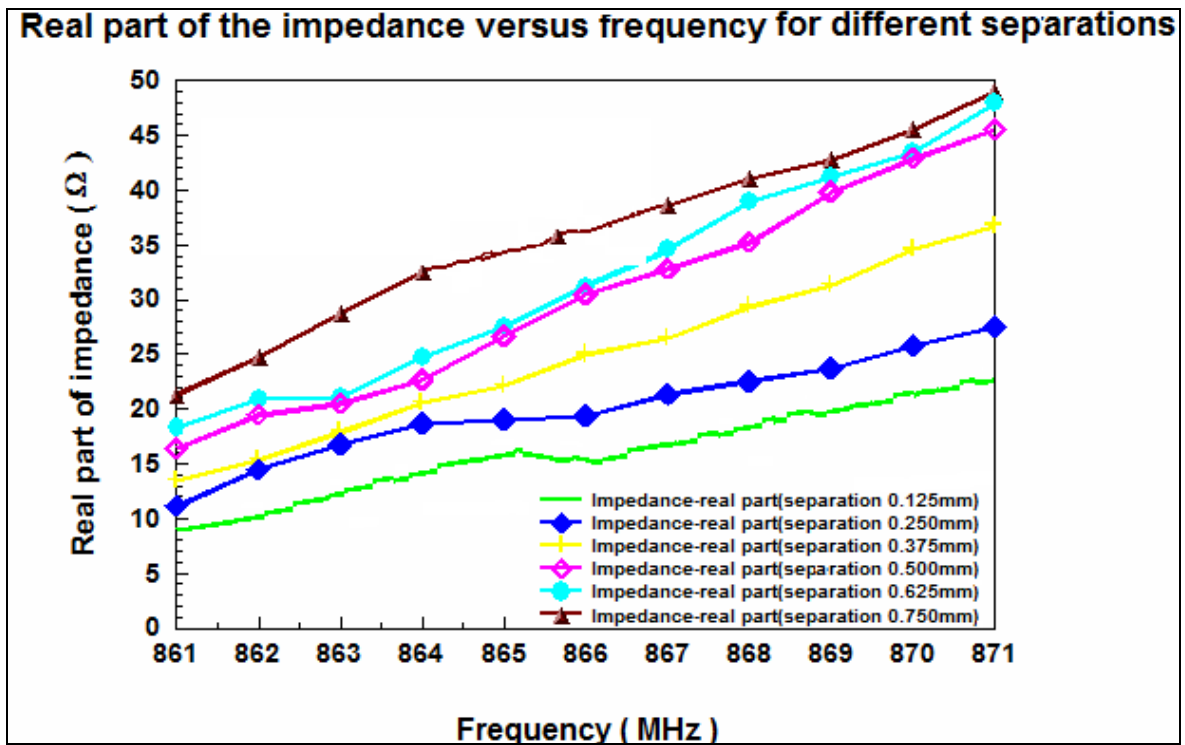


Figure 3.25.a) Real part of the impedance for tag antenna on water carboy for different separations

As it is shown in Figure 3.25 (a) that the increase in separation results with an increase in the real part of the impedance. While tag antenna has less than 10Ω real impedance at separation 0.125 mm , it has real impedance of approximately 40Ω at separation 0.750 mm at 868 MHz . Increase of separation improves tag antenna real part of impedance.

The effects of tag-to-carboy separation on imaginary part of the impedance is shown in Figure 3.25 (b);

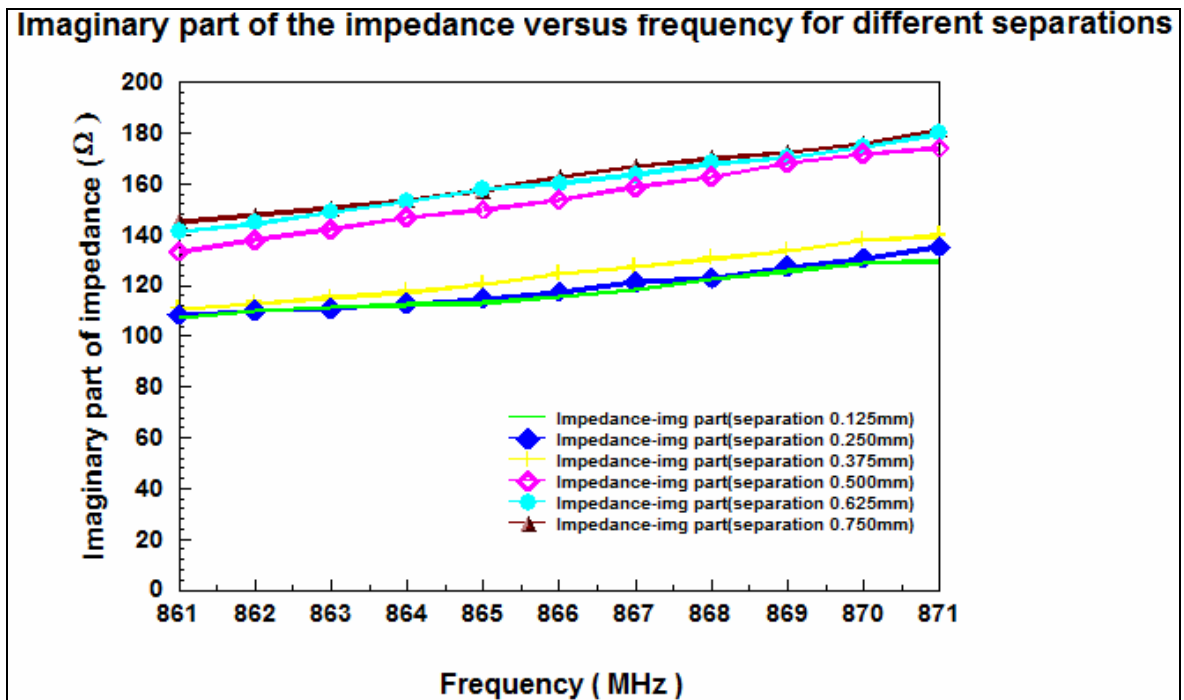


Figure 3.25.b) Imaginary part of the impedance for tag antenna on water carboy for different separations

Similar effects are observed for the imaginary part of the impedance as well. Therefore, we can say that the tag antenna is not terribly affected from plastic surfaces.

Simulations for gain are shown in Figure 3.26. It is observed that as the separation increases, gain decreases but the decrease is tolerable. Antenna has still acceptable gain when it is on plastics.

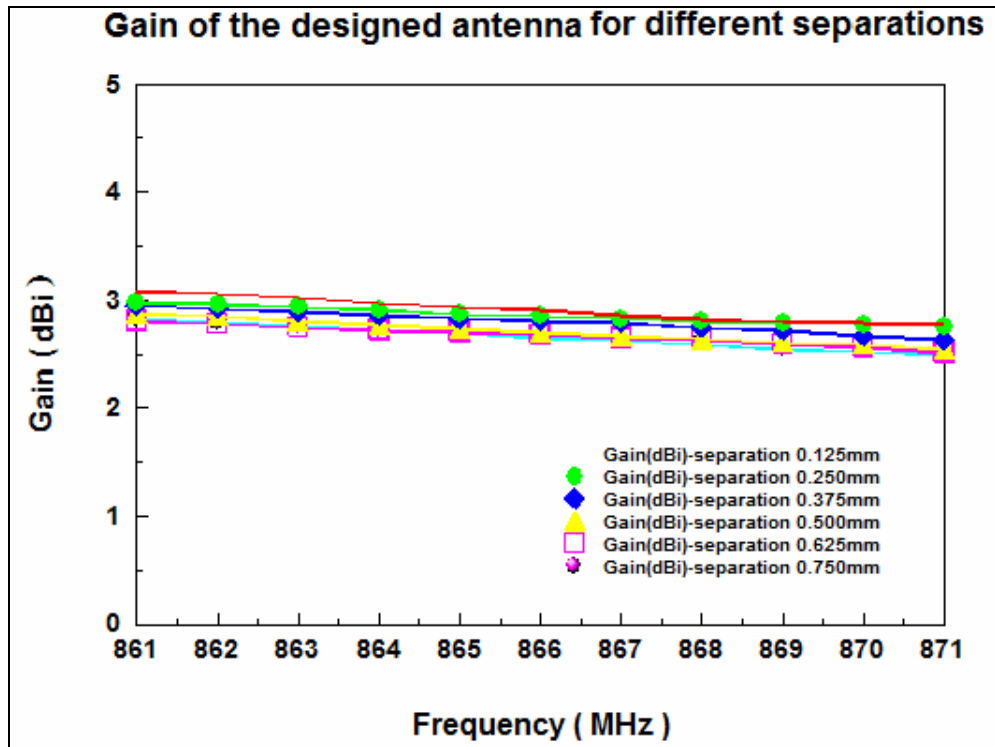


Figure 3.26. Gain of the tag antenna on water carboy for different separations

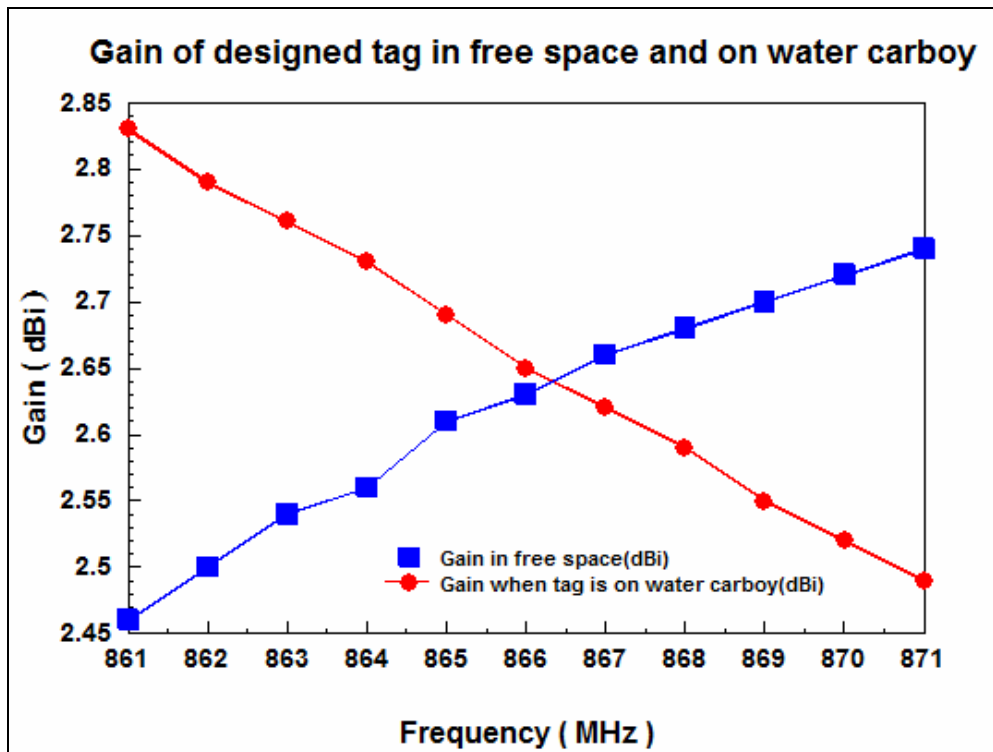


Figure 3.27. Gain of designed antenna in free space and on plastic water carboy

It is observed in Figure 3.27 that the plastic has effect on gain. There is at most 0.4 dB gain decrease over the frequency band. However, the difference between tag antenna in free space and tag antenna on plastic water carboy is approximately 0.1 dB at 868 MHz. So it can be said that the tag antenna has still good gain performance on plastic water carboy. Plastic surface affects antenna gain performance, but not much.

If size of the water carboy is increased, which height is increased to 55 cm and radius is increased to 25 cm it is observed that tag antenna gain performance continues to decrease. But, the tag antenna gain characteristic is not affected appreciably. Therefore, it can be said that tag antenna can be operated without degrading gain considerably, as indicated in Figure 3.28.

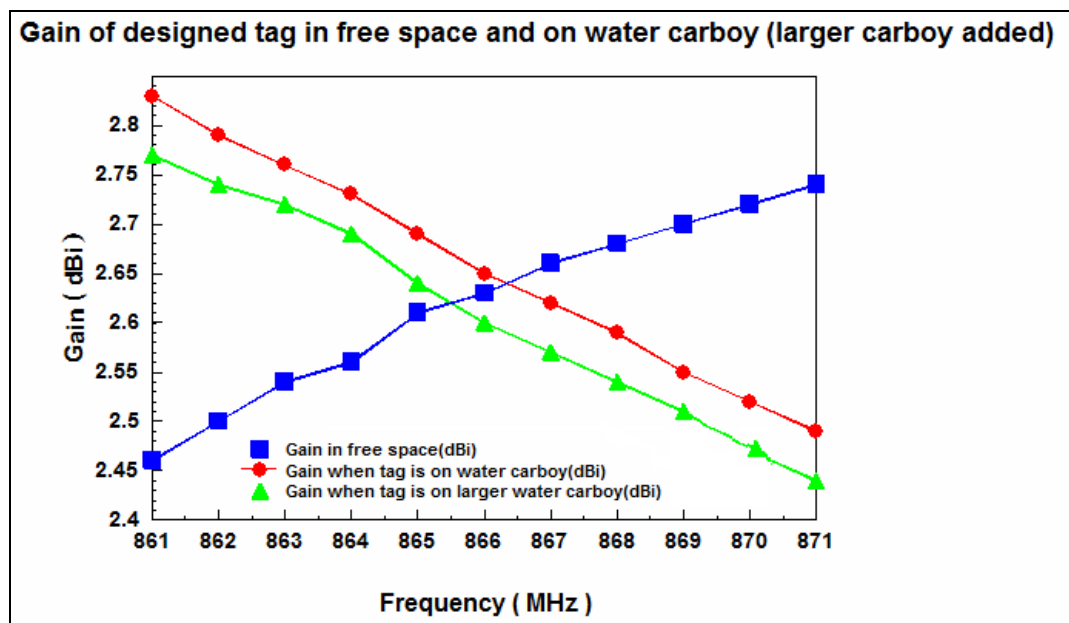


Figure 3.28. Gain of tag antenna in free space and on water carboy (larger carboy added)

We also made similar analysis for TI dipole. At 868 MHz, TI dipole antenna has input impedance of $1.84+j81.79 \Omega$ with gain of 0.0091 dBi while our antenna has input impedance of $40.99+j170.16 \Omega$ with gain 2.59 dBi.

Figure 3.29 (a) and (b) shows how real and imaginary part of the impedance changes with different separations for TI dipole antenna. For real part of the impedance, it is observed that when separation increases, it results in an increase in the real part of the impedance. But, it is at best 1.9Ω when TI dipole antenna on water carboy. But, the tag antenna achieves at least approximately 10Ω real impedance which is much larger than TI dipole.

For imaginary part, again increase in separation results with increase in imaginary part of the impedance. In terms of imaginary part, TI antenna seems acceptable but still our antenna has better imaginary part than TI dipole.

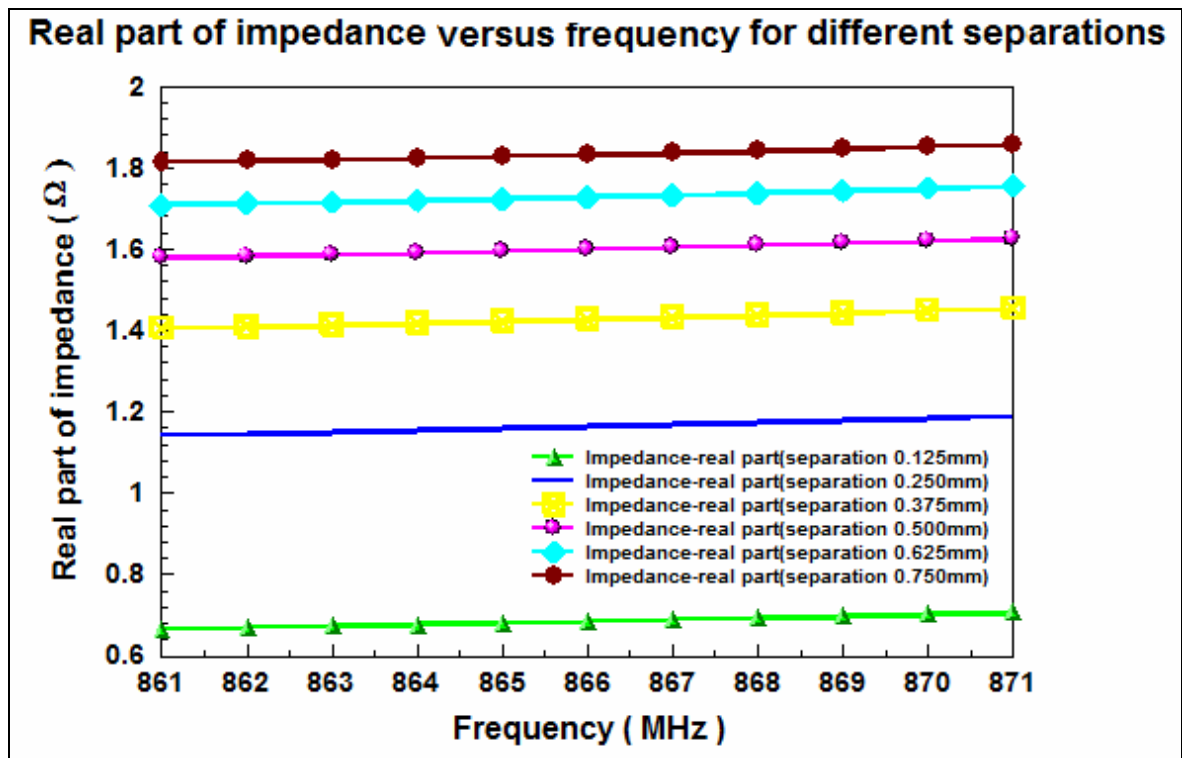


Figure 3.29.a) Real part of impedance for TI dipole on water carboy versus frequency for different separations

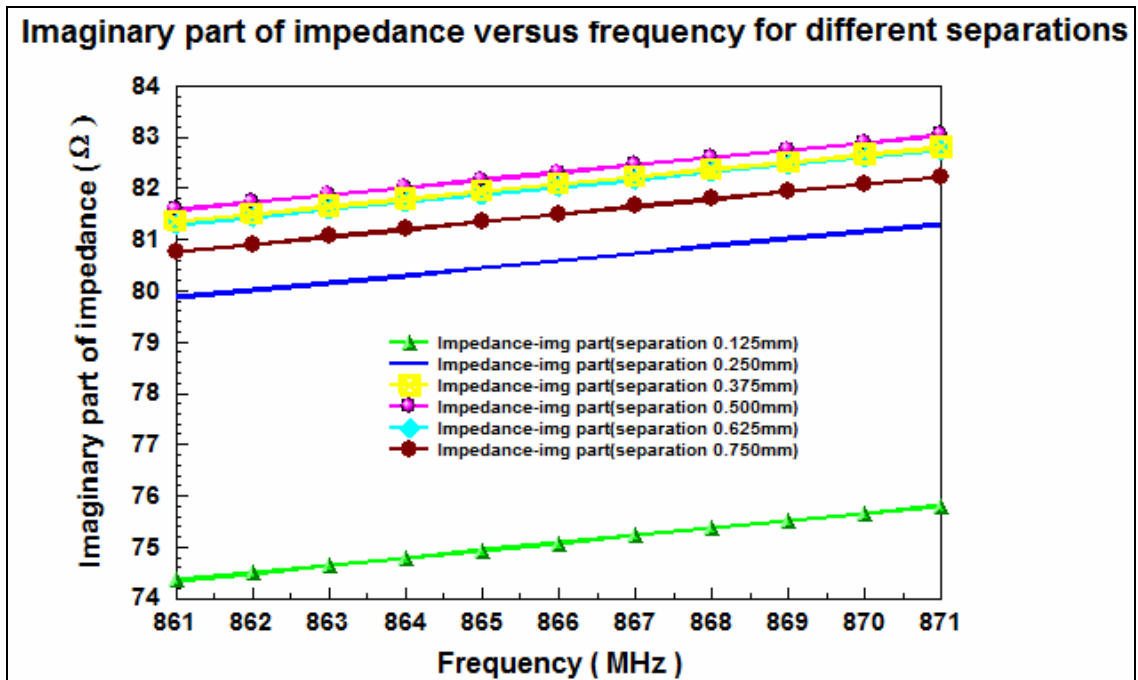


Figure 3.29.b) Imaginary part of impedance for TI dipole on water carboy versus frequency for different separations

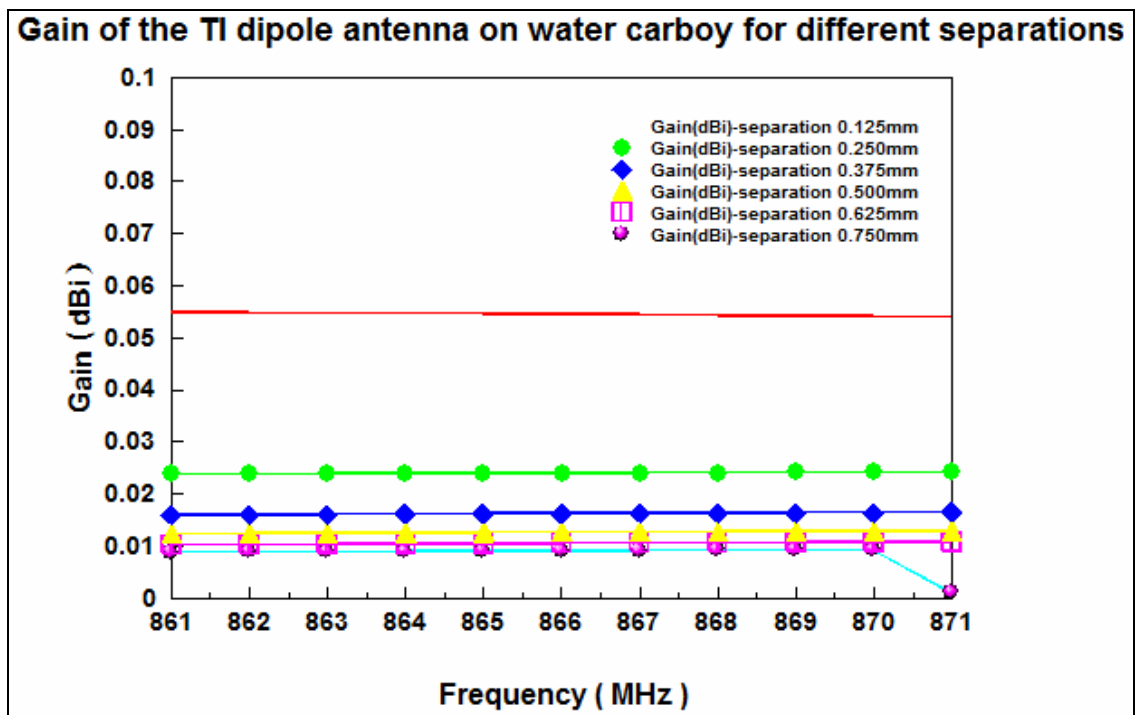


Figure 3.30. Gain of TI dipole on water carboy for different separations

It is seen in Figure 3.30 that, TI dipole has at most 0.05 dBi . Our tag antenna has approximately 2.45 dBi when placed on water carboy. So, the our tag performs better than TI dipole.

TI dipole has free space gain of 1.89 dBi. When it is placed on water carboy, major performance degraation occurs; gain approximately decreases to 0 dBi . Both regular sized water carboy (height is 45 cm and radius is 15 cm) and larger sized one (55 cm height and 25 cm radius) give similar results. So it can be said that, TI antenna is significantly affected from plastics surfaces as shown in Figure 3.31.

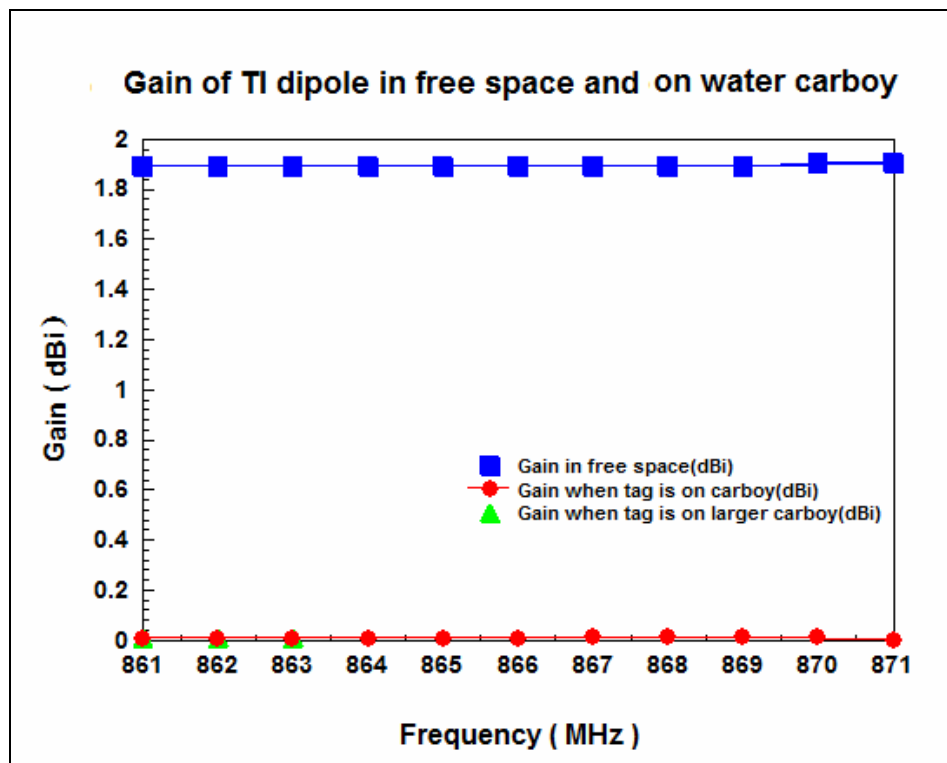


Figure 3.31. Gain of TI dipole in free space and on water carboy (larger carboy added)

3.3.3. Modeling and Design of Tag Antenna on Wooden Strip

After studying the effects tag placed on plastics and on/near-metal surfaces, next step is to study the effects of wooden surfaces. For this purpose, a wooden strip having dimensions $25 \times 45 \text{ cm}^2$ is modeled using FEKO. Dielectric constant of the wooden strip is

2.6 with loss factor 0.0026 . Wooden strip has a height of 3 cm . The tag is separated from wooden strip by 0.75 mm . FEKO model of tag antenna placed on wooden strip is shown in Figure 3.32;

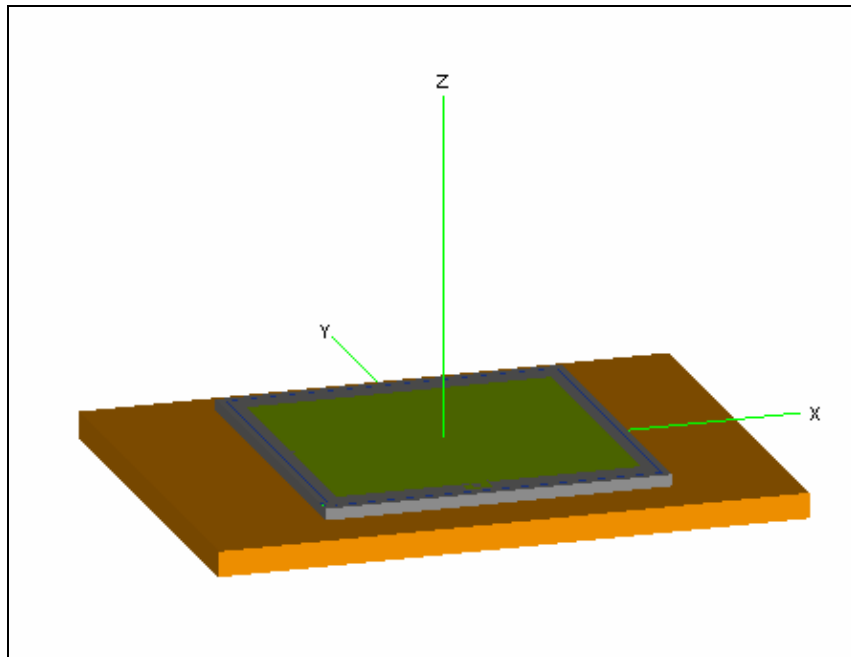


Figure 3.32. FEKO Model of designed tag antenna placed on wooden strip

After performing simulations on tag antenna when it is placed on wooden strip, impedance of $65.22+148.9 \Omega$ is observed. This setup did not affect designed tag antenna impedance much. Figure 3.33 (a) and (b) shows the real and imaginary part of the impedance versus frequency.

In Figure 3.33 (a), it is seen that real part of the impedance increases when separation increases. Tag antenna has at least 35Ω real impedance at 868 MHz . So designed tag antenna has less performance degradation in terms of real part of impedance. Separation affects real impedance a little bit, but not very much.

The same effect is observed for imaginary part too. Increasing the separation results in an increase in the imaginary part of the impedance. Designed tag antenna is good in terms of imaginary impedance, as well.

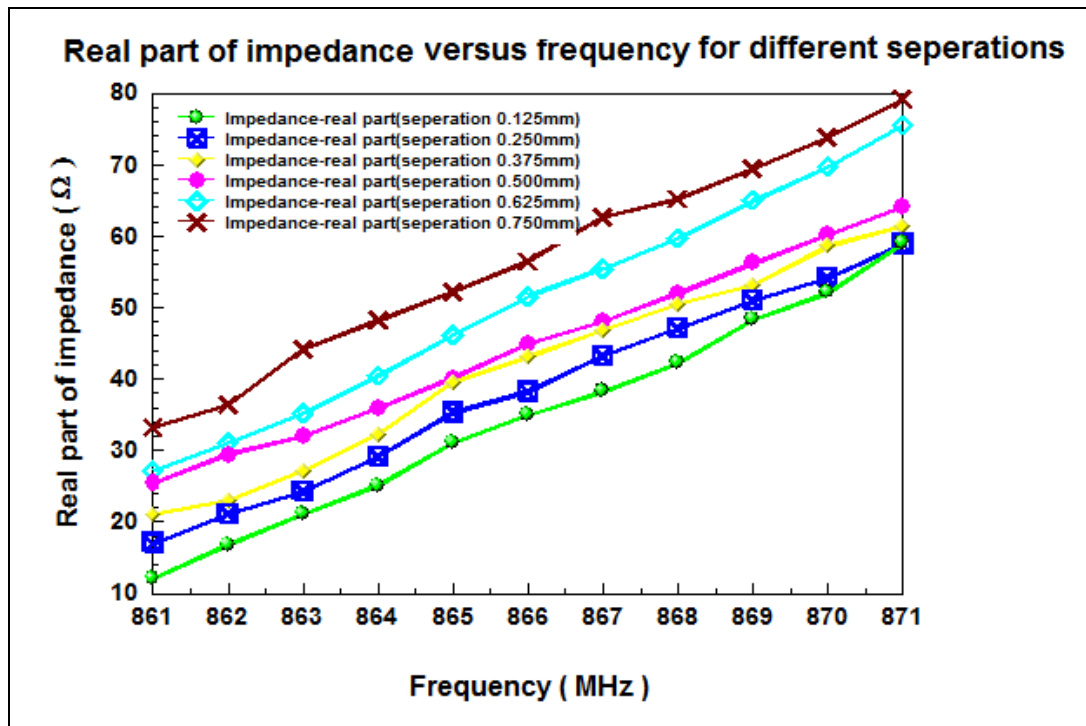


Figure 3.33.a) Real part of impedance for designed tag antenna on wooden strip versus frequency for different separations

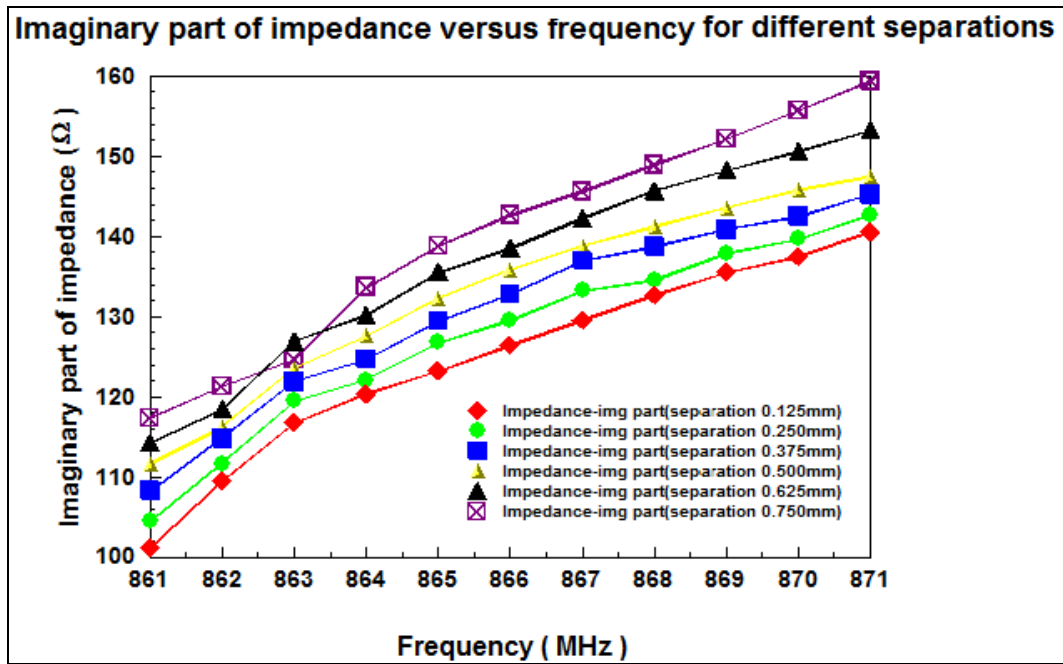


Figure 3.33.b) Imaginary part of impedance for designed tag antenna on wooden strip versus frequency for different separations

Designed tag antenna has gain of 2.6 dBi at 868 MHz. Figure 3.34 shows the gain of designed tag antenna on wooden strip for different separations;

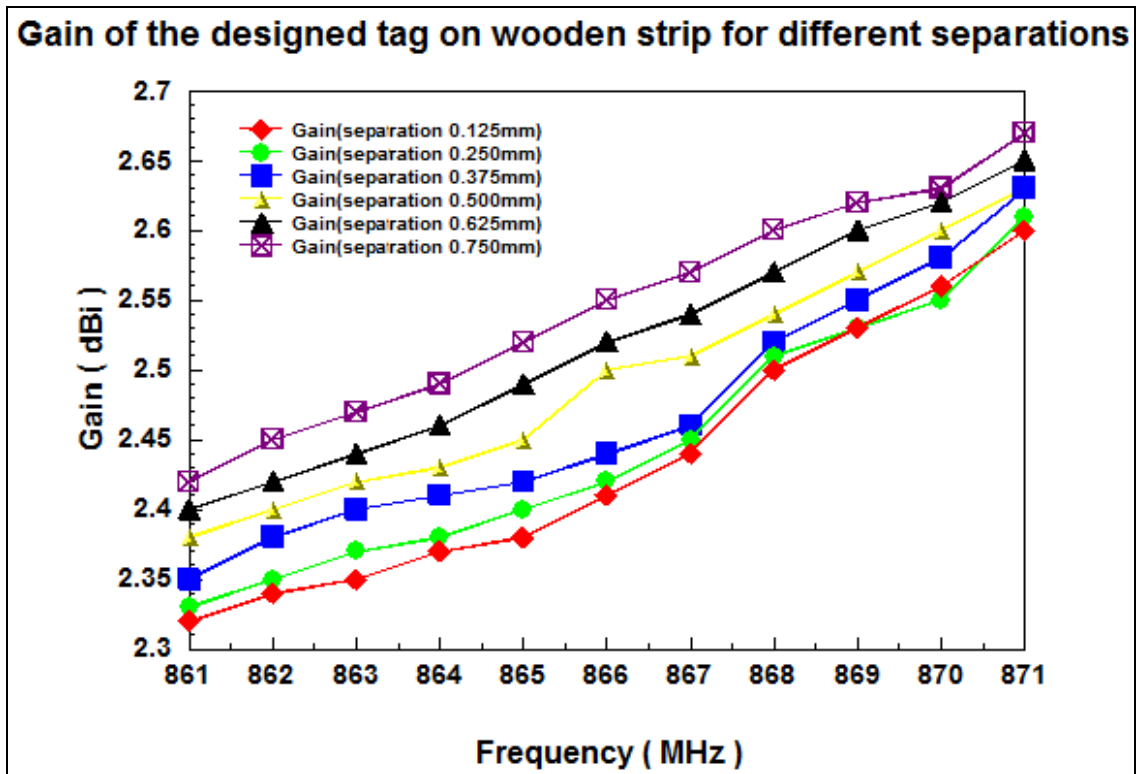


Figure 3.34. Gain of designed tag antenna on wooden strip for different separations

There is approximately 0.1 dB performance degradation seen from separation 0.750 mm to 0.125 mm.

Figure 3.35 shows the gain of tag antenna in free space and on wooden strip to show how tag antenna is affected when placed on wooden strip;

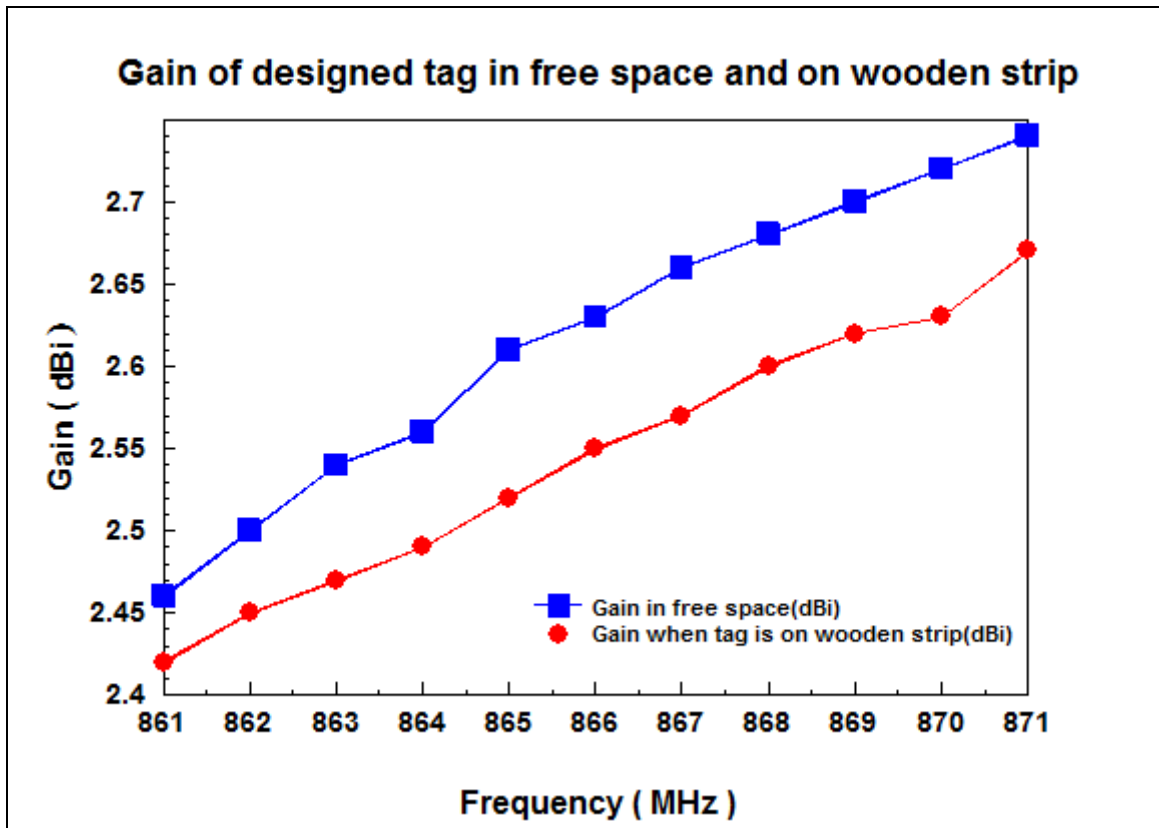


Figure 3.35. Gain of tag antenna in free space and on wooden strip (separation=0.75 mm)

Similar analysis is performed for TI dipole. TI dipole has maximum real impedance of approximately 3Ω , while designed tag antenna has minimum real impedance of approximately 30Ω at 868 MHz.

For imaginary part of the impedance, similar behavior is seen, too. Figure 3.36 (a) and (b) shows how real and imaginary part of the impedance changes with different separations;

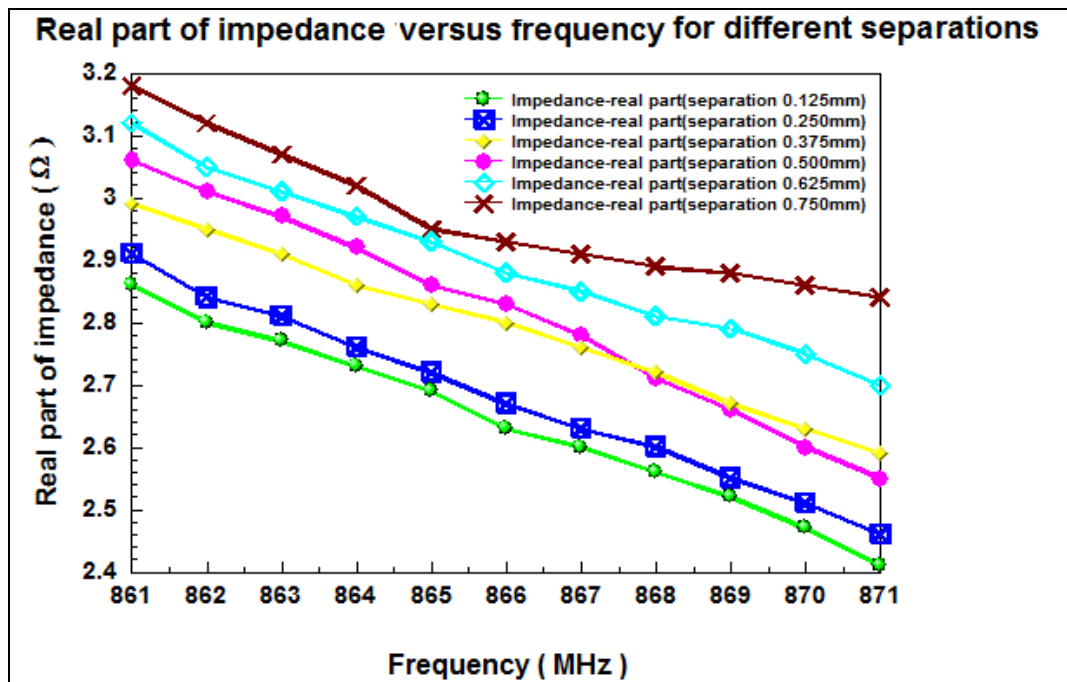


Figure 3.36.a) Real part of impedance for TI dipole antenna on wooden strip versus frequency for different separations

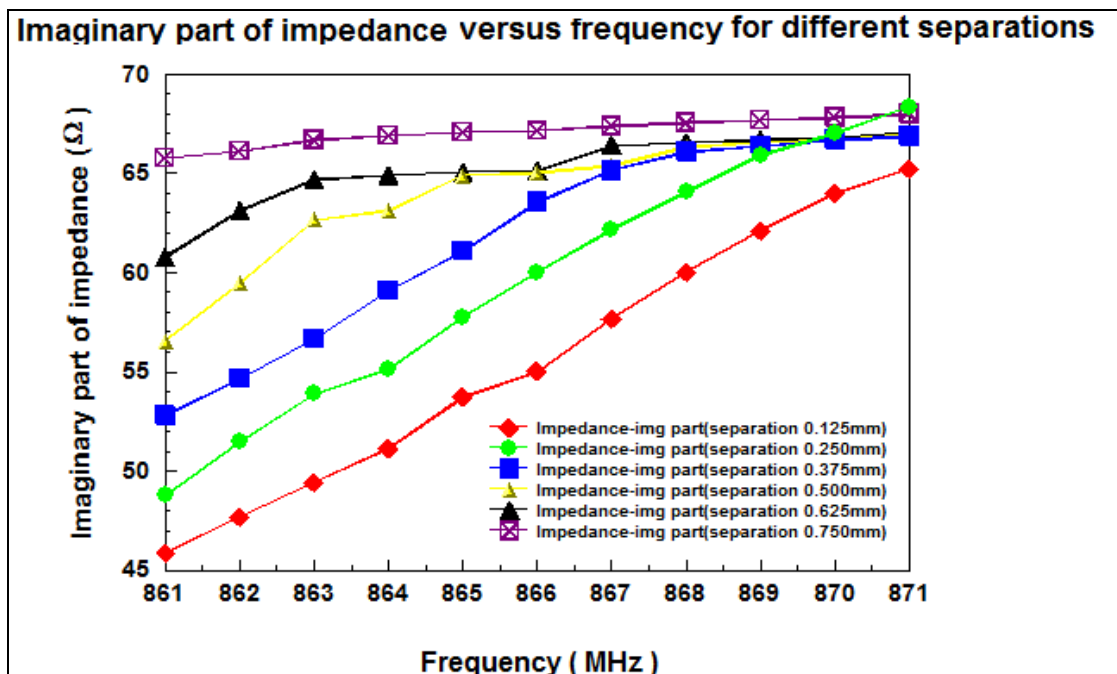


Figure 3.36.b) Imaginary part of impedance for TI dipole antenna on wooden strip versus frequency for different separations

When we look gain characteristic of TI dipole when it is on wooden strip, it is seen that it is achieved to have gain of approximately 0.95 dBi. The TI dipole is significantly affected from wooden surfaces. Figure 3.37 shows how gain characteristic changes for TI dipole on wooden strip for different separations;

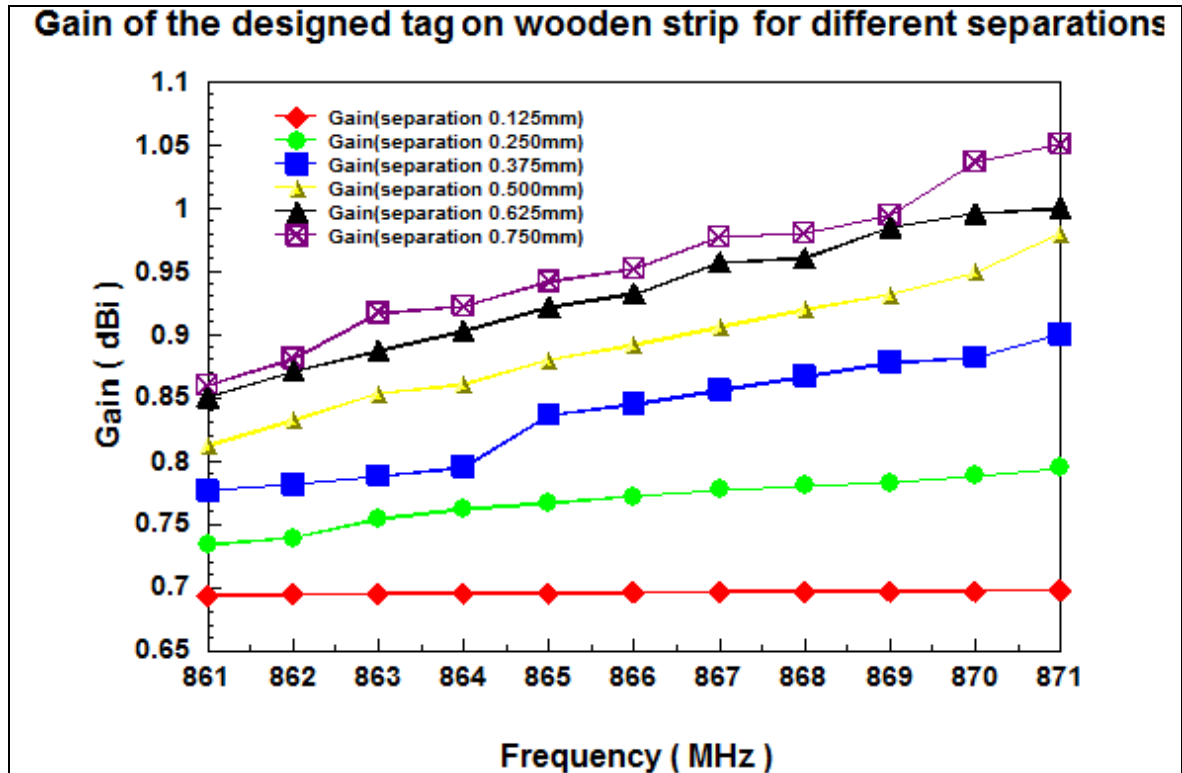


Figure 3.37. Gain of TI dipole antenna placed on wooden strip for different separations

It is seen from the Figure 3.37 that, increasing the separation increases gain. When separation decreases, performance degradation is observed for TI dipole. So, it can be said that TI dipole is significantly affected from wooden structures.

Free space analysis is given with on wooden strip analysis to determine the effect of wooden strip on TI dipole antenna. Figure 3.38 shows the gain of TI dipole in free space and TI dipole placed on wooden strip. Performance degradation in terms of gain is seen obvious, since, free space gain, 1.89 dBi decreases to 0.97 dBi.

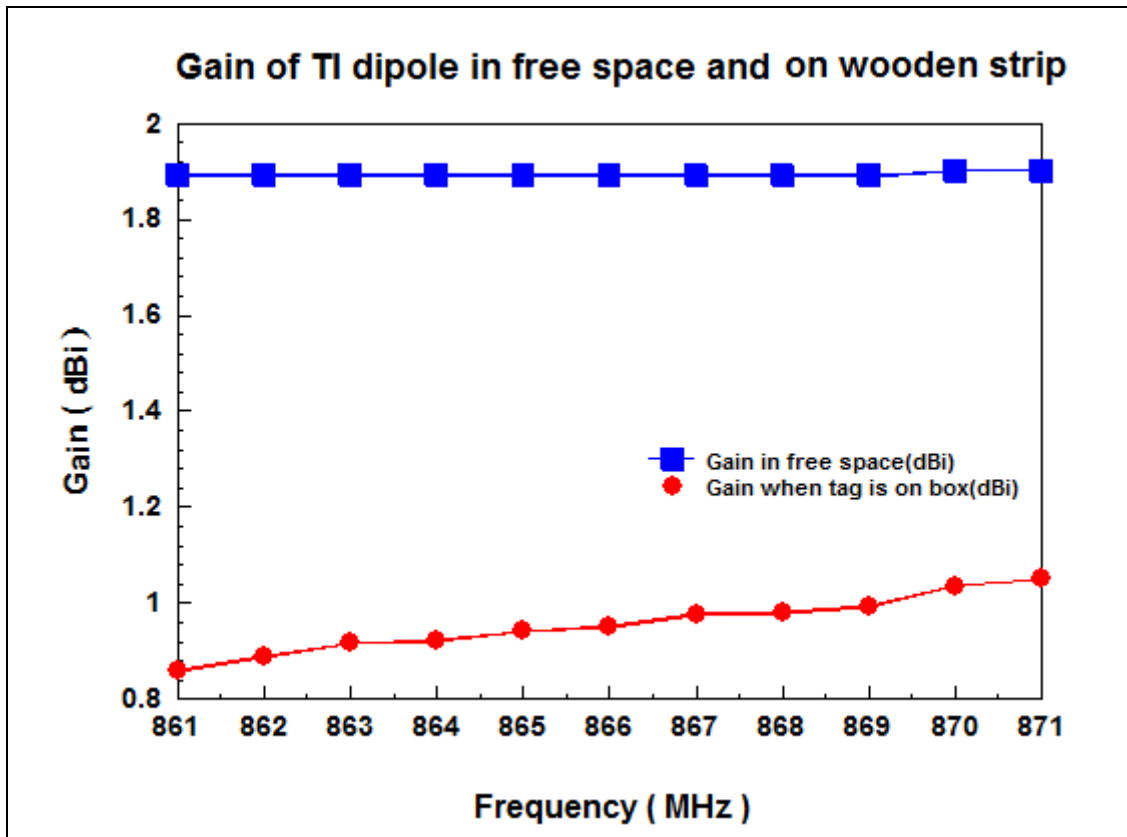


Figure 3.38. Gain of TI dipole in free space and on wooden strip

3.3.4. Modeling and design of tag antenna on Paper Box

Last, the effect of paper box on design tag is studied. Paper box with dimensions 30x65 cm² having a height of 10 cm is used for the model. Dielectric constant of 2 with a loss factor of 0.0044 is used in the design using FEKO. In model, separation between top of paper box and designed tag antenna is taken as 0.75 mm. Effect of different separations are also studied. FEKO model of tag antenna on paper box is shown in Figure 3.39.

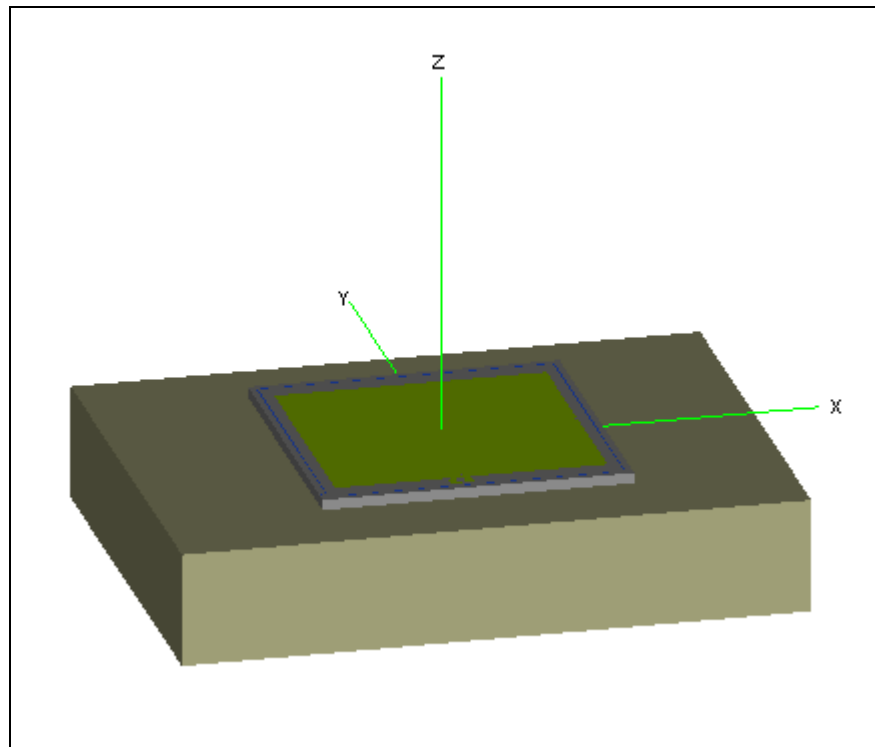


Figure 3.39. FEKO model of tag antenna placed on paper box

Simulations are performed on the model. Results show a complex impedance of $67.46 + j127.6 \Omega$ when tag antenna placed on paper box. When we look at the real part of the impedance, it is observed that it increases with separation.

For imaginary part of the impedance, values decrease compared to values obtained for tag antenna when placed on wooden strip. Figure 3.40 (a) and (b) shows how real and imaginary impedances change with different separations when tag antenna is placed on paper box.

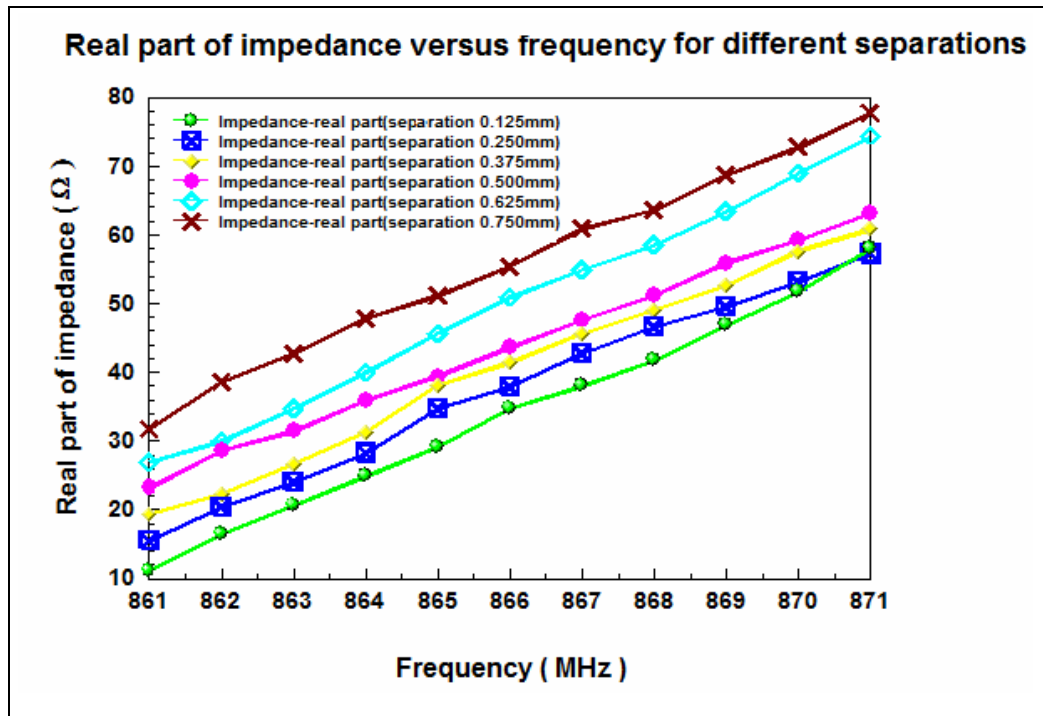


Figure 3.40.a) Real part of impedance for designed tag on paper box versus frequency for different separations

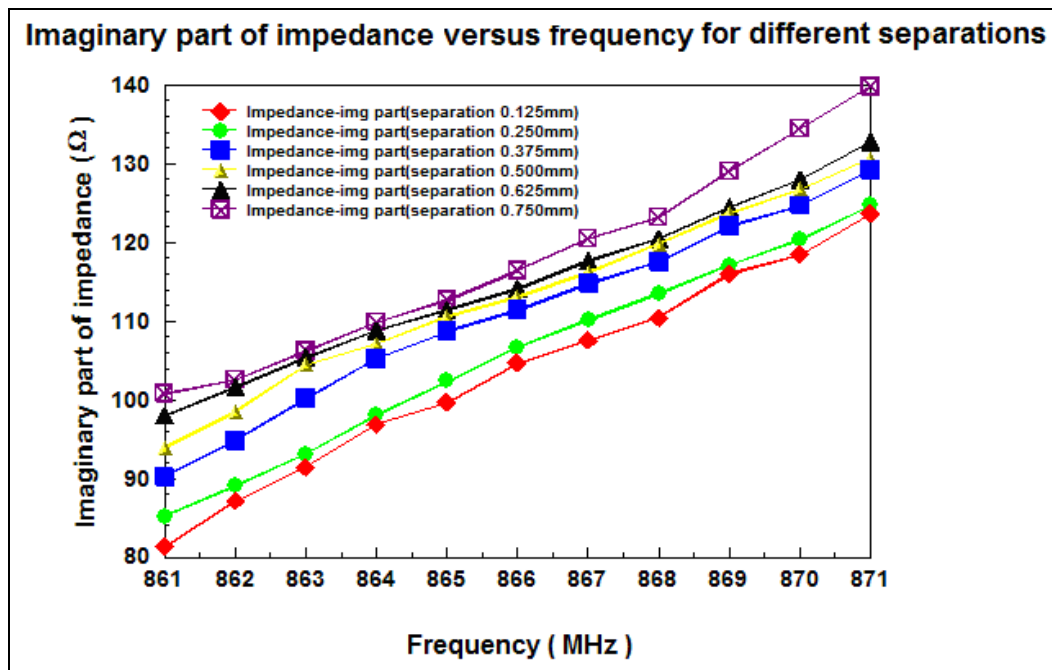


Figure 3.40.b) Imaginary part of impedance for designed tag on paper box versus frequency for different separations

Figure 3.41 shows the gain of tag antenna when it is on paper box for different separations;

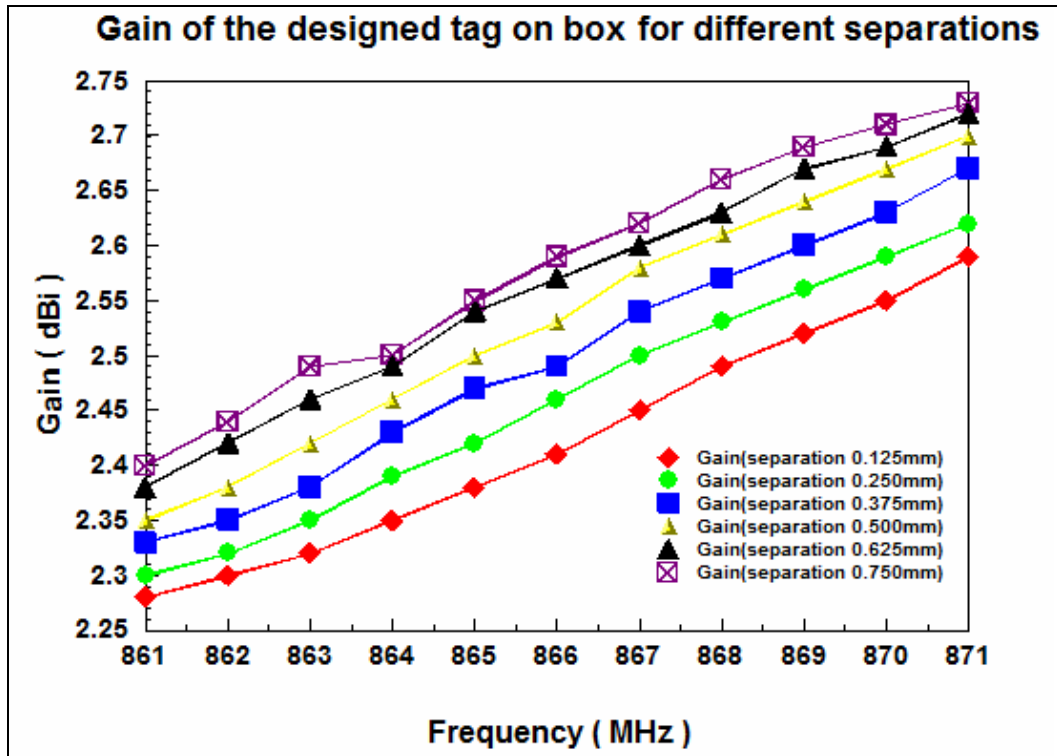


Figure 3.41. Gain of tag antenna when placed on paper box for different separations

It is seen that when separation between tag antenna and top of paper box decreases, small performance degradation is observed. But, we have still gain of more than 2.25 dBi. When separation increases, it causes performance increase in terms of gain. It is seen that gain reaches to 2.66 dBi when separation is 0.75 mm at 868 MHz.

Figure 3.42 shows gain analysis of tag antenna in free space and on paper box.

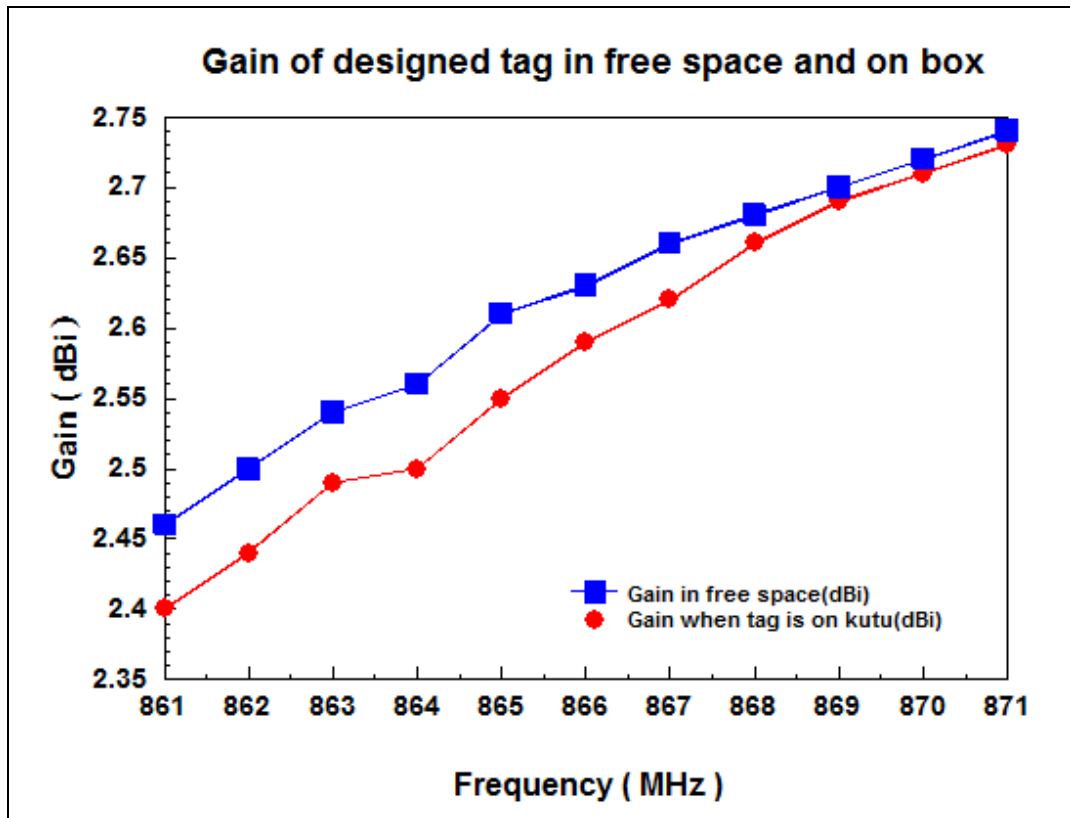


Figure 3.42. Gain of tag antenna in free space and on paper box

It is also important to study the effect of paper box on TI dipole antenna to make a comparison. While TI dipole has real impedance of approximately 3Ω at 861 MHz, real impedance decreases to 2.7Ω at 868 MHz.

If we look at the imaginary part of the impedance for TI dipole, separation causes an increase in imaginary impedance. But, imaginary impedance increases when frequency increases. Figure 3.43 (a) and (b) show the changes of real and imaginary impedance with different separations;

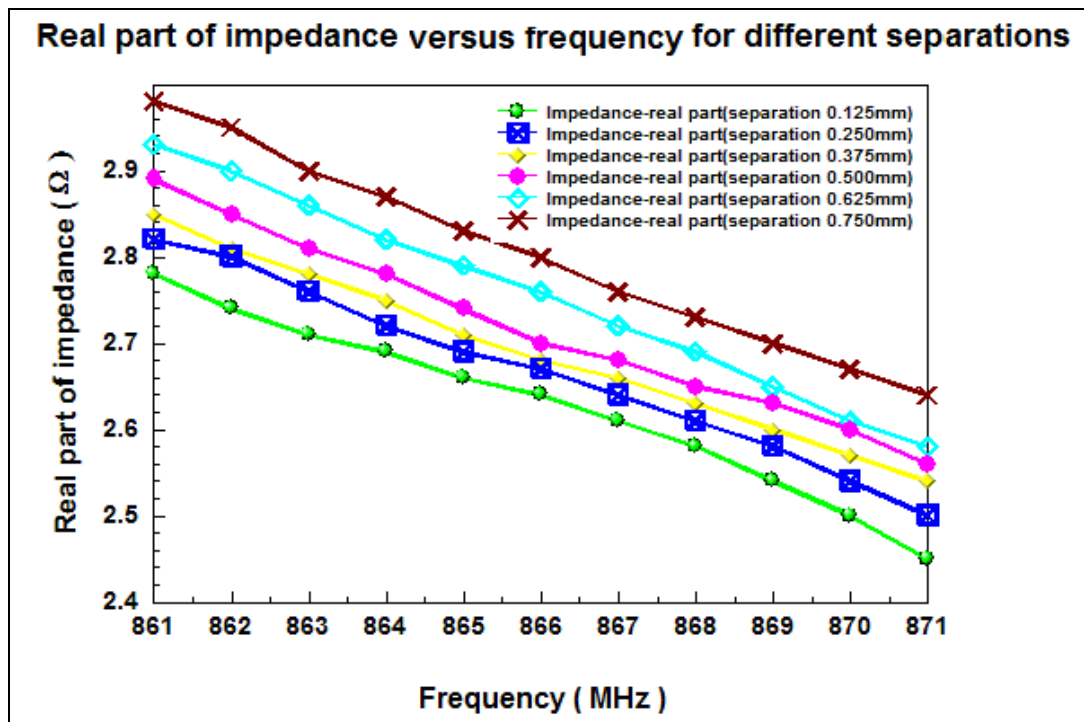


Figure 3.43.a) Real part of impedance for TI dipole on paper box versus frequency for different separations

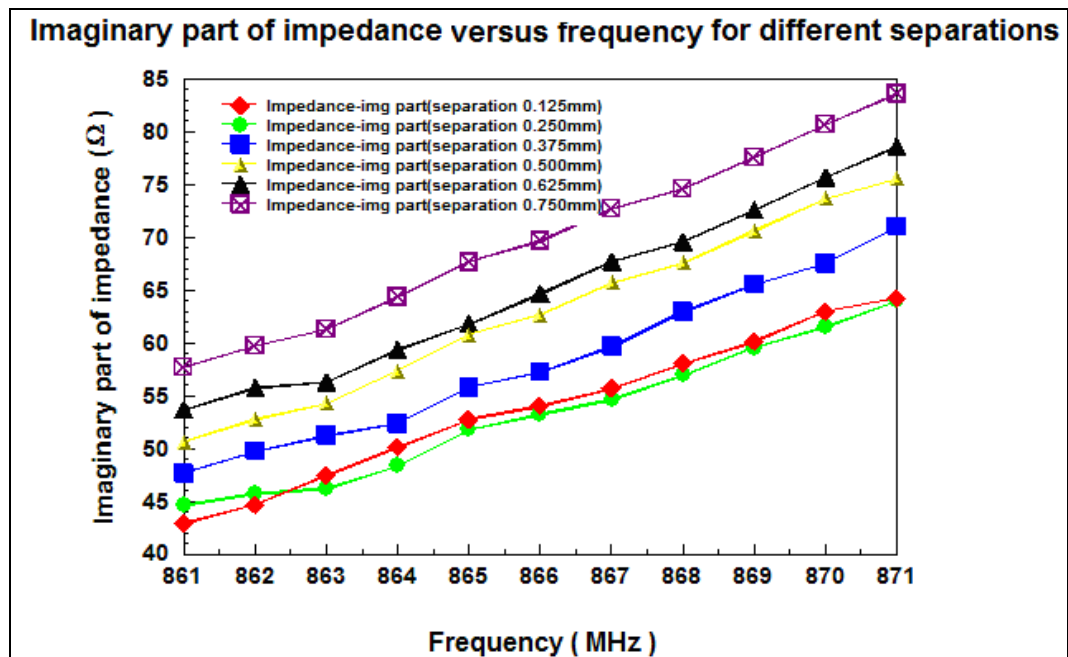


Figure 3.43.b) Imaginary part of impedance for TI dipole on paper box versus frequency for different separations

Gain characteristics of the TI dipole on paper box is studied to complete analysis. Figure 3.44 shows the gain of TI dipole antenna placed on paper box.

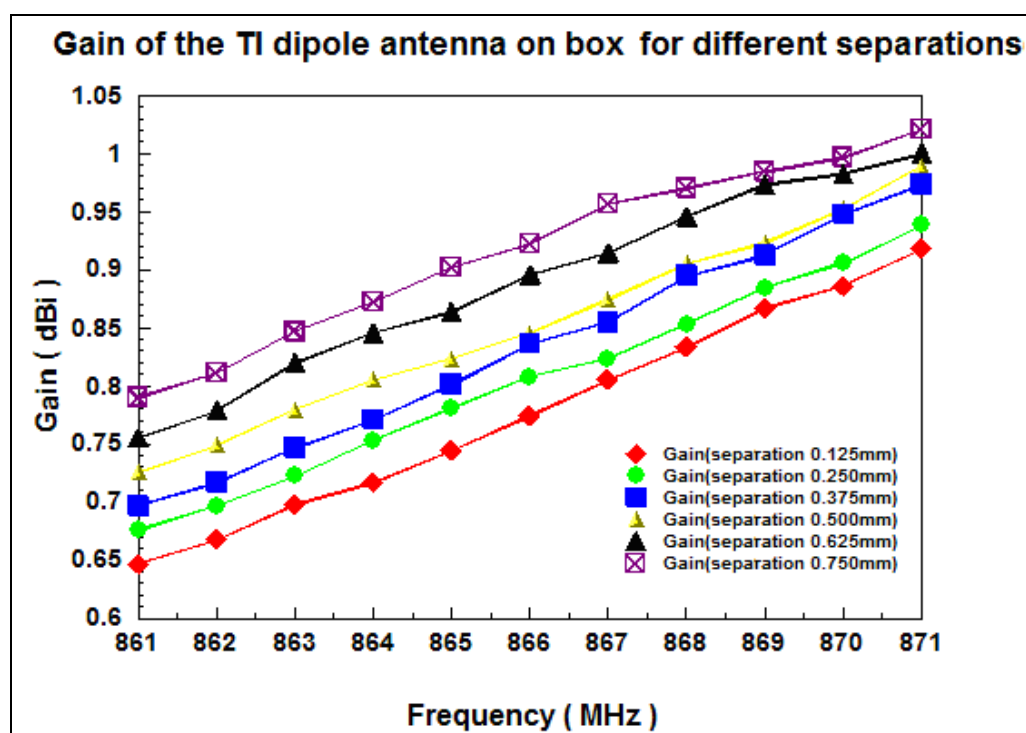


Figure 3.44. Gain of TI dipole on paper box for different separations

We can say that TI dipole is significantly affected when placed on paper box. The TI dipole has a gain of 1.89 dBi in free space, but it has only 0.8 dBi gain when it is placed on paper box. Figure 3.45 shows gain comparison;

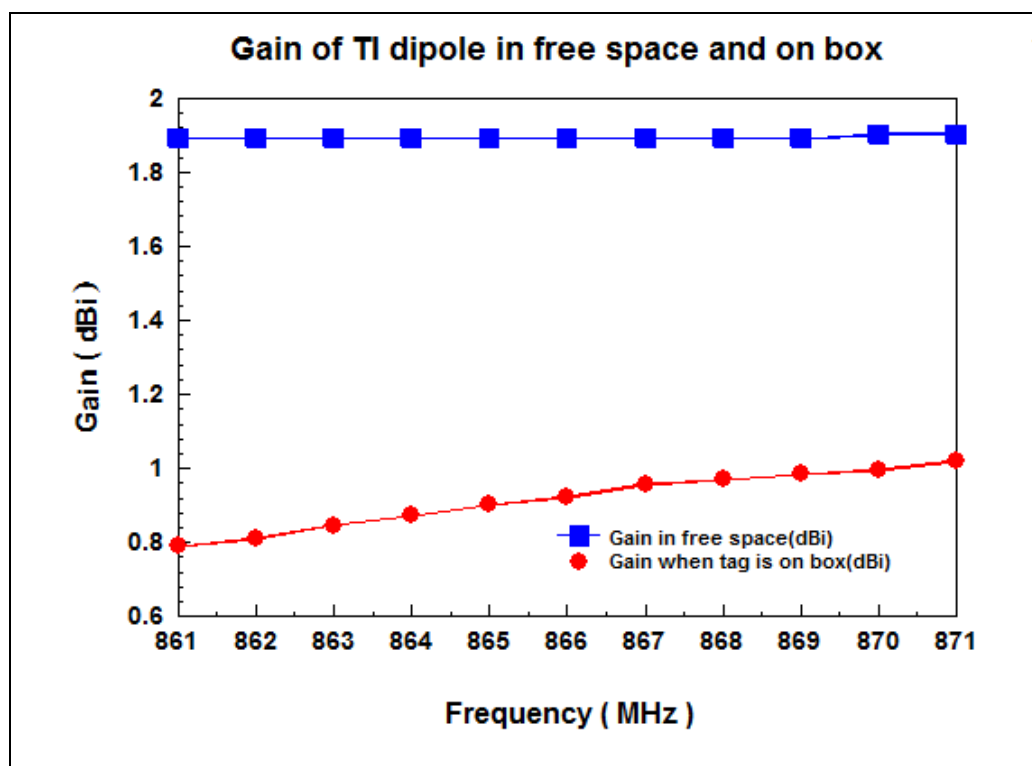


Figure 3.45. Gain of TI dipole in free space and on paper box

3.4. COMPARATIVE STUDY OF DIPOLE-LIKE STRUCTURES WITH OUR DESIGN

This section covers comparative study of designed tag and TI dipole antenna in terms of free space analysis, on metallic can analysis, on water carboy analysis, on wooden strip analysis and lastly on paper box analysis.

3.4.1. Free Space Analysis

Designed patch antenna has impedance of $35.12 + j161.87 \Omega$ with a gain of 2.68 dBi while TI dipole has impedance of $28.81 + j46.44 \Omega$ with a gain of 1.89 dBi in free space. Comparative results are given on Table 3.5;

Table 3.5. Comparative results for designed patch and TI dipole in free space

| Frequency (MHz) | G_{patch} (dBi) | $G_{TI\ dipole}$ (dBi) | Z_{patch} (Ω) | $Z_{TI\ dipole}$ (Ω) |
|-----------------|-------------------|------------------------|--------------------------|-------------------------------|
| 861 | 2.46 | 1.89 | 17.1+j124.7 | 35.8+j44.3 |
| 862 | 2.50 | 1.89 | 18.7+j128.9 | 34.7+j44.5 |
| 863 | 2.54 | 1.89 | 20.5+j133.3 | 33.6+j44.8 |
| 864 | 2.56 | 1.89 | 22.5+j138.1 | 32.6+j45.1 |
| 865 | 2.61 | 1.89 | 25.0+j143.3 | 31.6+j45.4 |
| 866 | 2.63 | 1.89 | 27.8+j149.0 | 30.6+j45.3 |
| 867 | 2.66 | 1.89 | 31.2+j155.1 | 29.7+j46.1 |
| 868 | 2.68 | 1.89 | 35.1+j161.9 | 28.8+j46.4 |
| 869 | 2.70 | 1.89 | 39.9+j169.3 | 28.0+j46.8 |
| 870 | 2.72 | 1.90 | 45.6+j177.5 | 27.2+j47.2 |
| 871 | 2.74 | 1.90 | 52.7+j186.5 | 26.4+j47.6 |

It can be understood from Table 3.5 that, designed patch performs better than TI dipole in terms of gain and impedance at 868 MHz via having impedance of $35.1+j161.9\ \Omega$ and gain of 2.68 dBi. Our patch design has 0.79 dBi more gain than TI dipole antenna in free space.

3.4.2. On Metallic Can Analysis

When designed patch antenna is placed on top of metallic CAN, small performance degradation is observed. But for TI dipole, major performance degradation is seen. The impedance which is $28.8+j46.4\ \Omega$ in free space drops to $0.01+j68.1\ \Omega$ for TI dipole. But for designed patch, it is seen impedance of $35.1+j161.9\ \Omega$ in free space analysis. When designed patch is placed on top of metallic CAN, impedance is $35.7+j163.8\ \Omega$. As it is seen that, there is considerably less degradation in terms of impedance. Table 3.6 gives the comparative results for both designed patch and TI dipole for on/near- metal placement.

Table 3.6. Comparative results for designed patch and TI dipole on metallic can

| Frequency (MHz) | G_{patch} (dBi) | $G_{TI\ dipole}$ (dBi) | Z_{patch} (Ω) | $Z_{TI\ dipole}$ (Ω) |
|-----------------|-------------------|------------------------|--------------------------|-------------------------------|
| 861 | 2.50 | 2.48 | 17.5+j126.3 | 0.01+j67.4 |
| 862 | 2.56 | 2.48 | 19.0+j130.4 | 0.01+j67.5 |
| 863 | 2.59 | 2.49 | 20.8+j134.9 | 0.01+j67.6 |
| 864 | 2.63 | 2.51 | 22.9+j139.7 | 0.01+j67.7 |
| 865 | 2.67 | 2.53 | 25.4+j145 | 0.01+j67.8 |
| 866 | 2.70 | 2.55 | 28.2+j150.6 | 0.01+j67.9 |
| 867 | 2.72 | 2.58 | 31.7+j157 | 0.01+j68 |
| 868 | 2.75 | 2.59 | 35.7+j163.8 | 0.01+j68.1 |
| 869 | 2.77 | 2.66 | 40.6+j171.4 | 0.01+j68.2 |
| 870 | 2.79 | 2.69 | 46.6+j179.7 | 0.01+j68.3 |
| 871 | 2.80 | 2.72 | 54+j189 | 0.01+j68.4 |

3.4.3. On Water Carboy Analysis

Comparative results for tag on water carboy are given in Table 3.7,

Table 3.7. Comparative results for designed tag and TI dipole on water carboy

| Frequency (MHz) | G_{patch} (dBi) | $G_{TI\ dipole}$ (dBi) | Z_{patch} (Ω) | $Z_{TI\ dipole}$ (Ω) |
|-----------------|-------------------|------------------------|--------------------------|-------------------------------|
| 861 | 2.83 | 0.01 | 21.7+j140.9 | 1.81+j80.8 |
| 862 | 2.79 | 0.01 | 24.6+j145.7 | 1.82+j80.9 |
| 863 | 2.76 | 0.01 | 28.4+j149.1 | 1.82+j81.1 |
| 864 | 2.73 | 0.01 | 33.5+j152.2 | 1.82+j81.2 |
| 865 | 2.69 | 0.01 | 34.3+j157.9 | 1.83+j81.4 |
| 866 | 2.65 | 0.01 | 36.2+j161.4 | 1.83+j81.5 |
| 867 | 2.63 | 0.01 | 38.4+j165.3 | 1.84+j81.7 |
| 868 | 2.59 | 0.01 | 40.99+j170.16 | 1.84+j81.8 |
| 869 | 2.55 | 0.01 | 43.2+j174.4 | 1.85+j81.9 |
| 870 | 2.52 | 0.01 | 45.3+j179.7 | 1.85+j82.1 |
| 871 | 2.49 | 0.009 | 49.8+j182.2 | 1.86+j82.2 |

3.4.4. On Wooden Strip Analysis

Table 3.8 shows comparative results for designed patch and TI dipole on wooden strip;

Table 3.8. Comparative results for designed patch and TI dipole on wooden strip

| Frequency (MHz) | G_{patch} (dBi) | $G_{TI\ dipole}$ (dBi) | Z_{patch} (Ω) | $Z_{TI\ dipole}$ (Ω) |
|-----------------|-------------------|------------------------|--------------------------|-------------------------------|
| 861 | 2.42 | 0.79 | 33.2+j117.3 | 3.18+j65.8 |
| 862 | 2.45 | 0.81 | 36.4+j121.3 | 3.12+j66.1 |
| 863 | 2.47 | 0.85 | 44.1+j124.7 | 3.07+j66.7 |
| 864 | 2.49 | 0.87 | 48.2+j33.7 | 3.02+j66.9 |
| 865 | 2.52 | 0.90 | 52.2+j138.8 | 2.95+j67.1 |
| 866 | 2.55 | 0.92 | 56.5+j142.7 | 2.93+j67.4 |
| 867 | 2.57 | 0.96 | 62.7+j145.6 | 2.91+j67.3 |
| 868 | 2.60 | 0.97 | 65.2+j148.9 | 2.89+j67.6 |
| 869 | 2.62 | 0.98 | 69.5+j152.1 | 2.88+j67.7 |
| 870 | 2.63 | 1.0 | 73.8+j155.7 | 2.86+j67.8 |
| 871 | 2.67 | 1.02 | 79.2+j159.3 | 2.84+j68 |

3.4.5. On Paper Box Analysis

Table 3.9 gives the comparative results for designed patch and TI dipole when placed on paper box.

Table 3.9. Comparative results for designed patch and TI dipole on paper box

| Frequency (MHz) | G_{patch} (dBi) | $G_{TI\ dipole}$ (dBi) | Z_{patch} (Ω) | $Z_{TI\ dipole}$ (Ω) |
|-----------------|-------------------|------------------------|--------------------------|-------------------------------|
| 861 | 2.40 | 0.79 | 31.8+j100.8 | 2.98+j57.7 |
| 862 | 2.44 | 0.81 | 38.6+j102.6 | 2.95+j59.8 |
| 863 | 2.49 | 0.85 | 42.8+j106.2 | 2.90+j61.3 |
| 864 | 2.50 | 0.87 | 47.9+j109.9 | 2.87+j64.4 |
| 865 | 2.54 | 0.90 | 51.1+j112.6 | 2.83+j67.6 |
| 866 | 2.59 | 0.92 | 55.4+j116.4 | 2.80+j69.7 |
| 867 | 2.62 | 0.96 | 60.8+j120.5 | 2.76+j72.7 |
| 868 | 2.66 | 0.97 | 63.7+j123.1 | 2.73+j74.6 |
| 869 | 2.69 | 0.98 | 68.8+j129 | 2.70+j77.6 |
| 870 | 2.71 | 1.0 | 72.7+j134.5 | 2.67+j80.7 |
| 871 | 2.73 | 1.02 | 77.8+j139.8 | 2.64+j83.6 |

All of the studies performed on designed patch and TI dipole antenna show that designed tag performs better than TI does in terms of gain and impedance. While TI dipole has performance degradation on metal, plastics, paper and wood; designed patch is not affected considerably.

3.5. MEASUREMENTS

Before fabricating the designed antenna on dielectric substrate with height of 3.175 mm, similar structure having dimensions of 84x84 mm² is fabricated on Rogers RO 3006 dielectric substrate which has dielectric constant of 6.15 and height of 1.57 mm. After we performed measurements and we realized that fabricated patch antenna was not adequate in terms of gain and radiation efficiency. Hence, we decided to increase the height of dielectric substrate from 1.57 mm to 3.175 mm and use Taconic RF 43 type dielectric substrate which has dielectric constant of 4.3 and loss factor of 0.0033.

Top and bottom sides of the designed patch drawn in Eagle for prototyping in Figure 3.46 (a) and (b);

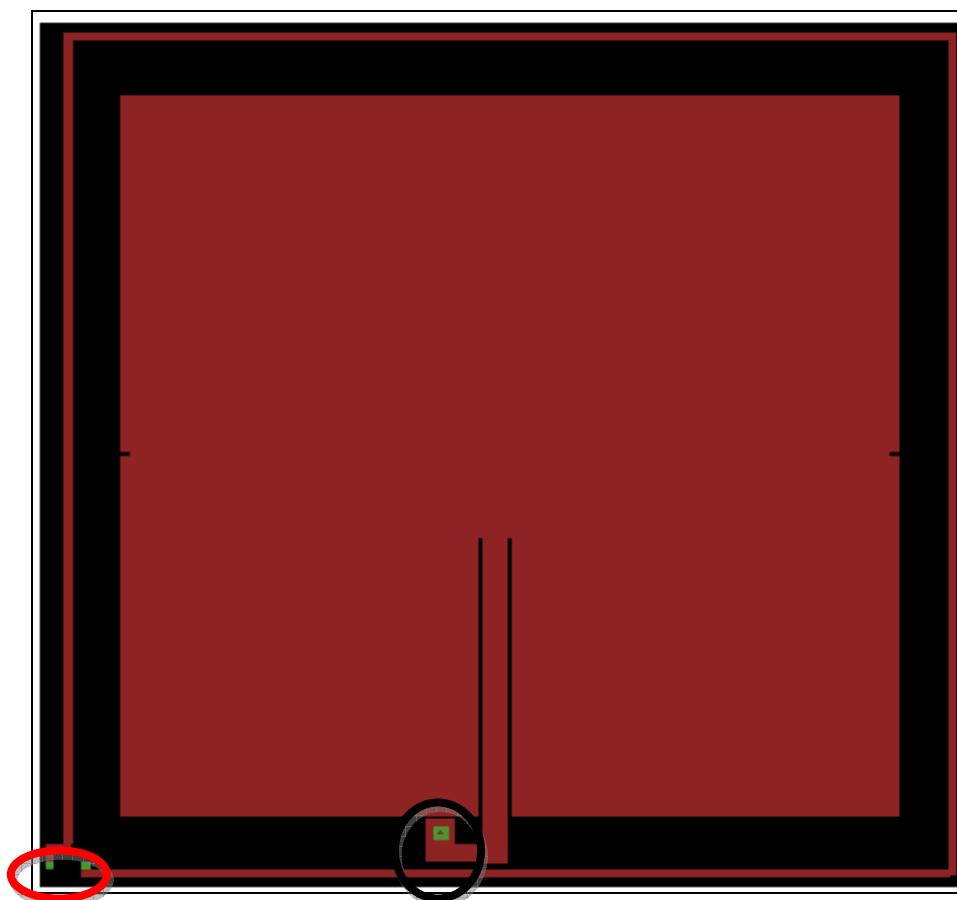


Figure 3.46.a) Top view of the EAGLE drawing of patch antenna

On both figures, via points are shown with green color. There are three vias used for the final design. One of the vias, pointed with black circle, is used to feed the UHF antenna. The other one, pointed with red circle, is used to feed the HF antenna, and the remaining via is used to connect bottom spiral to the upper one.

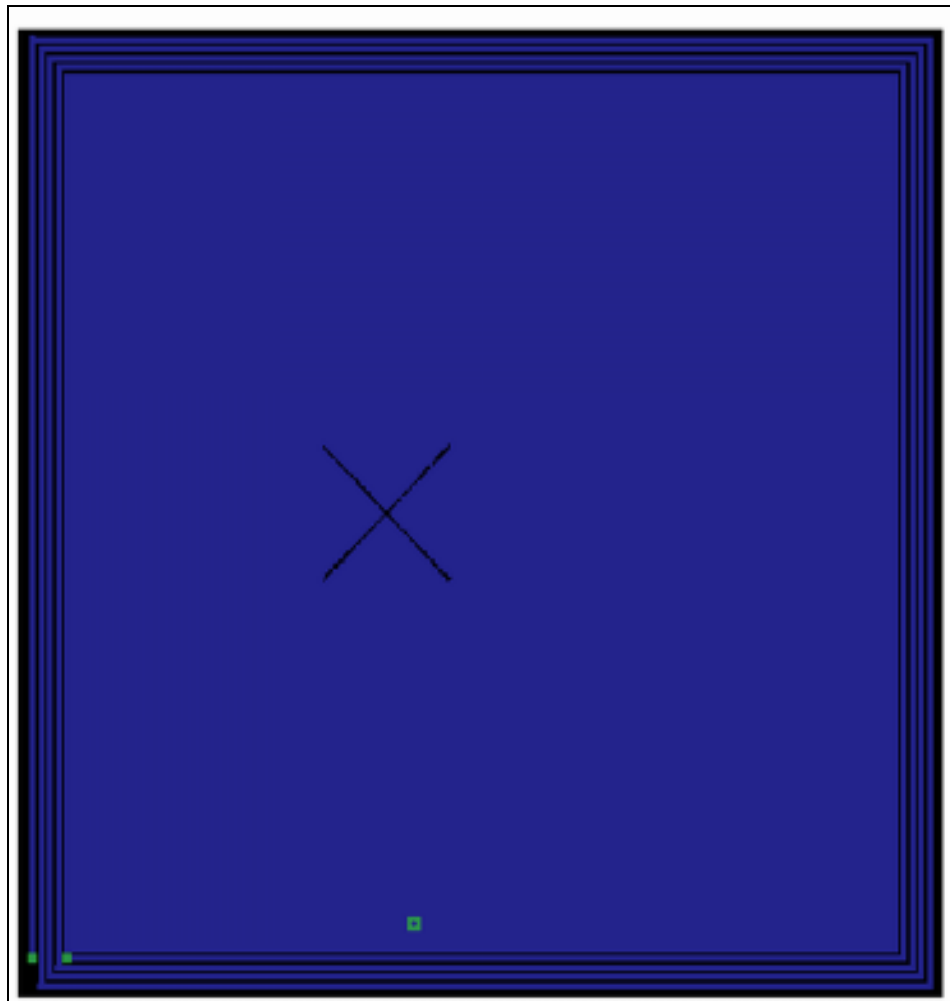


Figure 3.46.b) Bottom view of EAGLE drawing of patch antenna

It was difficult to fabricate the patch antenna on dielectric substrate, since there were very small line separations in the design such as 0.3 mm.

After the prototypes being fabricated, the vias are drilled using electric drill which has drilling bit of 1.2 mm. Top and bottom views of the latest prototype are given on Figures 3.47 (a) and (b);



Figure 3.47.a) Top view of latest prototype



Figure 3.47.b) Bottom view of latest prototype

3.5.1. One-Port Impedance Measurements

3.5.1.1. One-Port Impedance Measurements for HF Antenna

One port of the network analyzer is connected to the feed of the HF antenna. HF antenna combined with UHF antenna is previously shown in Figures 3.47 (a) and (b). We measured impedance of at 13.56 MHz which corresponds to $2.54 \mu H$. Figure 3.48 shows how inductance changes with frequency including simulations.

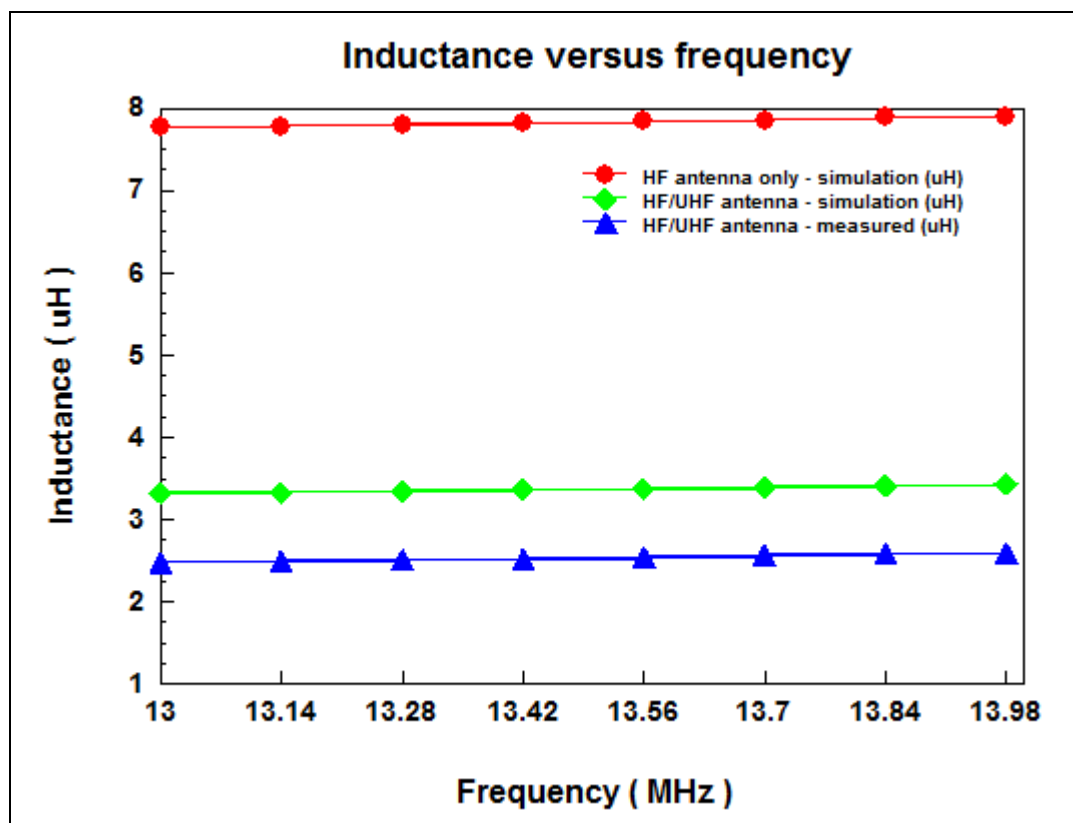


Figure 3.48. Inductance versus frequency

It is seen in Figure 3.48 that, when dielectric substrate, upper patch antenna and bottom side ground plane are added, there is inductance loss observed compared to pure inductance in free space. There is also difference between the measurement and simulation result.

3.5.1.2. One-Port Impedance Measurements for UHF Antenna in free space

We achieved an impedance of $35.1+j161.9 \Omega$ during simulation. During measurements, we obtained $40.3+j163.5 \Omega$. It is seen that there is small difference in terms of real and imaginary part of the impedance. Comparative results for designed tag antenna in simulation and measurement are shown in Figure 3.49 (a) and (b);

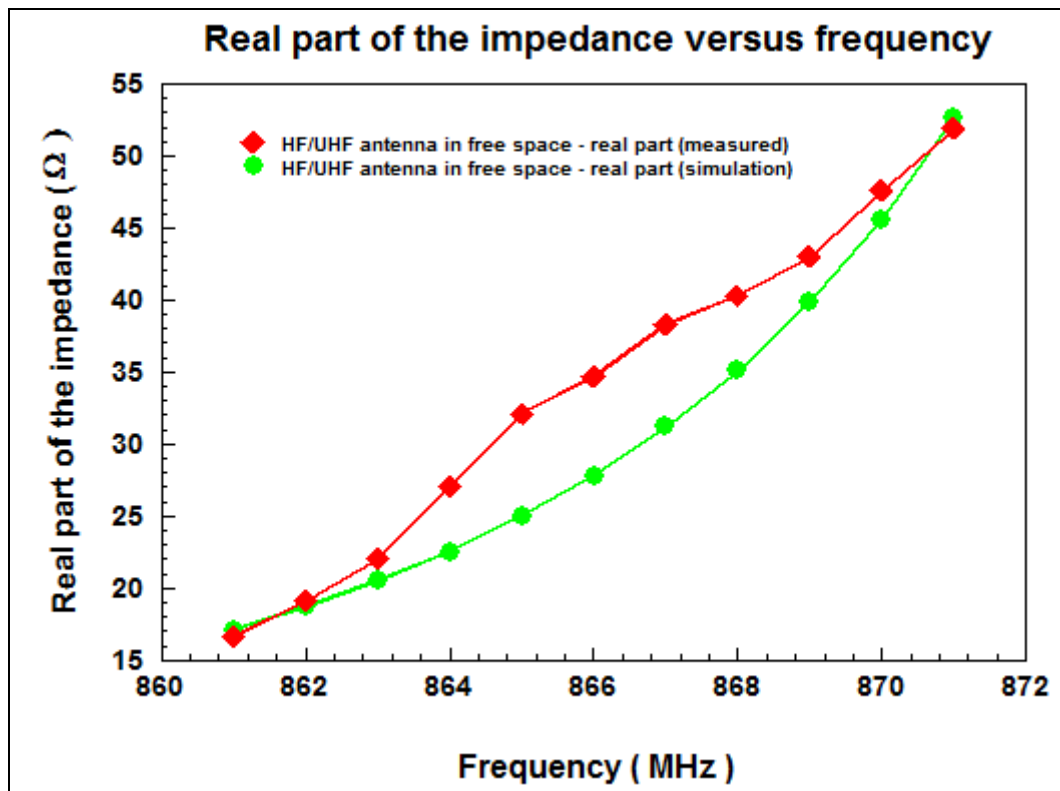


Figure 3.49.a) Real part of impedance for simulation and measurement

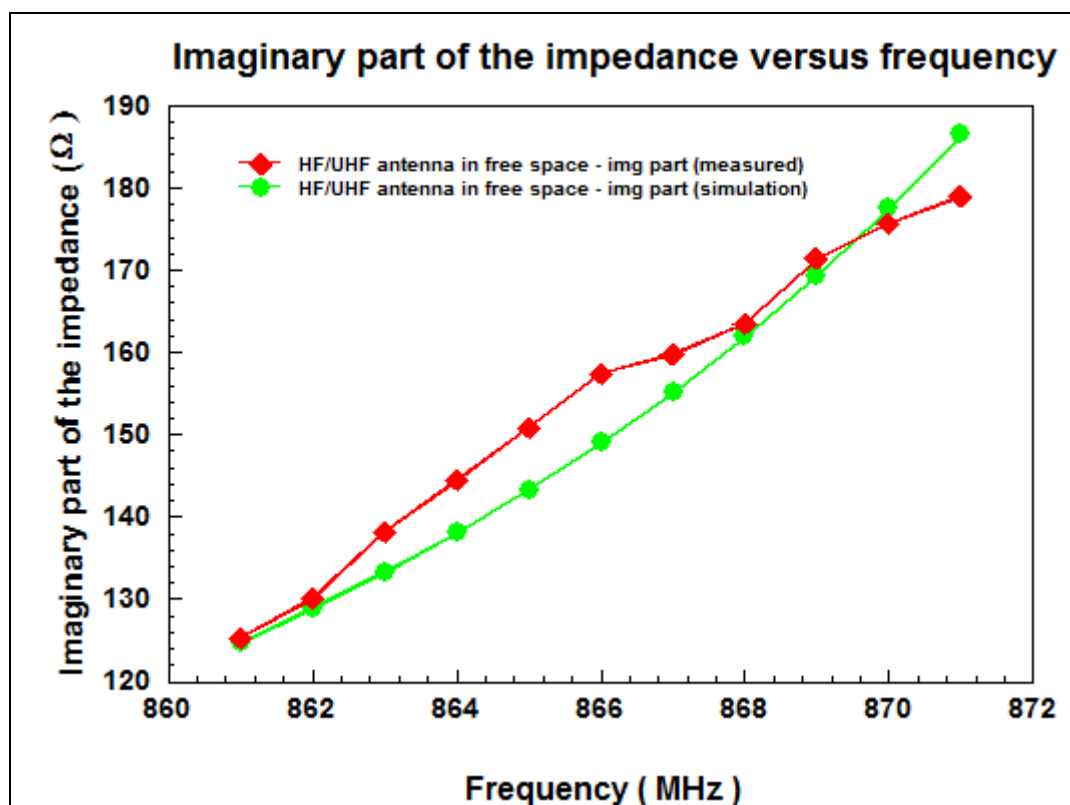


Figure 3.49.b) Imaginary part of the impedance for simulation and measurement

3.5.1.3. One-port impedance measurements for UHF antenna on metallic can

After getting results for designed tag antenna in free space, next step is to perform measurements when tag antenna is on metallic can having height of 32.5 cm and radius of 13.5 cm. Figure 3.50 shows the designed tag placed on top of metallic can;

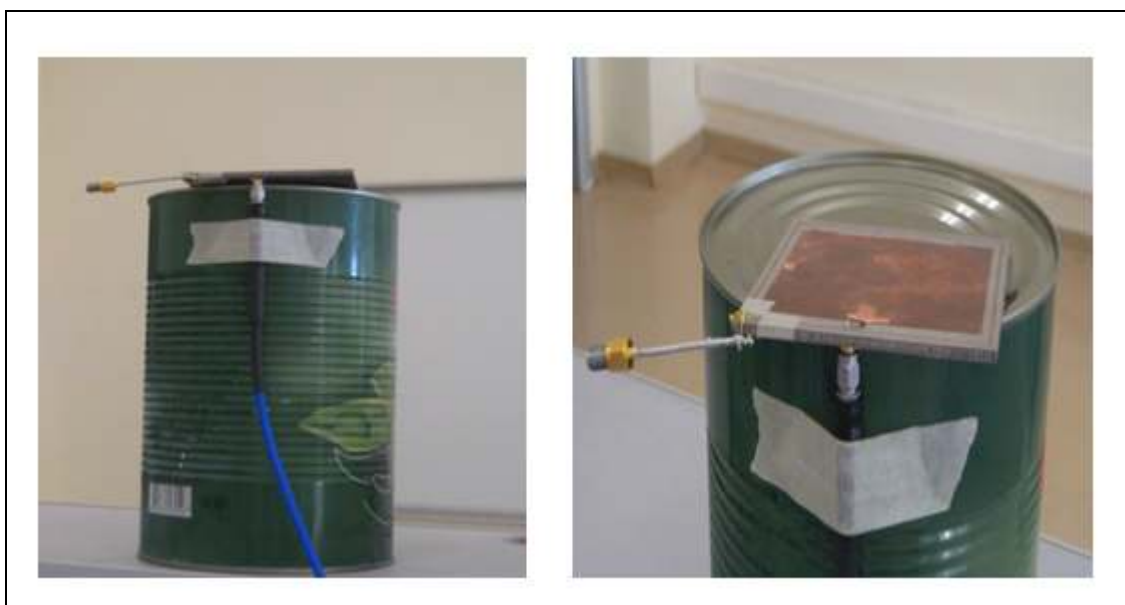


Figure 3.50. Designed tag antenna on metallic can

We obtained impedance of $35.7+j163.8 \Omega$ during simulation. Measurement result shows $31+j147.3 \Omega$. There is some difference between simulation and measurement results. But the difference is small. Compared to measurements, there is not much degradation Figure 3.51 (a) and (b) show how real and imaginary part of the impedance changes with frequency in free space and on metallic can;

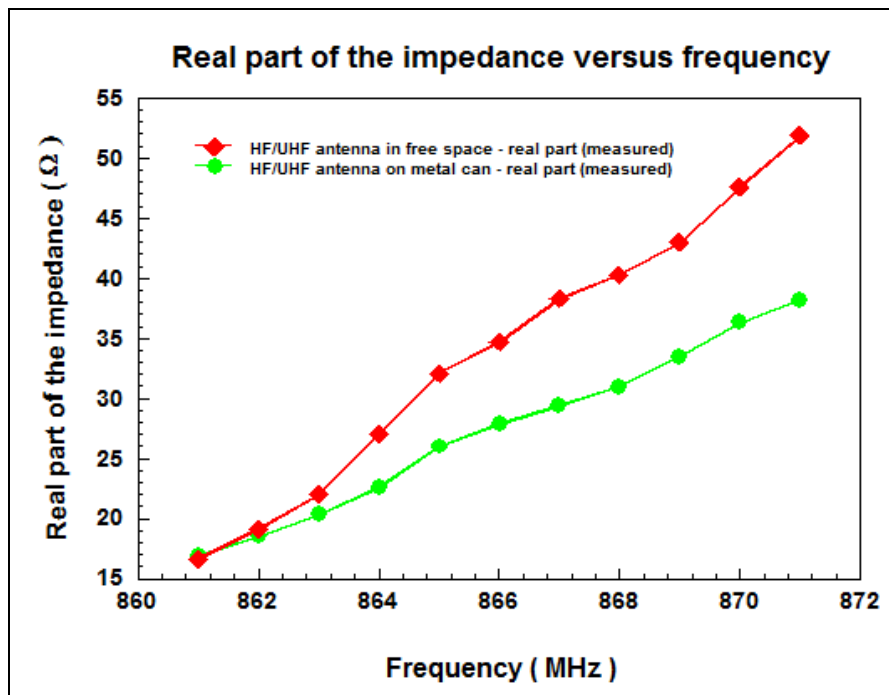


Figure 3.51.a) Measurement of real part of the impedance versus frequency when tag antenna in free space and on metallic can

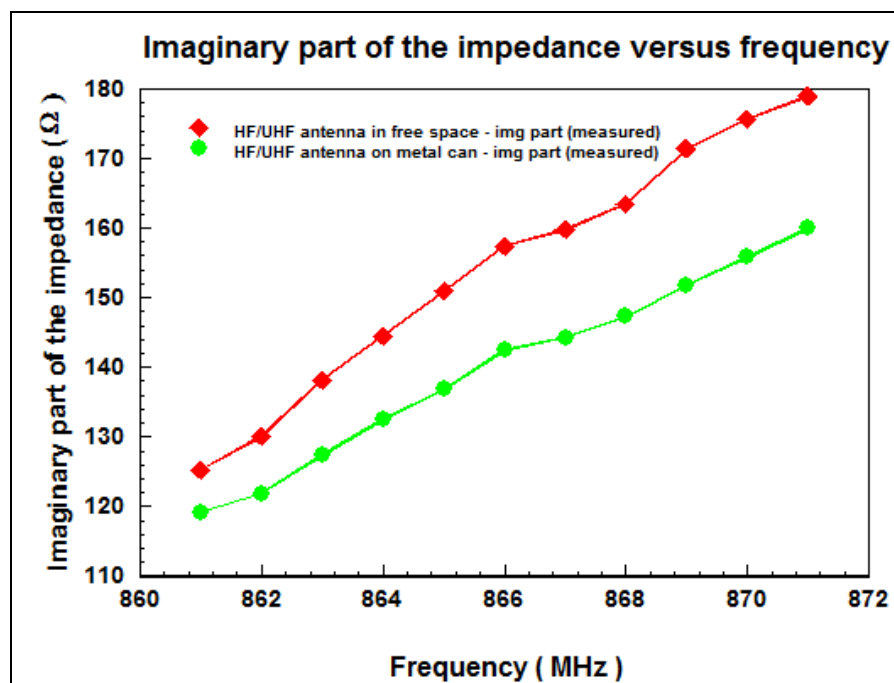


Figure 3.51.b) Measurement of imaginary part of the impedance versus frequency when tag antenna in free space and on metallic can

Figure 3.52 (a) and (b) show how real and imaginary part of the tag antenna on metallic can changing with frequency in simulation and measurements;

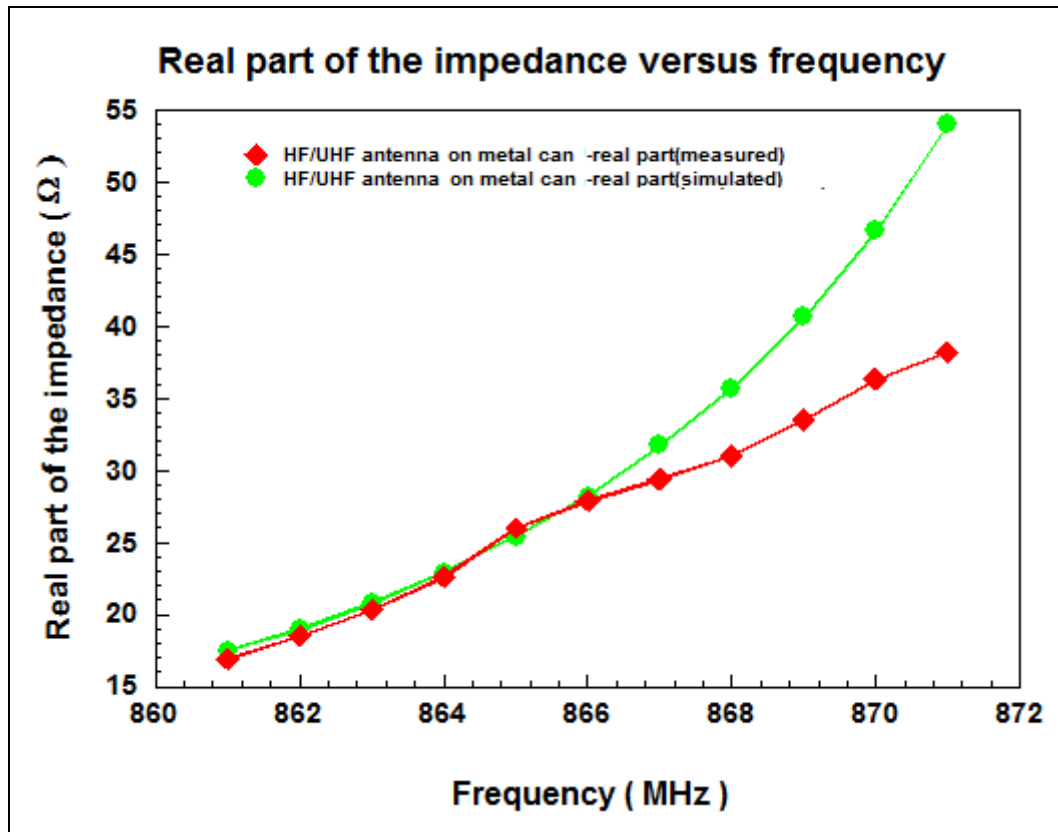


Figure 3.52.a) Real part of the impedance versus frequency for measurement and simulation

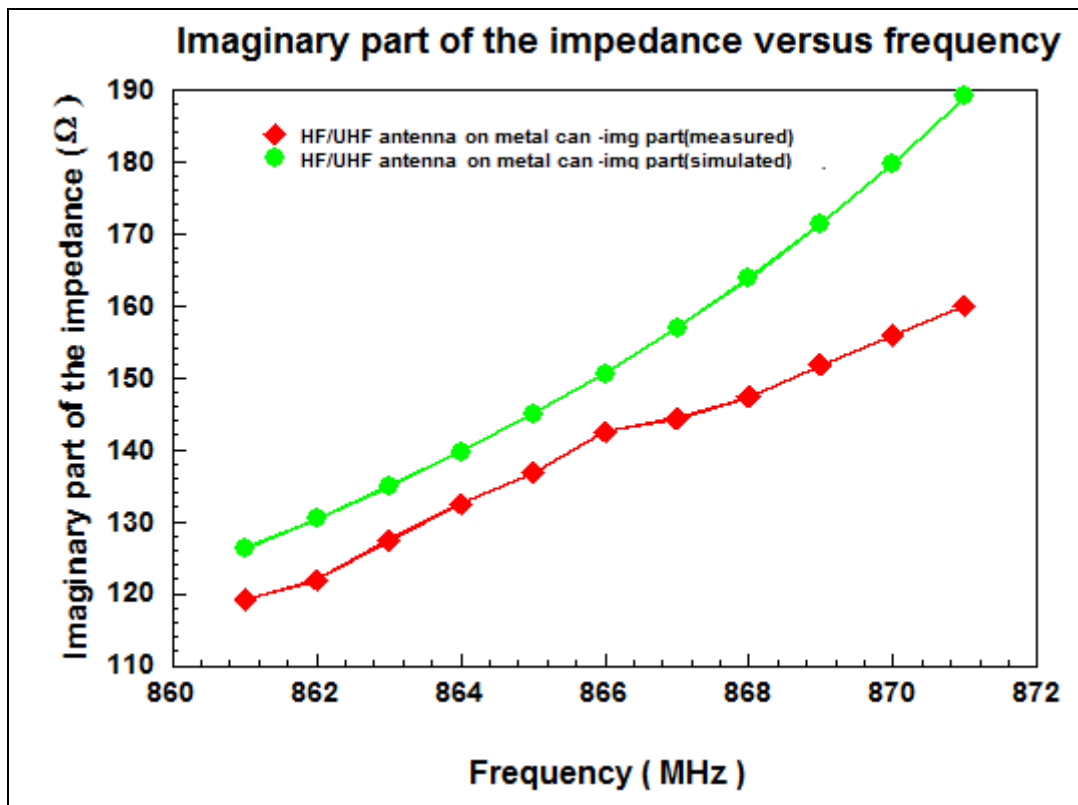


Figure 3.52.b) Imaginary part of the impedance versus frequency for measurement and simulation

3.5.1.4. One-port impedance measurements for UHF antenna on water carboy

Figure 3.53 shows tag antenna placed on water carboy having height of 41 cm and radius of 18 cm,



Figure 3.53. Designed tag antenna on water carboy

An impedance of $40.99+j170.16 \Omega$ was obtained in simulation. Measurements show that the impedance is $39.2+j172.4 \Omega$. Figures 3.54 (a) and (b) both measurement and simulation results are parallel and close to each other.

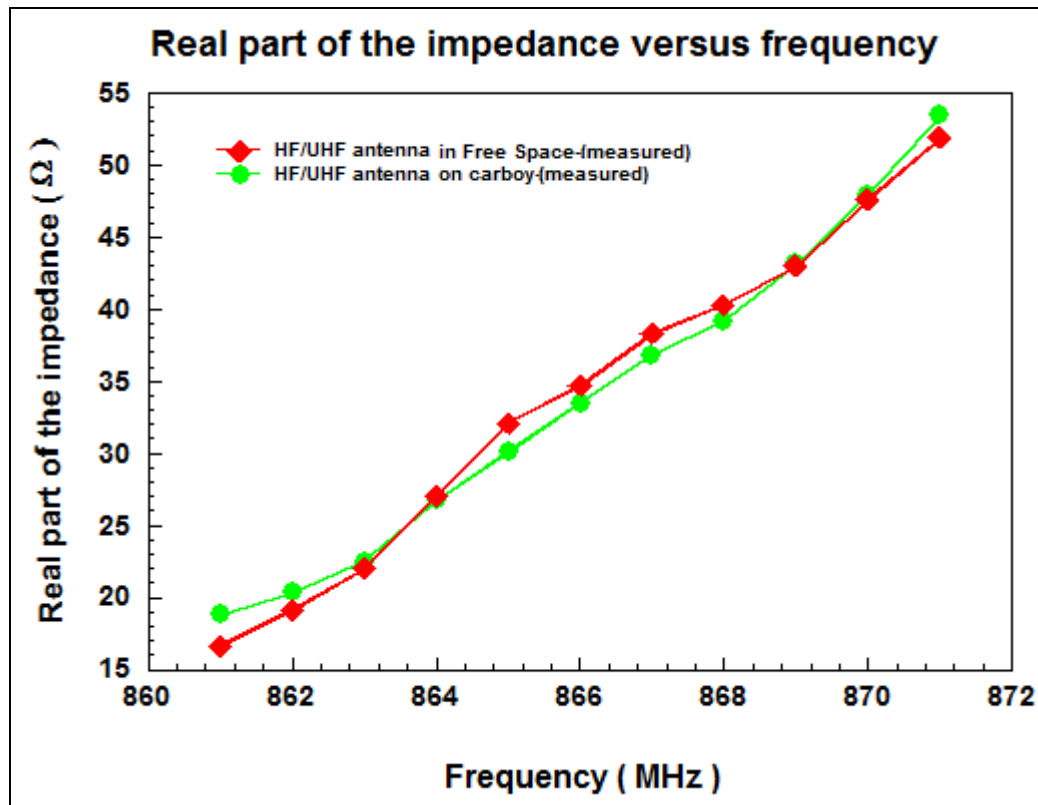


Figure 3.54.a) Measurement of real part of the impedance versus frequency when tag antenna in free space and on water carboy

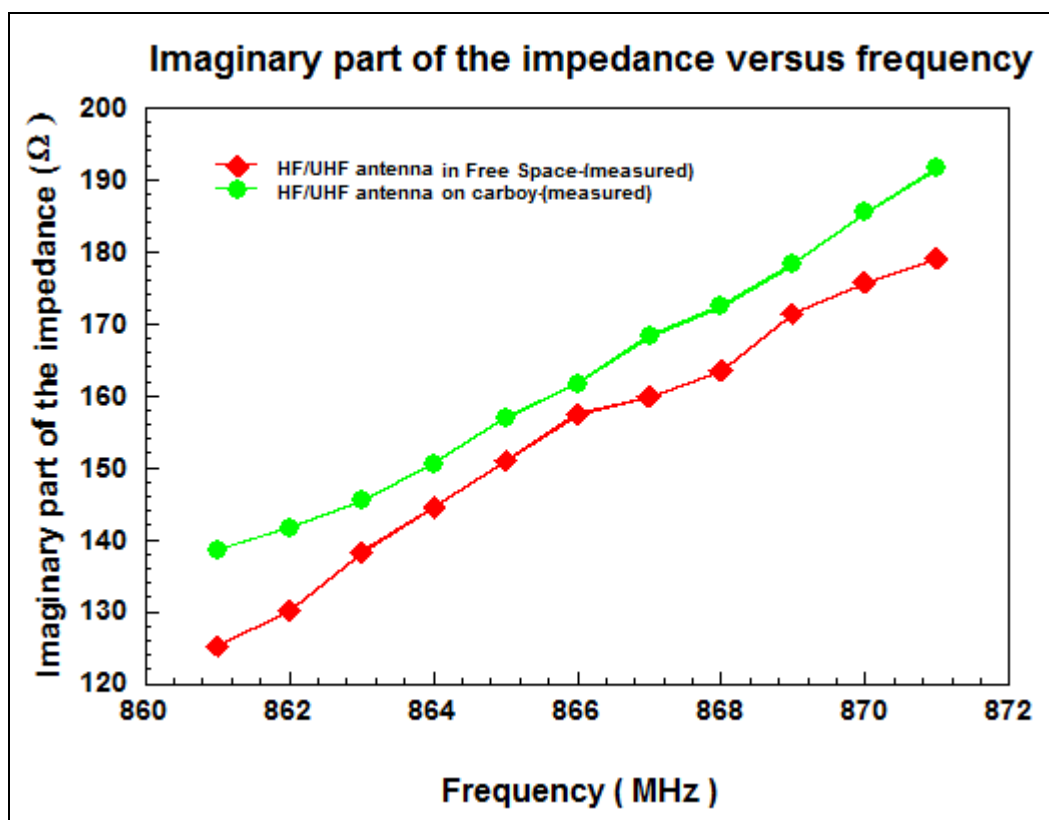


Figure 3.54.b) Measurement of imaginary part of the impedance versus frequency when tag antenna in free space and on water carboy

Figure 3.55 (a) and (b) shows the measured and simulated results with frequency for the tag antenna placed on plastic water carboy;

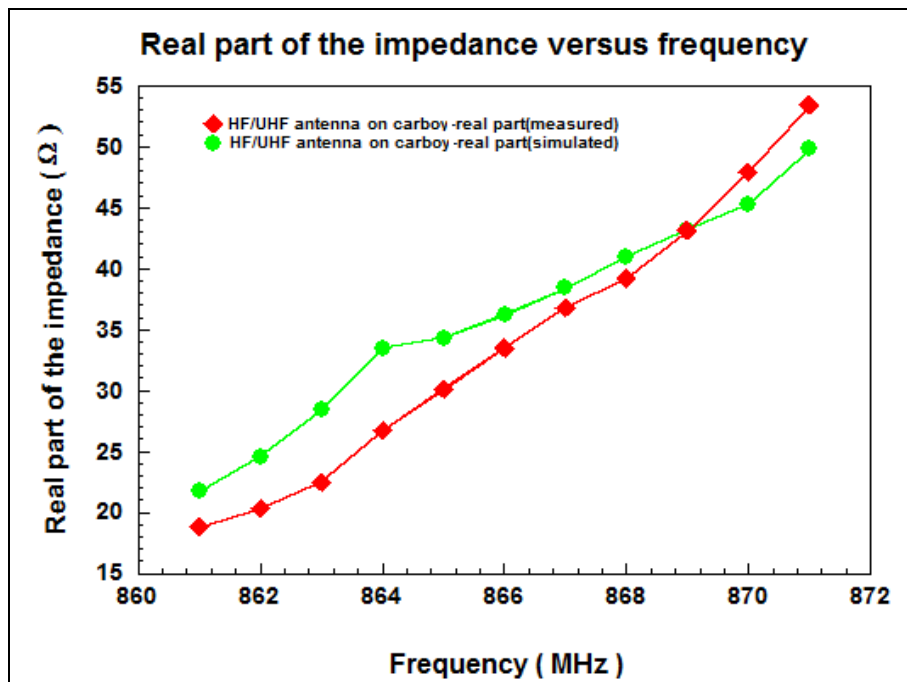


Figure 3.55.a) Real part of the impedance versus frequency for measurement and simulation

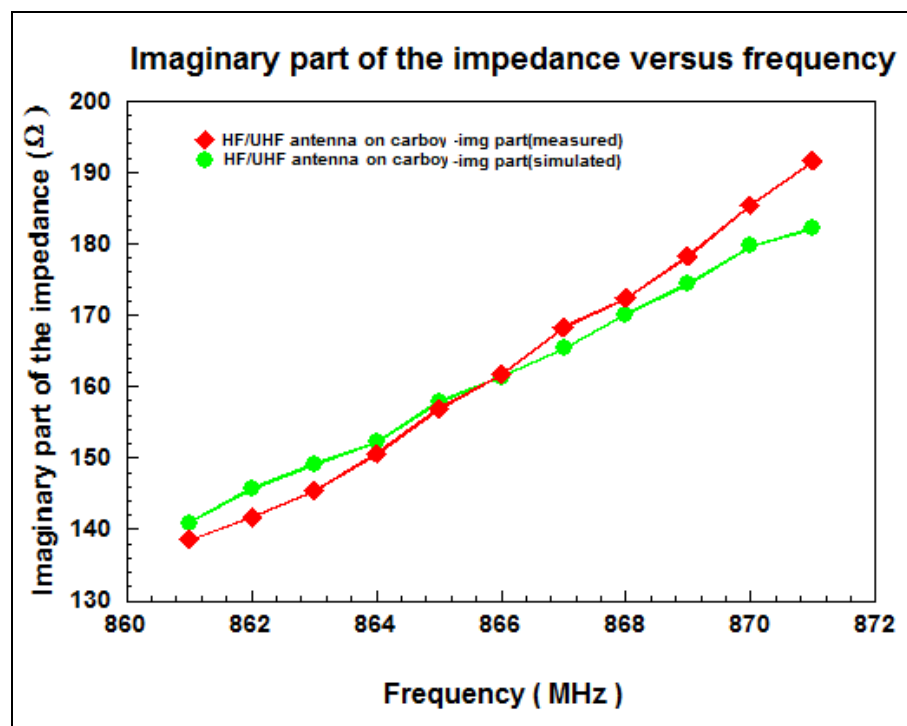


Figure 3.55.b) Imaginary part of the impedance versus frequency for measurement and simulation

3.5.1.5. *One-port impedance measurements for UHF antenna on wooden strip*

Figure 3.56 shows how the tag antenna is placed on top of the wooden strip having dimensions of 27.4x46.2 cm².

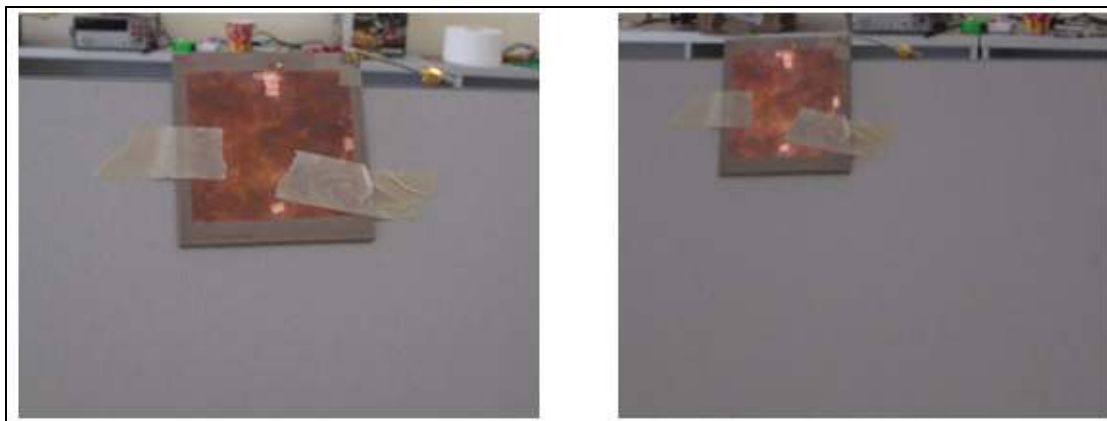


Figure 3.56. Designed tag on wooden strip

An impedance of $53.3+j141.2 \Omega$ is obtained with measurement at 868 MHz. As it is shown in Figure 3.57 (a) and (b) there is some difference between tag antenna in free space and tag antenna on wooden strip.

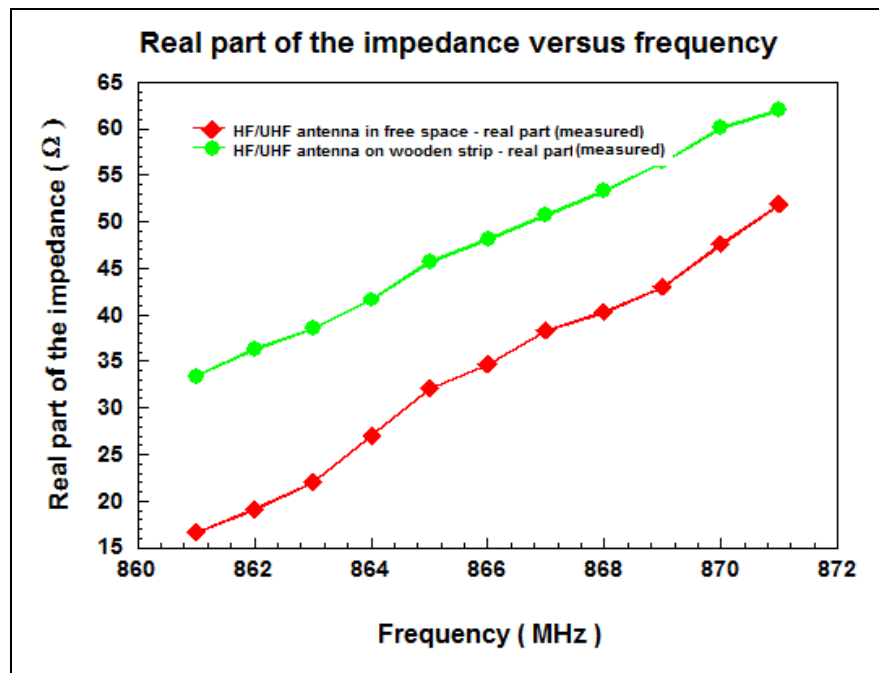


Figure 3.57.a) Measurement of real part of the impedance versus frequency when tag antenna in free space and on wooden strip

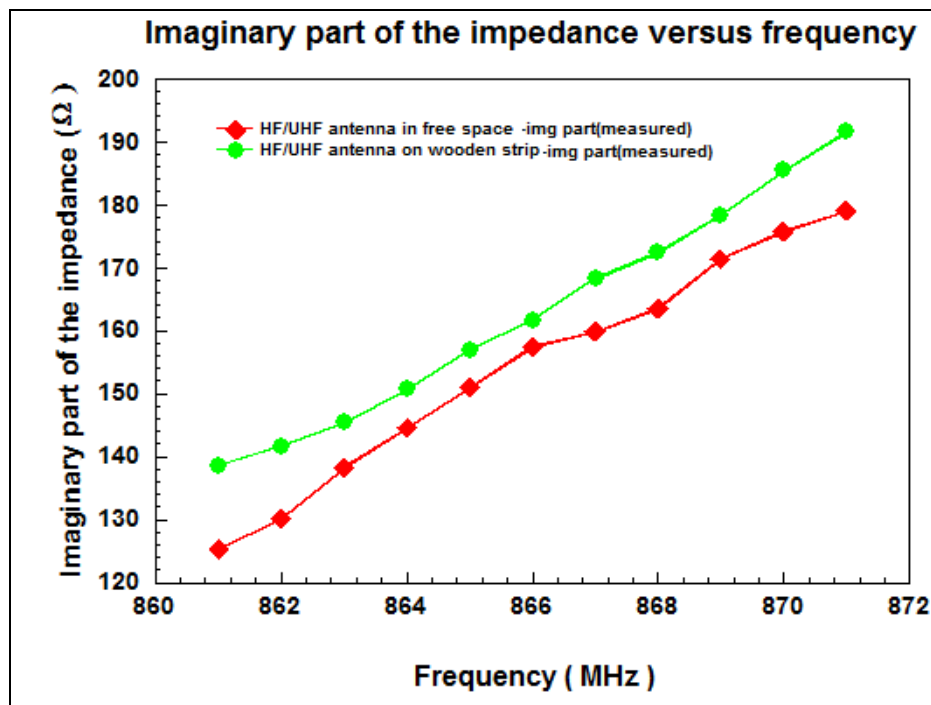


Figure 3.57.b) Measurement of imaginary part of the impedance versus frequency when tag antenna in free space and on wooden strip

Figure 3.58 (a) and (b) show how real and imaginary part of the impedance change with frequency for simulation and measurement results.

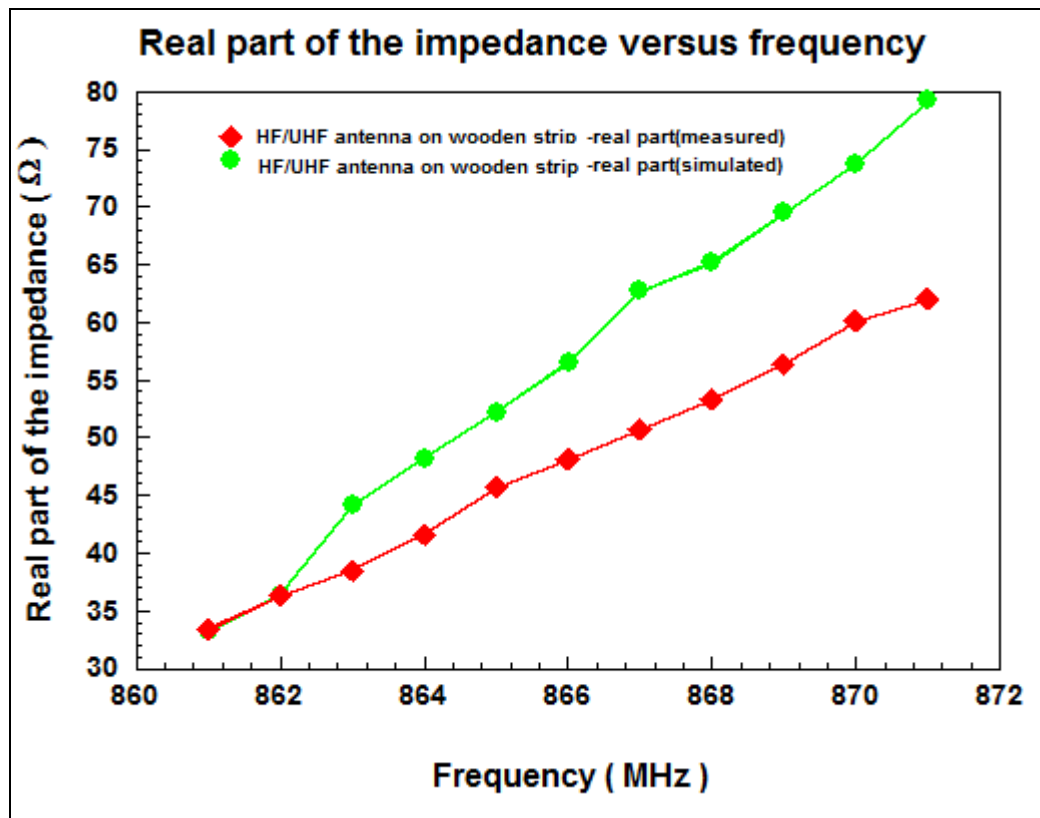


Figure 3.58.a) Real part of the impedance versus frequency for measurement and simulation ($53.3 + j141.2 \Omega$ with measurement and $65.2 + j148.9 \Omega$ with simulation)

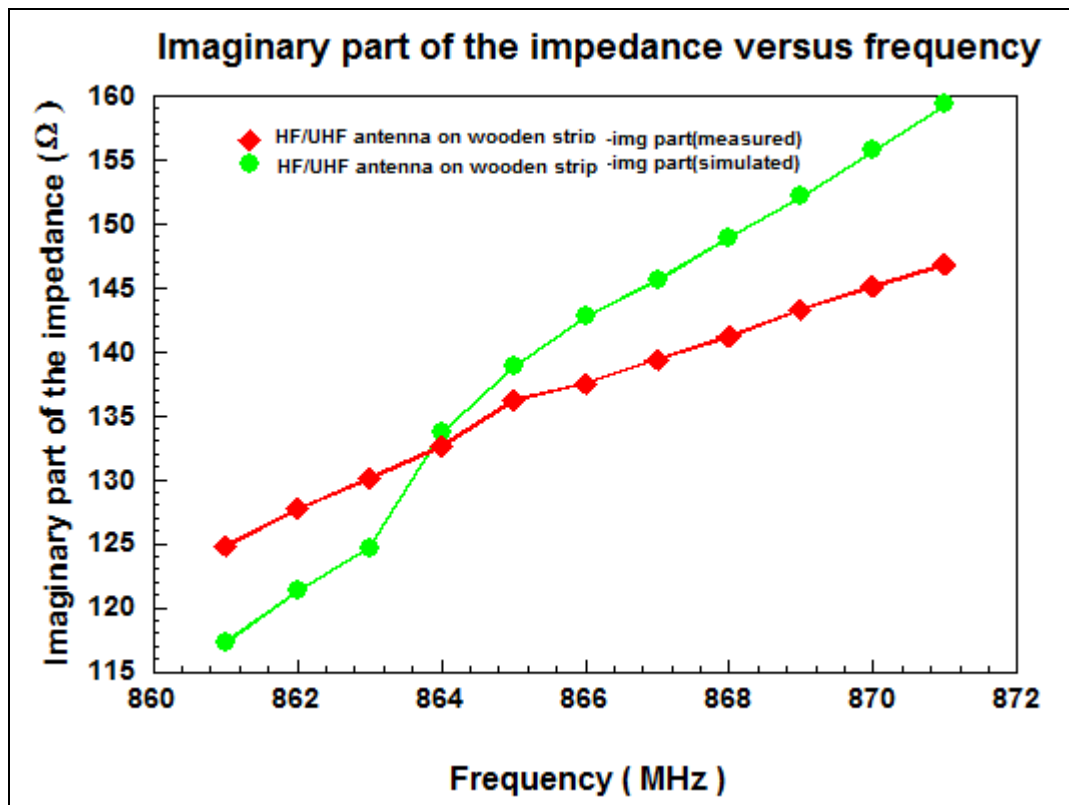


Figure 3.58.b) Imaginary part of the impedance versus frequency for measurement and simulation ($53.3 + j141.2 \Omega$ with measurement and $65.2 + j148.9 \Omega$ with simulation)

3.5.1.6. One-port impedance measurements for UHF antenna on paper box

Measurements are performed when tag antenna placed on paper box. In Figure 3.59, designed antenna on paper box having dimensions of $33 \times 67 \text{ cm}^2$ is given.

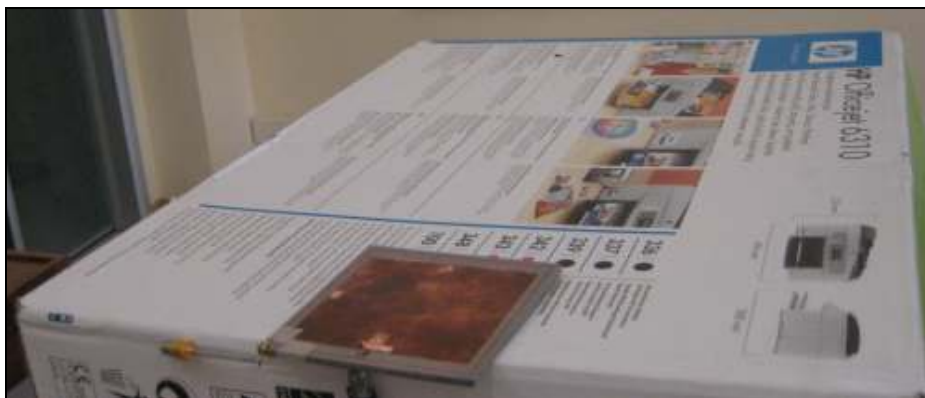


Figure 3.59. Designed tag on paper box

We performed measurements when tag antenna is on paper box. We observed $46.8+j164.7 \Omega$, which was $40.3+j163.5 \Omega$ when the antenna is in free space. As it is seen that there is very small difference between both tag antenna in free space and tag antenna on paper box. Figure 3.60 (a) shows how real part of the impedance changes with frequency;

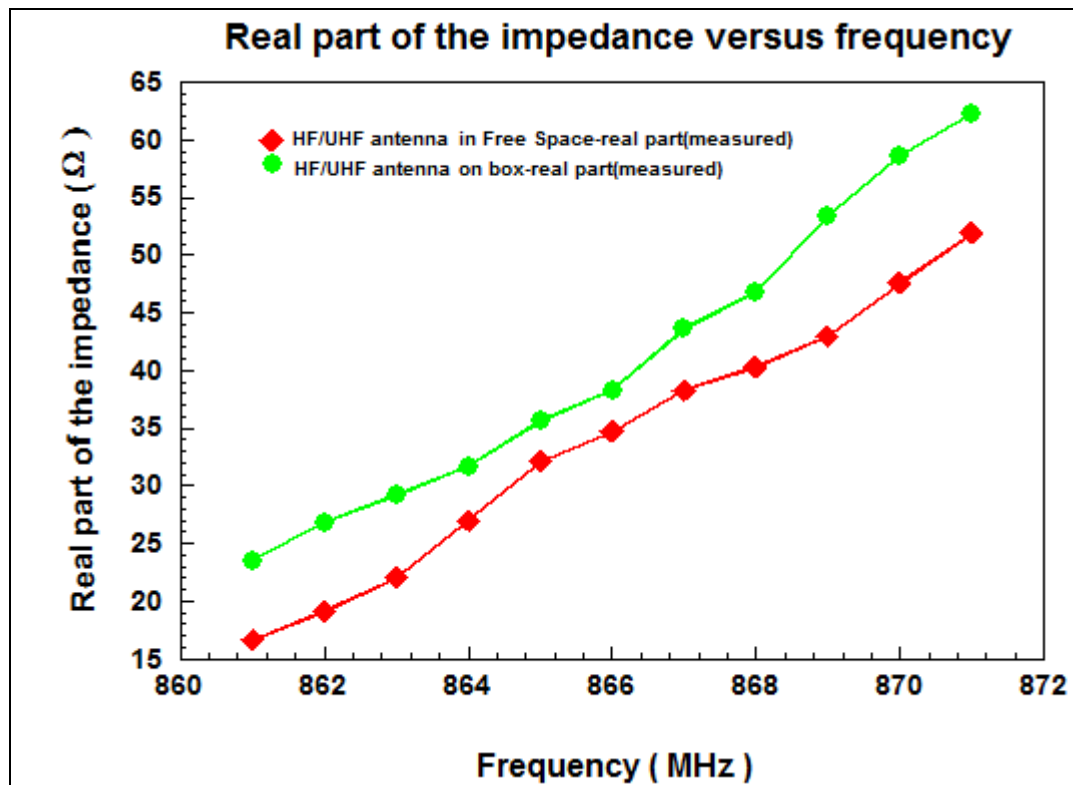


Figure 3.60.a) Measurement of real part of the impedance for tag antenna in free space and on paper box

Figure 3.60 (b) shows imaginary part versus frequency for tag antenna in free space and tag antenna on paper box.

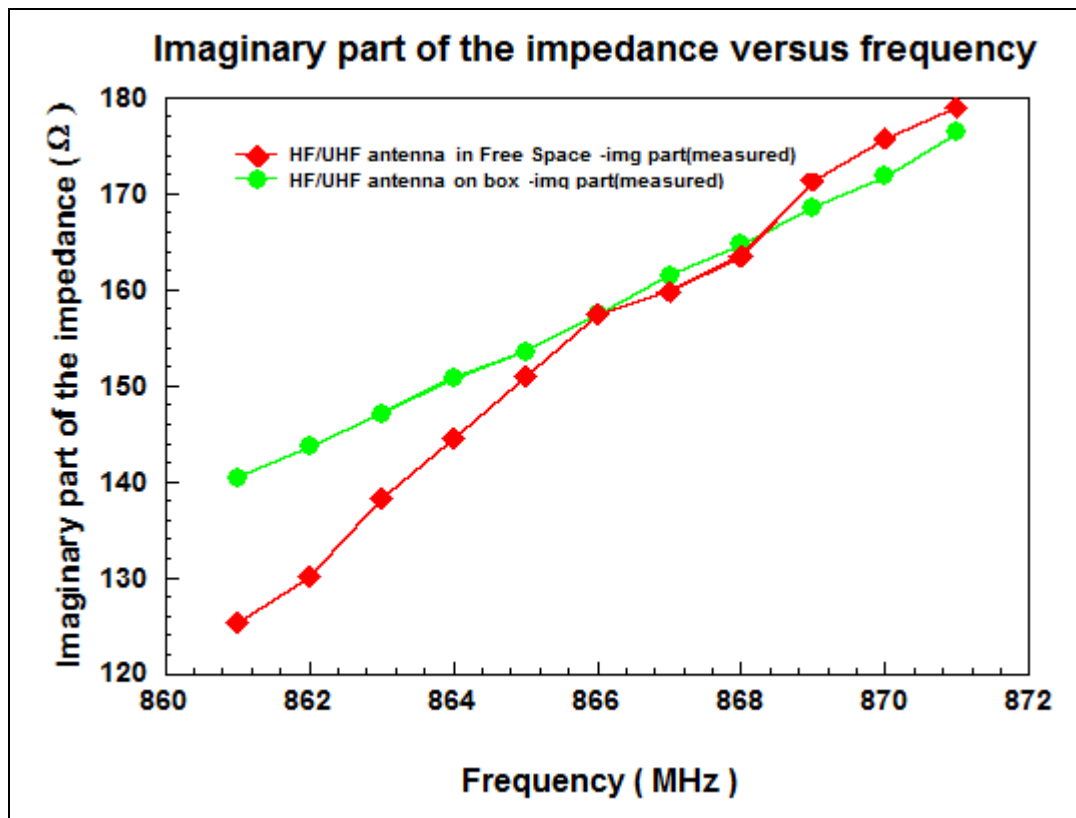


Figure 3.60.b Measurement of imaginary part of the impedance for tag antenna in free space and on paper box

After comparing measurement results, we compared simulation and measurement results to each other. Simulation results show that we have $63.7+j123.1 \Omega$, whereas measurements show $46.8+j164.7 \Omega$. Figure 3.61 (a) and (b) shows how real and imaginary part of the impedance changes with frequency for simulation and measurement.

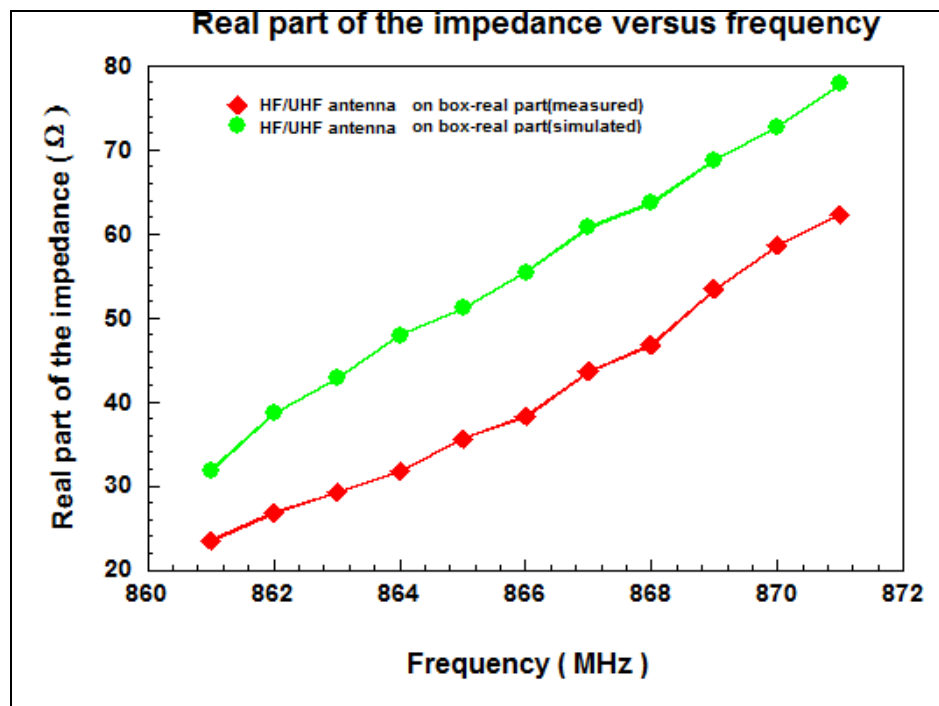


Figure 3.61.a) Real part of the impedance versus frequency for measurement and simulation

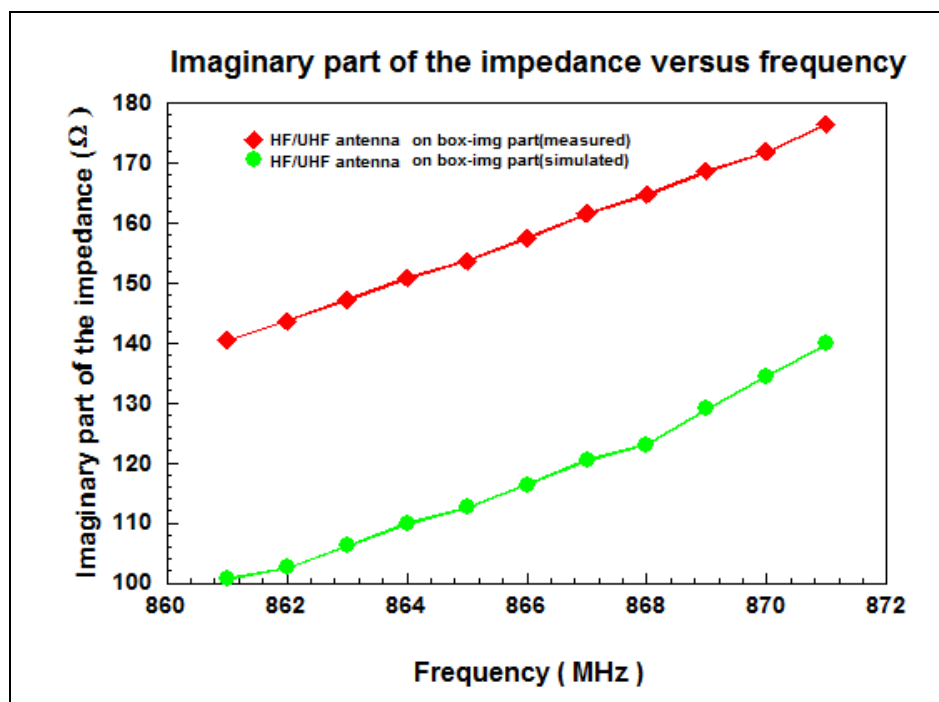


Figure 3.61.b) Imaginary part of the impedance versus frequency for measurement and simulation

3.5.2. Two-port (gain) measurements

Two-port measurements are performed for gain analysis. Previously measured and optimized two dipole antennas resonant at 868 MHz are used. Two dipoles are separated 4.55 m from each other. When two dipoles are measured and S_{21} is recorded as -41 dB. When the designed antenna is located 4.55 m far away from dipole antenna (which is 15λ stating that we are withing far-field region), the S_{21} is found to be -46 dB. After performing calculation, S_{21} is found to be -38 dB. It is calculated that mismatch factor causes 7.84 dB loss. The gain of the designed antenna is $S_{21DESIGNED} - S_{21DIPOLE} = GAIN$. It is found approximately 3 dBi. As it is seen that, this value for the gain is close to simulated one and also better than gain of referenced dipole antenna which has a gain of approximately 2.18 dBi [17].

Dipole antenna used during measurement is given in Figure 3.62 and measurement set up is seen in Figure 3.63,



Figure 3.62. Dipole antenna with balun used during measurement as reference

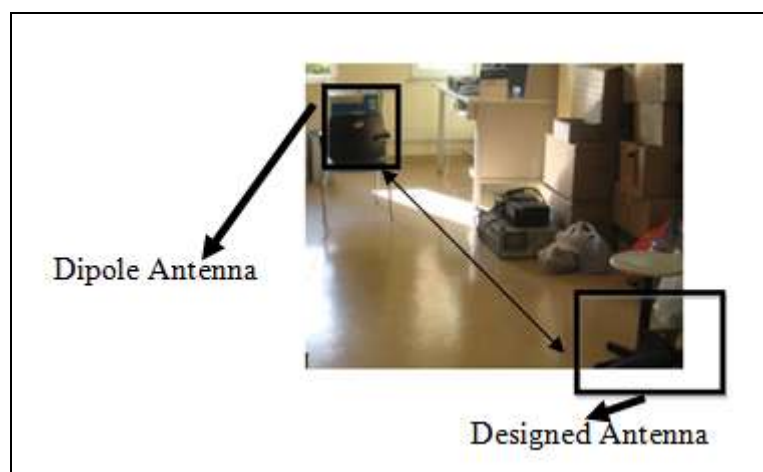


Figure 3.63. Measurement setup for gain analysis: far side: dipole antenna, near side: designed antenna and separation: 4.55 m (15λ confirms that we are within far-field)

4. HF/UHF READER ANTENNA DESIGN, SIMULATION AND MEASUREMENTS

4.1. Design and Simulation of HF/UHF Reader Antenna

In the previous section, it is objected to study the effects different kinds of environmental changes such as; metal, plastics, wood and paper on designed tag. To investigate the read/write capability of HF/UHF tag, we need a HF/UHF reader antenna.

4.1.1. Yagi UHF Reader Antenna Design and Simulations

A transmitter antenna which has high gain and easy to design is needed. Yagi antenna is a simple choice. The antenna consists of three different elements; driver, reflector and director. 3-element Yagi antenna structure is shown in Figure 4.1;

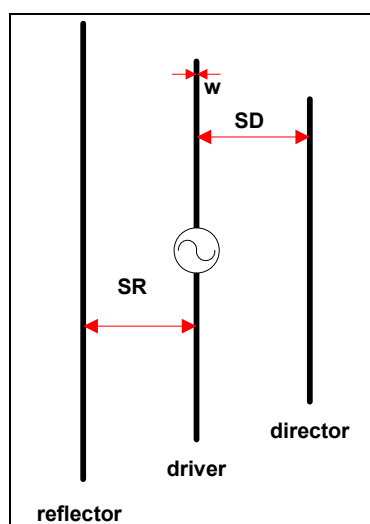


Figure 4.1. Three-element Yagi antenna structure

Theoretical design gives gain of 8.82 dBi [21], [22] is achieved for the three element Yagi antenna which has reflector length of 0.49λ , driver length of 0.4781λ and director length of 0.45λ . **SD** and **SR** are the separation between the reflector and driver, and the

separation between driver and director are respectively 0.15λ . Diameter of each element are given 0.0025λ [21], [22].

This antenna structure and dimensions are taken as reference for our Yagi antenna which is used for reader antenna. Some changes on the length of the antennas are performed to simplify design and calculations. At the end, 3-element Yagi antenna is designed which has reflector length of 0.48λ , driver length of 0.46λ and director length of 0.42λ . The separations **SD** and **SR** are both chosen as 0.14λ . The width of each element is given 0.0025λ . Gain of 7.89 dBi is obtained with a radiation impedance of $43.6-j6 \Omega$ and having VSWR value of 1.2 at 868 MHz. FEKO model of designed Yagi antenna is given in Figure 4.2;

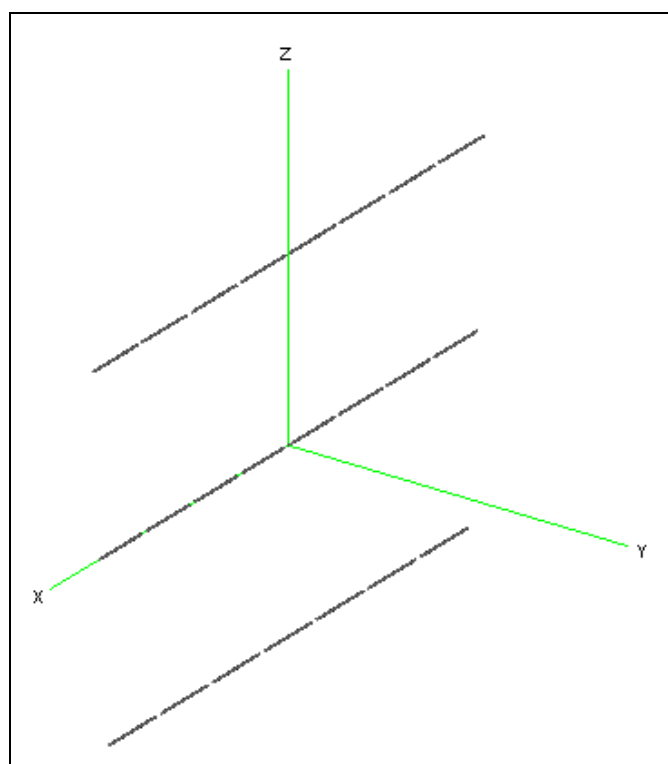


Figure 4.2. FEKO Model of designed Yagi antenna

Antenna gain characteristics of designed Yagi antenna is given in Figure 4.3. It is seen that it has directional shape.

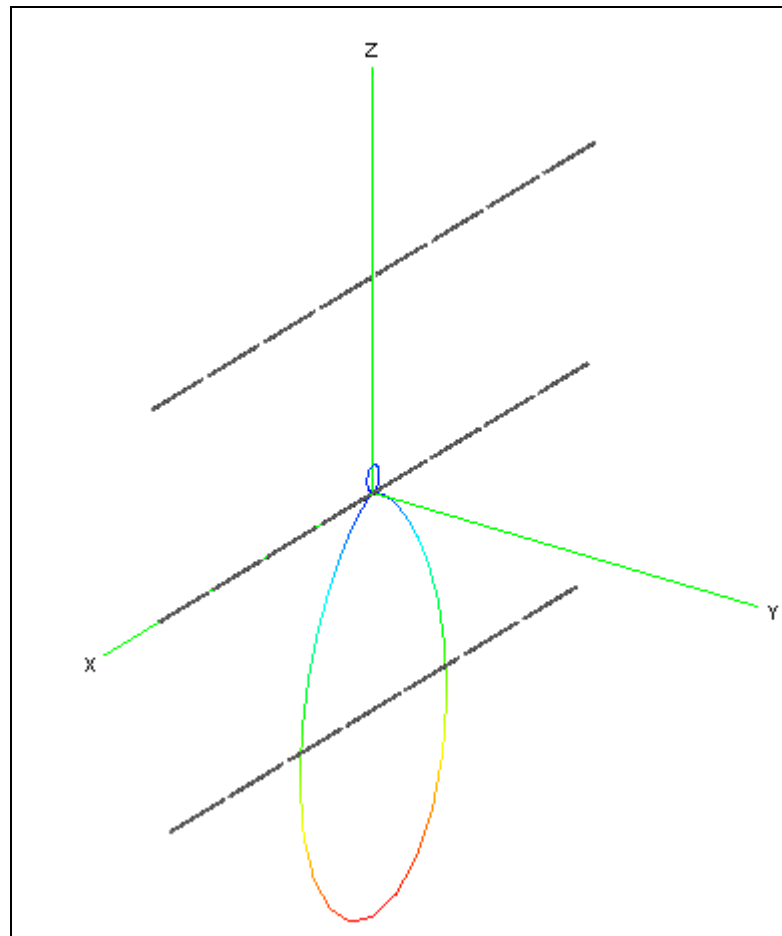


Figure 4.3. Antenna gain characteristics of designed Yagi ($\phi=0, \theta$ changes)

4.1.2. HF Reader Antenna Design and Simulations

We also need to design an HF reader antenna. 3 turns spiral having dimensions of $350 \times 250 \text{ mm}^2$ is used. Figure 4.4 shows the HF reader antenna;

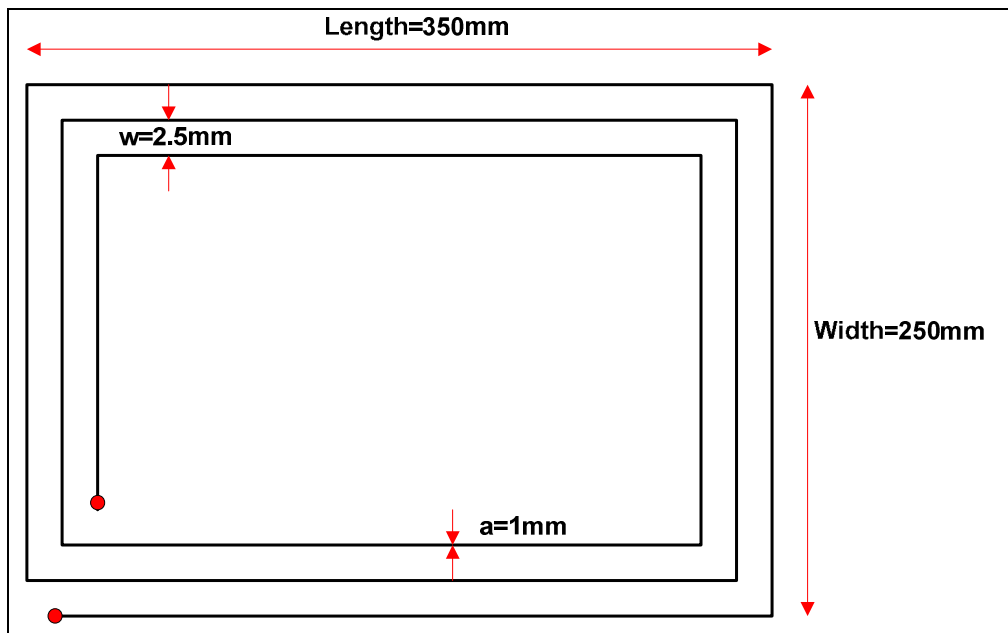


Figure 4.4. HF reader antenna

In Figure 4.4, “ a ” is the diameter of the spiral used and “ w ” is the separation between each spirals. FEKO model of the HF reader antenna is given in Figure 4.5;

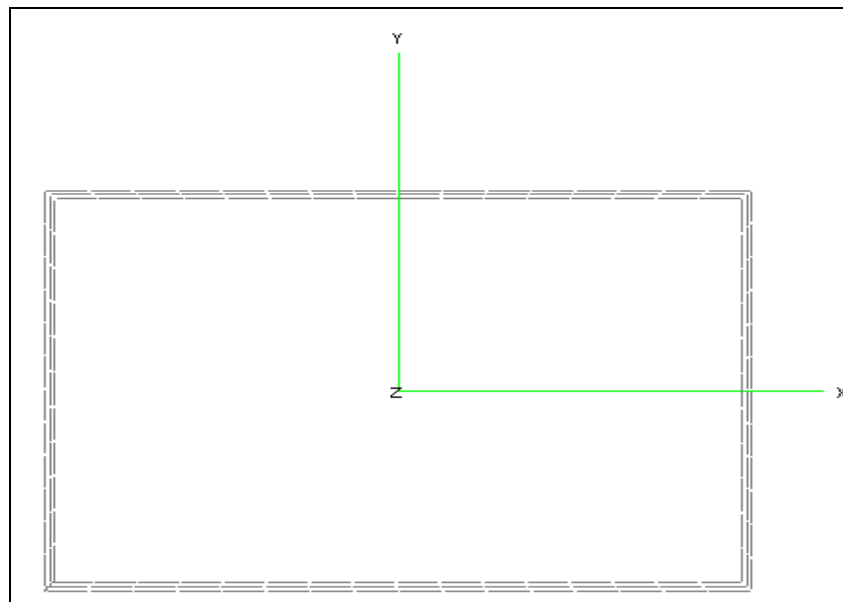


Figure 4.5. FEKO model of designed HF reader antenna

Before simulating inductance, theoretical calculations are performed. Theoretical inductance value is calculated as $12.6 \mu\text{H}$ for the reader antenna using (3.7).

After designing the HF reader antenna on FEKO, we achieved an inductance value of $13.5 \mu\text{H}$. During simulation, it is seen that when the separation between spirals is increased, there is an increase in inductance. According to near-field standards, magnetic field strength near the antenna should be less than 5 A/m and at 10 m range this magnetic strength value can not exceed $42 \text{ dB}\mu\text{A/m}$. During FEKO simulations, 1.026 mW is used to feed HF reader antenna not to exceed these limits.

4.2. Measurements for HF/UHF Reader Antenna

4.2.1. Measurements for UHF Yagi Reader Antenna

After getting all simulation results for both HF and UHF reader, next step is to realize the reader antennas and perform measurements. First, Yagi which is used as UHF reader antenna is realized. Figure 4.6 shows the realized Yagi reader antenna.

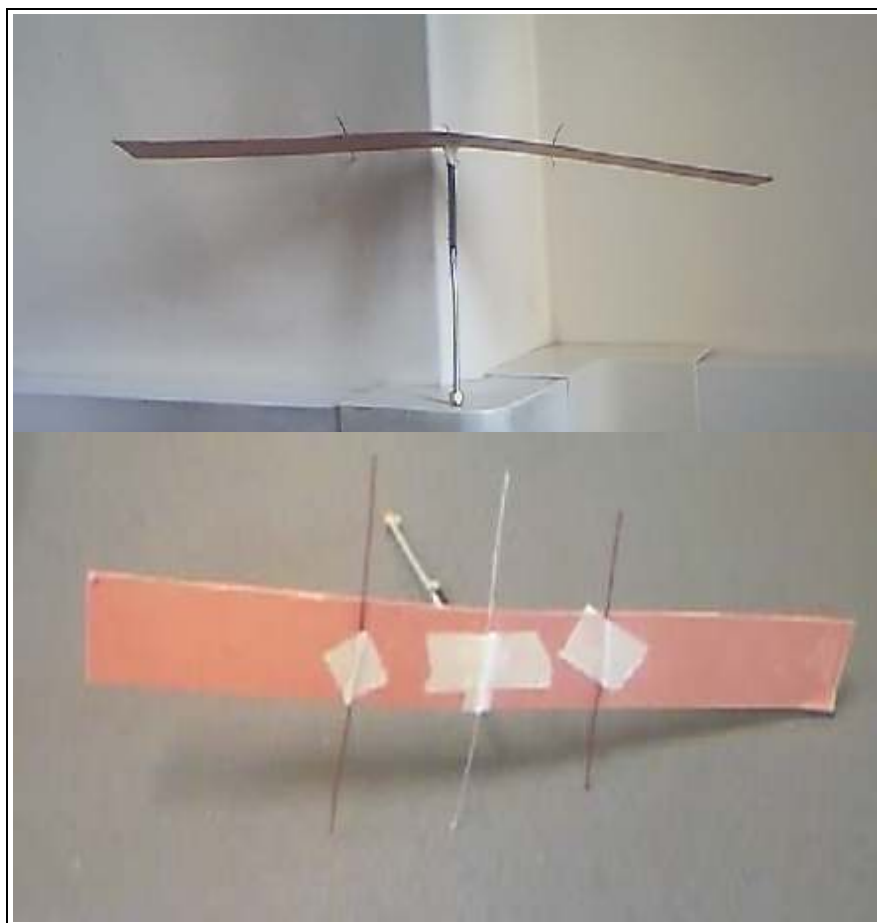


Figure 4.6. Realized Yagi antenna

After realization, we did perform gain and impedance measurements. Measurement results shows that we have a gain of approximately 7.80 dBi. We also have impedance of 53.8Ω and VSWR values of 1.08. So it can be said that the realized antenna is very close to perfect match. Impedance measurement result is given in Figure 4.7 and VSWR is shown in Figure 4.8;

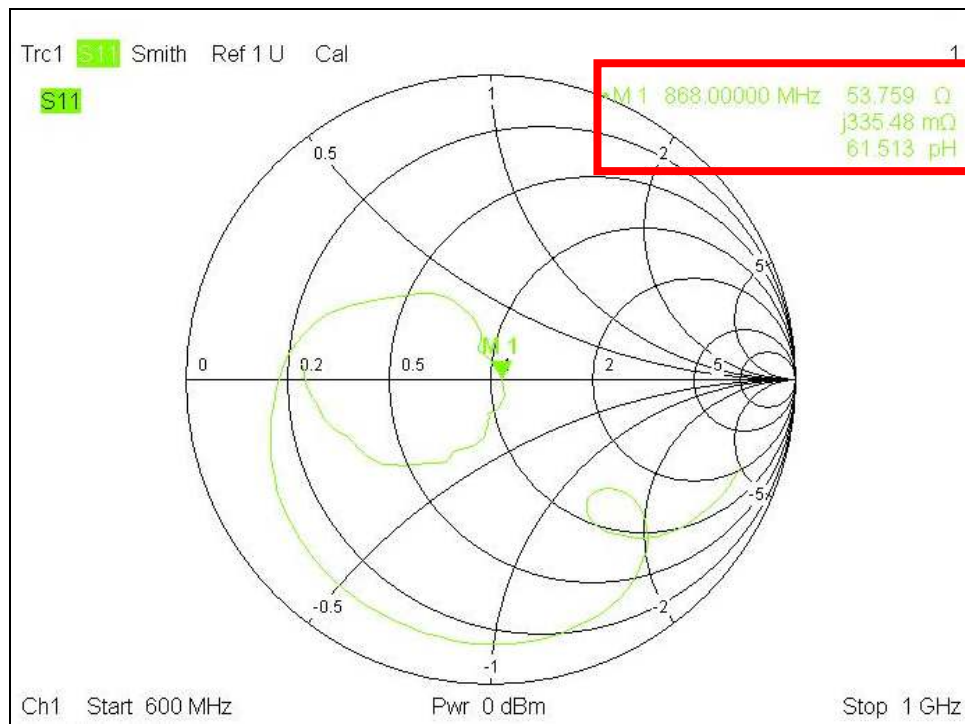


Figure 4.7. Impedance measurement for realized Yagi antenna



Figure 4.8. VSWR measurement for Yagi antenna

4.2.2. Measurements for HF reader antenna

Three turn spiral is used with having width diameter of 1 mm . There is a separation of 2.5 mm between each spiral. All of the dimensions of the HF reader antenna are given in Figure 4.4. Figure 4.9 shows the realized HF reader antenna.



Figure 4.9. Realized HF reader antenna

After realization of HF reader antenna, next step is to perform measurements for inductance. LCR meter is used to perform inductance measurements. It is achieved to have inductance value of approximately 10 μH at 100 KHz. Although not at 13.56 MHz, we took this result reliable. Setup which is used to measure inductance value of the reader antenna is given in Figure 4.10;

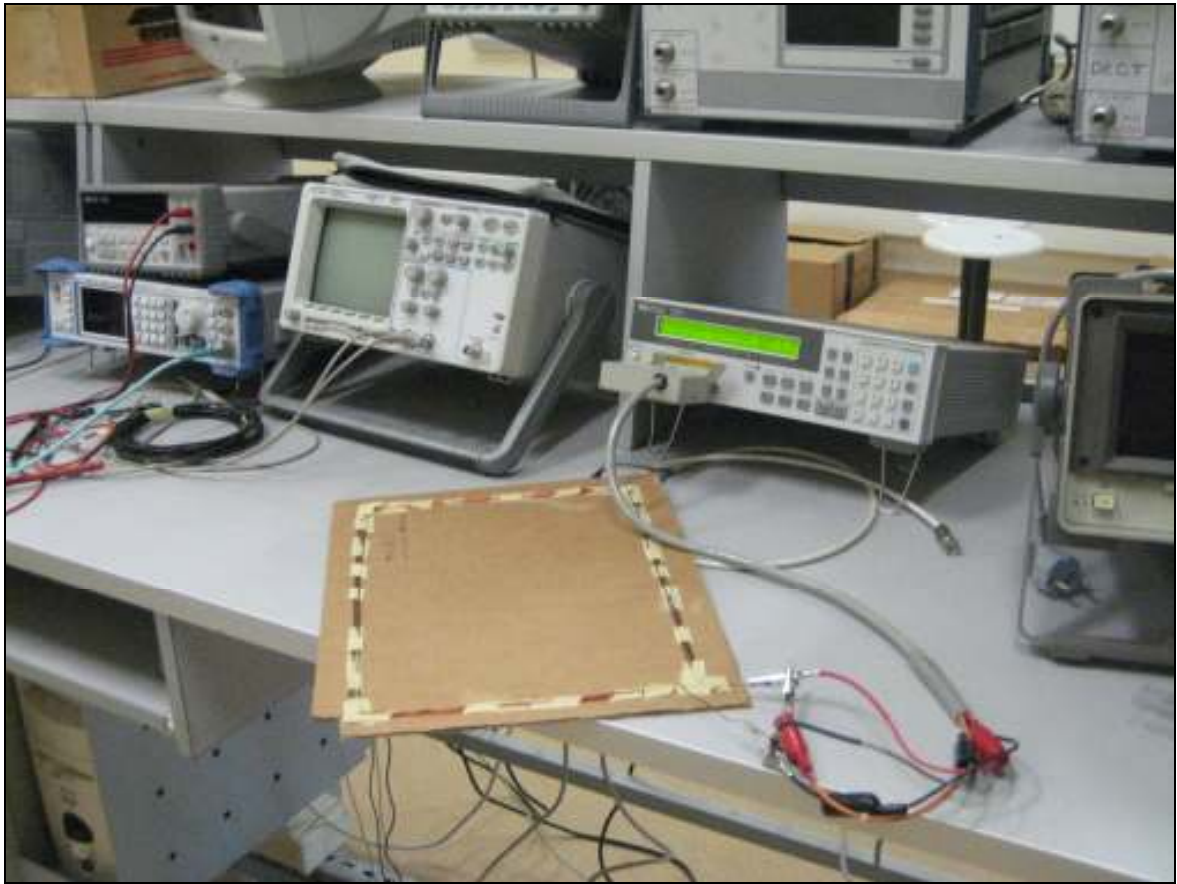


Figure 4.10. Measurement setup used to measure inductance of HF reader coil

5. IMPROVING READ/WRITE RANGE CAPABILITY OF HF TRANSPONDER

In this chapter, we propose a method which can be used to extend the read/write range capability of a HF tag.

5.1. RANGE EXTENSION

First we theoretically find the maximum read/range distance of a HF tag based on required minimum voltage at which HF tag is operational using the following steps:

- 1) We calculate the magnetic flux density for different distances (25 cm to 110 cm) using (2.7) which was previously given in chapter 2.
- 2) Then we calculate the mutual inductance. (2.12) is used to calculate mutual inductance.
- 3) After calculating mutual inductance, coupling coefficient which will be used to calculate induced voltage in next step is found. (2.13) is used to calculate coupling coefficient.
- 4) Next step is to calculate the induced voltage on HF tag side. (2.32) is used to find theoretical value of induced voltage;
- 5) After finding the value of induced voltage, quality factor should be calculated. (2.24) is used to calculate Q.

In (2.24) which was given in chapter 2, R_2 (internal resistance of HF tag antenna) which includes both radiation resistance, $R_{RADIATION}$ and loss resistance, R_{LOSS} . $R_{LOSS} \cdot R_{RADIATION}$ is

obtained in FEKO, however R_{LOSS} is ignored by FEKO. So it should also be calculated to find the exact value of R_2 . (5.1) is used to find R_{LOSS} .

$$R_{LOSS} = \frac{\sqrt{\pi f \mu}}{\sqrt{\sigma} 2 \omega} \quad (5.1)$$

In (5.1), f is the frequency which tag operates, μ is the permeability of the medium, σ is the conductivity of wire and ω is the angular frequency. We choose a capacitance value for C_p which makes tag resonant at 13.56 MHz as shown in Figure 2.10. So we have only R_L left unassigned. We choose R_L as 1.3 K Ω , which is the load resistance. When we put all these, Q is found as 35.84.

- 6) The minimum voltage, V_2 which HF tag antenna is operational. (2.18) is used to find the minimum voltage.
- 7) After getting all results for the previous steps, last step is to calculate the magnetic field intensity, H using (2.40).

After theoretical derivation, next step is to perform simulations for comparing both theoretical and analytical results. We used to get the values of H , L_1 and L_2 . In simulations, 4 turns of spiral is used in reader side and 5 turns of spiral is used in HF tag side. The distances are varied from 25 cm to 110 cm between reader antenna and HF tag. In Figure 5.1, FEKO model of reader and tag system is shown:

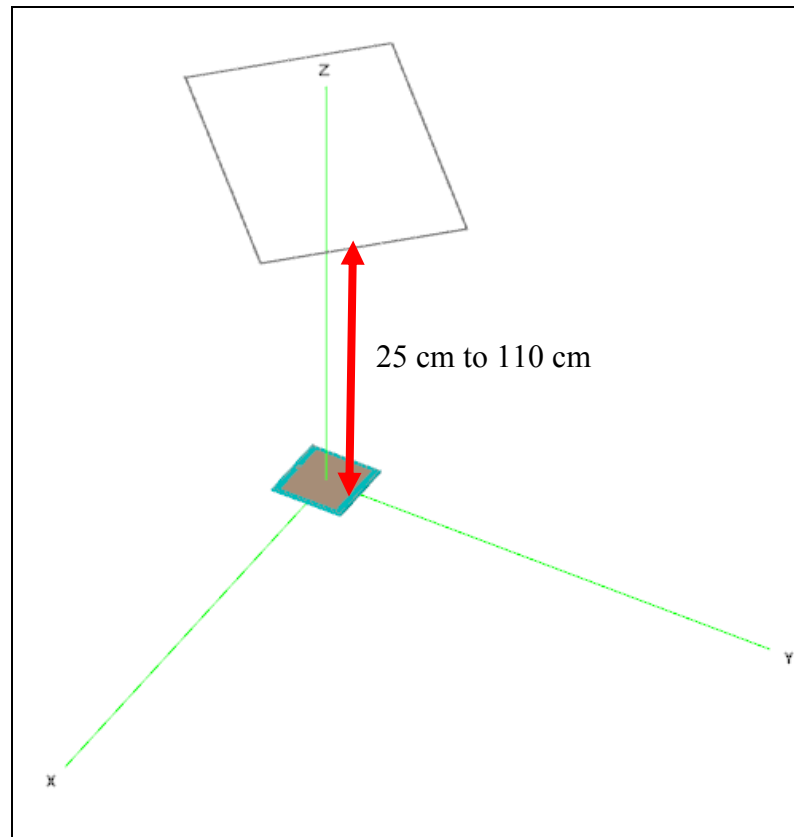


Figure 5.1. FEKO model of reader- tag system

Comparative results for both analytical and FEKO simulation analysis are given in Table 5.1,

Table 5.1. Comparative results for both theoretical and analytical analysis

| Distance (cm) | H_{FEKO} (mA/m) | $V_{2\text{FEKO}}$ (V) | $H_{\text{ANALYTICAL}}$ (mA/m) | $V_{2\text{ANALYTICAL}}$ (V) |
|---------------|--------------------------|------------------------|--------------------------------|------------------------------|
| 25 | 607 | 4.46 | 545.3 | 4.02 |
| 30 | 412.7 | 3.98 | 385.1 | 3.72 |
| 35 | 289.6 | 3.44 | 262.4 | 3.12 |
| 40 | 209.4 | 3.28 | 188.7 | 2.95 |
| 45 | 155.5 | 3.12 | 135.2 | 2.71 |
| 50 | 118.3 | 2.98 | 102.5 | 2.59 |
| 55 | 91.9 | 2.66 | 72.1 | 2.28 |
| 60 | 72.7 | 2.54 | 55.4 | 2.17 |
| 65 | 58.4 | 2.38 | 42.1 | 2.03 |
| 70 | 47.7 | 2.1 | 24.8 | 1.89 |
| 75 | 39.4 | 1.74 | 19.5 | 1.57 |
| 80 | 32.9 | 1.44 | 7.3 | 1.28 |
| 85 | 27.8 | 1.22 | 1.4 | 1.12 |
| 90 | 23.6 | 1.04 | 0.92 | 0.97 |
| 95 | 20.3 | 0.89 | 0.65 | 0.79 |
| 100 | 17.6 | 0.78 | 0.34 | 0.62 |
| 105 | 15.3 | 0.68 | 0.21 | 0.53 |
| 110 | 13.4 | 0.59 | 0.09 | 0.41 |

We need to find out how much voltage is obtained within range 25 cm to 110 cm. We use Yagi as UHF transmitter and UHF tag antenna as receiver. FEKO model of Yagi transmitter antenna and UHF tag antenna as receiver part system is given in Figure 5.2,

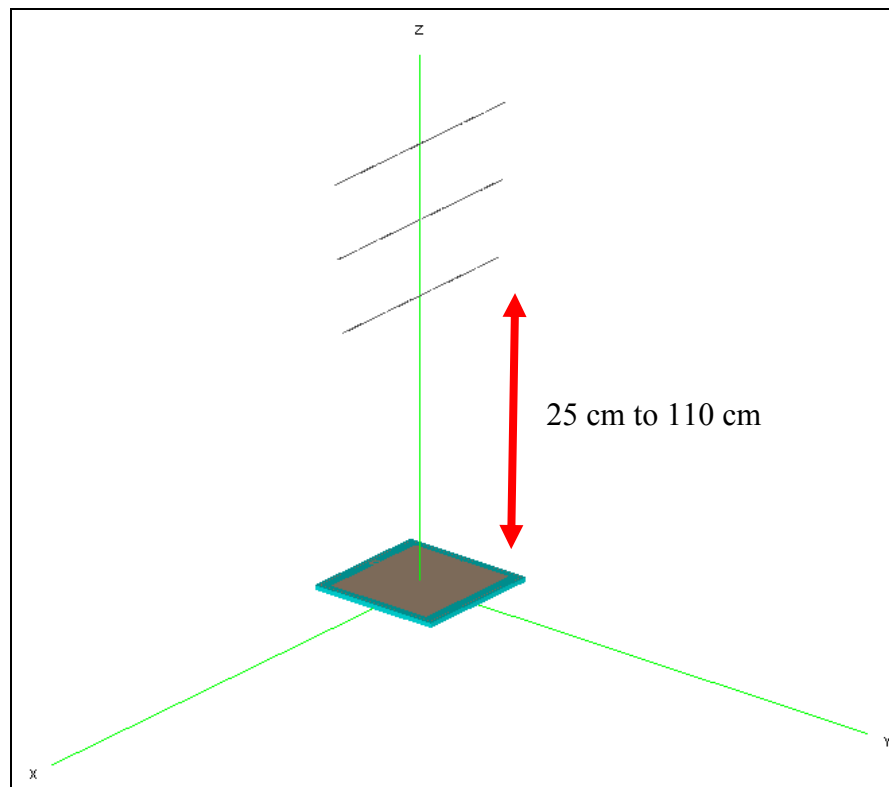


Figure 5.2. FEKO model of Yagi transmitter and UHF tag system

As it is seen in Table 5.1, minimum voltage level 2.5 V is achieved at 50 cm distance. We need to study how much ΔV is required to reach minimum operating voltage 2.5 V for various distances. Table 5.2 shows the ΔV voltage values required to reach minimum operating voltage, 2.5 V to operate the tag;

Table 5.2. ΔV required to reach minimum operating voltage 2.5 V for HF tag

| Distance (cm) | $V_{2_ANALYTICAL}$ (V) | ΔV required for min. operating voltage (V) |
|---------------|-------------------------|----------------------------------------------------|
| 50 | 2.59 | 0 |
| 55 | 2.28 | 0.22 |
| 60 | 2.17 | 0.33 |
| 65 | 2.03 | 0.47 |
| 70 | 1.89 | 0.61 |
| 75 | 1.57 | 0.93 |
| 80 | 1.28 | 1.22 |
| 85 | 1.12 | 1.38 |
| 90 | 0.97 | 1.53 |
| 95 | 0.79 | 1.71 |
| 100 | 0.62 | 1.88 |
| 105 | 0.53 | 1.97 |
| 110 | 0.41 | 2.09 |

We used Yagi antenna as transmitter and tag antenna as receiver. FEKO model of UHF reader-tag system is shown in Figure 5.3,

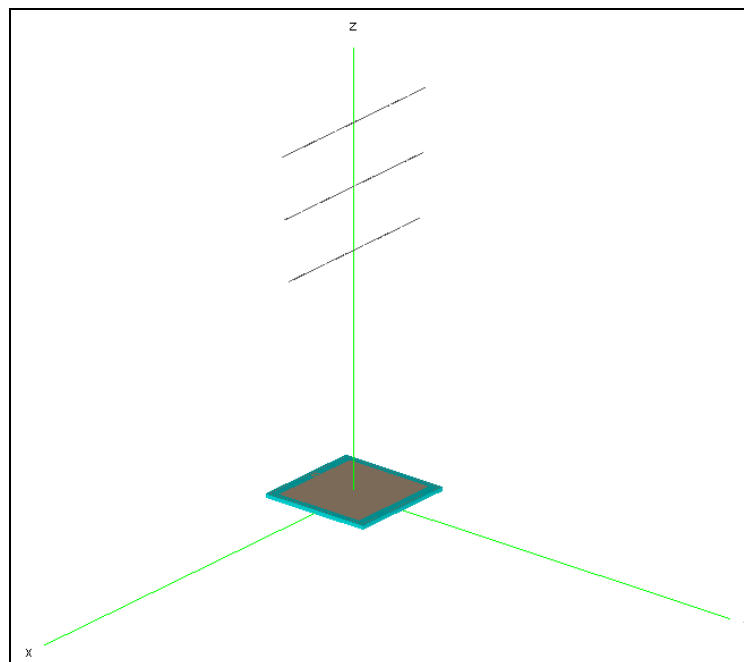


Figure 5.3. FEKO model of UHF reader-tag system

Previously, we showed that we have an impedance of $35.12+j161.87 \Omega$ for the tag antenna. To find the available source voltage on tag, we added a complex impedance of $35.12-j161.87 \Omega$ to the tag antenna feed point as a load to achieve maximum power transfer. According to standards issued for UHF RFID, input power can be used changes within 0.5 W to 2 W. We applied 6.731 V to obtain power of 0.5 W and 13.46 V to achieve 2W to study induced voltage levels between 25 cm to 110 cm distances. We need to study whether we can compensate required voltage differences to extend the read/write range. Minimum operating voltage for HF tag is taken as 2.5 V. Table 5.3, 5.4 and 5.5 show the available voltage levels for different separations when 0.5 W, 2 W and 4 W UHF reader antenna is used. 1-stage to 5-stages voltage doubler can be used to increase the available source voltage for UHF tag which will be used to extend the read/write range of HF tag. While there is increase in voltage levels with using voltage doublers 1-stage to 5-stage, there is also decrease in efficiency. So, all voltage levels obtained should be multiplied by efficiency factors.

Table 5.3. Available source voltages for different distances when 0.5 W UHF reader is used

| Distance(cm) | V _{av} (mV) 69% efficiency one-stage | V _{av} (mV) 66.5% efficiency two-stages | V _{av} (mV) 64% efficiency three-stages | V _{av} (mV) 61.5% efficiency four-stages | V _{av} (mV) 59% efficiency five-stages |
|--------------|--------------------------------------------------------|-----------------------------------------------------------|-----------------------------------------------------------|------------------------------------------------------------|-------------------------------------------------------|
| 25 | 152.2 | 293.3 | 564.7 | 1086.5 | 2086.8 |
| 30 | 117.5 | 226.5 | 435.7 | 839.7 | 1610.8 |
| 35 | 92.1 | 177.5 | 341.8 | 657.6 | 1265.1 |
| 40 | 86.5 | 166.6 | 320.7 | 618.5 | 1187.1 |
| 45 | 82.6 | 158.9 | 306.2 | 590.4 | 1133.7 |
| 50 | 80.3 | 154.5 | 298.7 | 574.5 | 1100.4 |
| 55 | 78.1 | 150.1 | 290.4 | 558.8 | 1070.1 |
| 60 | 75.1 | 144.7 | 279.3 | 537.2 | 1029.4 |
| 65 | 71.5 | 137.8 | 266.4 | 510.1 | 979.2 |
| 70 | 59.6 | 114.6 | 222.2 | 426.7 | 817.4 |
| 75 | 51.3 | 98.7 | 191.3 | 366.3 | 712.5 |
| 80 | 49.2 | 94.4 | 182.6 | 351.5 | 675.4 |
| 85 | 46.4 | 89.8 | 172.7 | 331.7 | 636.8 |
| 90 | 43.7 | 84.9 | 162.1 | 311.9 | 598.2 |
| 95 | 41.6 | 80.3 | 154.5 | 297 | 570.4 |
| 100 | 39.5 | 76.4 | 146.4 | 282.2 | 541.6 |
| 105 | 36.7 | 69.9 | 136.3 | 262.4 | 502.3 |
| 110 | 34.7 | 66.8 | 128.7 | 247.5 | 474.5 |

When we look at the Table 5.3, we see that we are able to extend 50 cm to 55 cm using three-staged voltage doubler. If we use five-staged level, we are able to extend 50 cm HF read/write range to 70 cm. Available source voltages for different distance when 2 W UHF reader antenna used is given in Table 5.4,

Table 5.4. Available source voltages for different distances when 2W UHF reader is used

| Distance (cm) | V_{av} (mV) 69% efficiency one-stage | V_{av} (mV) 66.5% efficiency two-stages | V_{av} (mV) 64% efficiency three-stages | V_{av} (mV) 61.5% efficiency four-stages | V_{av} (mV) 59% efficiency five-stages |
|---------------|----------------------------------------------|----------------------------------------------------|----------------------------------------------------|-----------------------------------------------------|------------------------------------------------|
| 25 | 302.6 | 586.2 | 1129.7 | 2175.5 | 4274.6 |
| 30 | 254.5 | 491.9 | 946.8 | 1820.6 | 3495.7 |
| 35 | 211.3 | 408.4 | 784.5 | 1509.6 | 2894.6 |
| 40 | 192.8 | 369.7 | 710.9 | 1366.5 | 2623.7 |
| 45 | 172.1 | 331.7 | 638.8 | 1229.6 | 2360.6 |
| 50 | 160.8 | 311.6 | 598.8 | 1153.7 | 2210.4 |
| 55 | 156.3 | 302.6 | 581.9 | 1118.4 | 2148.4 |
| 60 | 149.7 | 289.1 | 554.3 | 1068.5 | 2051.3 |
| 65 | 139.5 | 270.2 | 519.7 | 1000.2 | 1920.1 |
| 70 | 128.5 | 249.8 | 479.6 | 922.7 | 1771.5 |
| 75 | 102.5 | 200.1 | 384.4 | 739.5 | 1426.2 |
| 80 | 100.8 | 196.1 | 378.7 | 725.6 | 1392.7 |
| 85 | 90.6 | 174.3 | 335.6 | 645.3 | 1239.8 |
| 90 | 85.6 | 164.6 | 316.9 | 609.1 | 1169.4 |
| 95 | 82.5 | 158.9 | 304.6 | 588.6 | 1125.5 |
| 100 | 78.3 | 149.7 | 293.1 | 563.2 | 1081.3 |
| 105 | 73.8 | 144.5 | 279.1 | 535.8 | 1027.3 |
| 110 | 71.4 | 138.5 | 268.4 | 514.5 | 989.1 |

Compared to situation when 0.5 W UHF reader antenna, we are able to increase the read/write range of HF tag to 80 cm from 50 cm, which was at most 70 cm when 0.5 W UHF reader is preferred. Green bold labeled values show the limits that we can use to compensate the ΔV values required to reach minimum operating voltage 2.5 V. Table 5.5 shows the available source voltages for different distances when 4 W UHF reader antenna is used.

Table 5.5. Available source voltages for different distances when 4 W UHF reader is used

| Distance (cm) | V_{av} (mV) 69% efficiency one-stage | V_{av} (mV) 66.5% efficiency two-stages | V_{av} (mV) 64% efficiency three-stages | V_{av} (mV) 61.5% efficiency four-stages | V_{av} (mV) 59% efficiency five-stages |
|---------------|-------------------------------------------------|----------------------------------------------------|----------------------------------------------------|-----------------------------------------------------|------------------------------------------------|
| 25 | 609.4 | 1173.6 | 2270.4 | 4347.3 | 8345.5 |
| 30 | 509.8 | 981.5 | 1897.5 | 3642.6 | 6898.3 |
| 35 | 421.8 | 814.7 | 1569.6 | 3017.3 | 5795.2 |
| 40 | 382.6 | 737.4 | 1421.3 | 2733.5 | 5247.5 |
| 45 | 343.5 | 663.6 | 1278.4 | 2459.7 | 4721.4 |
| 50 | 321.9 | 613.8 | 1291.6 | 2302.1 | 4421.2 |
| 55 | 312.5 | 603.6 | 1163.8 | 2238.8 | 4298.7 |
| 60 | 298.7 | 577.8 | 1112.2 | 2137.2 | 4104.6 |
| 65 | 280.4 | 539.8 | 1040.7 | 2000.6 | 3841.3 |
| 70 | 259.4 | 498.5 | 962.7 | 1845.3 | 3542.2 |
| 75 | 206.6 | 399.4 | 769.5 | 1476.4 | 2837.9 |
| 80 | 203.6 | 391.8 | 754.8 | 1451.7 | 2785.2 |
| 85 | 181.2 | 352.2 | 671.6 | 1290.6 | 2477.4 |
| 90 | 171.3 | 328.7 | 634.1 | 1217.5 | 2340.1 |
| 95 | 164.8 | 318.1 | 610.8 | 1166.4 | 2258.4 |
| 100 | 158.1 | 303.8 | 585.3 | 1126.5 | 2163.2 |
| 105 | 149.9 | 288.9 | 557.4 | 1071.8 | 2056.6 |
| 110 | 143.7 | 279.1 | 537.1 | 1030.6 | 1978.8 |

When we look at Table 5.5, we see that we are able to extend HF tag read/write range to 105 cm at best situation. So we can say that, 50 cm can be extended to 105 cm at best situation. If voltage doubler which have stages more than 5, we can extend the read/write range to distances more than 105 cm. This shows and verifies that proposing this new method, read/write range extension is possible using proper staged voltage doubler.

After having simulation results, we also performed measurements to see if simulation and measurement results are in corroboration. So, we studied the rectifier circuit. Next section, rectifier circuit design is given:

5.2. RECTIFIER CIRCUIT DESIGN, SIMULATION & MEASUREMENT

We designed a rectifier circuit using AWR Design Environment RF circuit design tool. Circuit scheme for the designed rectifier is shown in Figure 5.4;

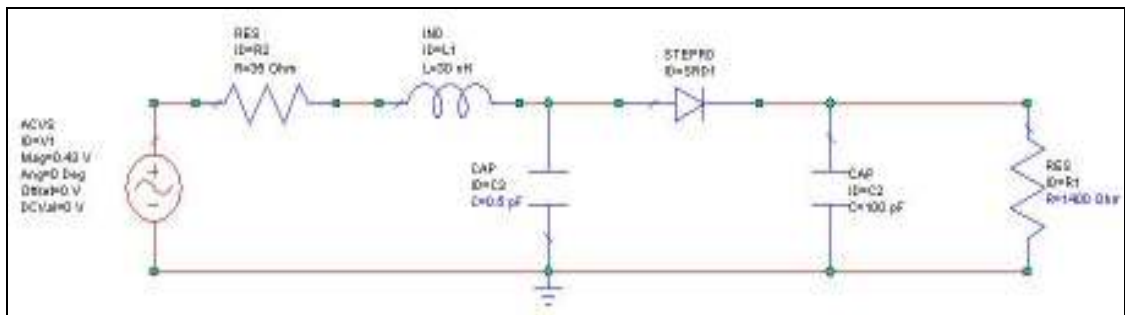


Figure 5.4. Circuit scheme of rectifier

All of the variables given in Figure 5.4 are optimized for maximum efficiency. Left-hand side of the circuit shows the model of designed tag which has input impedance of $35.12 + j161.87 \Omega$. Schottky diode which is suitable for RF circuit designs is used. When load $R=1400 \Omega$ on the right-hand side of the circuit is used, we have an efficiency of 63%. Input-output characteristics for the rectifier circuit is shown in Figure 5.5. In that figure, input AC voltage is shown with blue color and rectified voltage is shown with green color. When there is 0.43 V applied, corresponding power is calculated as 0.68 mW. When this voltage is rectified, corresponding output power is calculated as 0.43 mW.

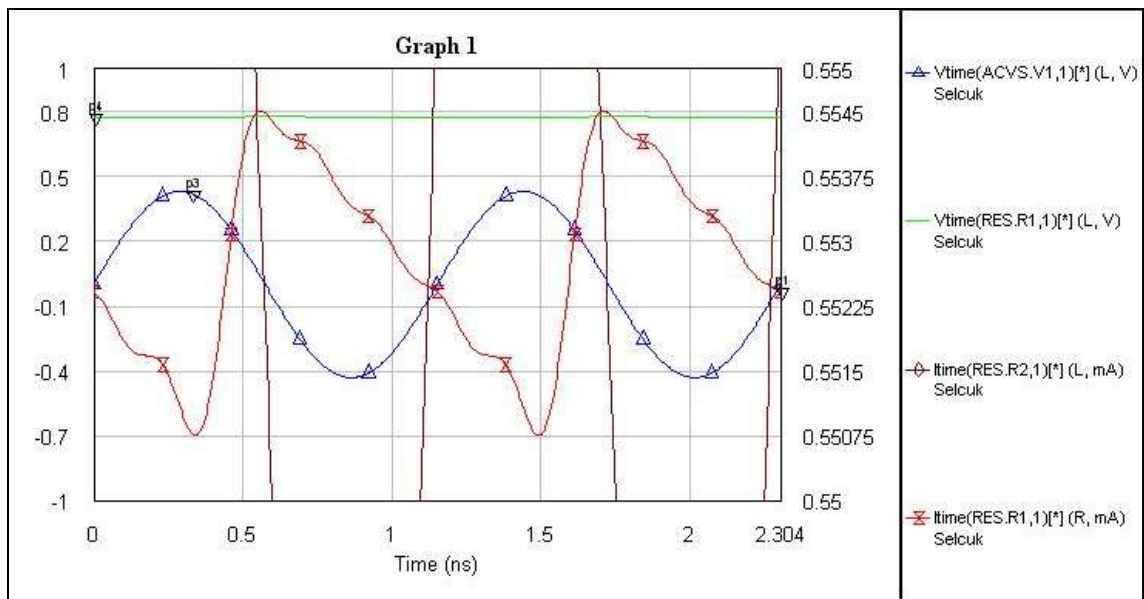


Figure 5.5. Input-out characteristics of rectifier circuit

After designing the rectifier circuit on AWR Design Environment, we realized the circuit on FR4 type dielectric substrate. We sketched the schematic of the circuit using Eagle, and then have prototypes made. EAGLE drawing of the rectifier circuit is shown in Figure 5.6;



Figure 5.6. EAGLE drawing of the rectifier circuit

Top view of the rectifier prototype is given in Figure 5.7,



Figure 5.7. Top view of rectifier circuit

After having the prototypes for the rectifier circuit, we performed measurements with Yagi antenna transmitting and the tag antenna receiving. Measurement setup is shown in Figure 5.8 (there is separation of 60 cm between Yagi and designed tag);

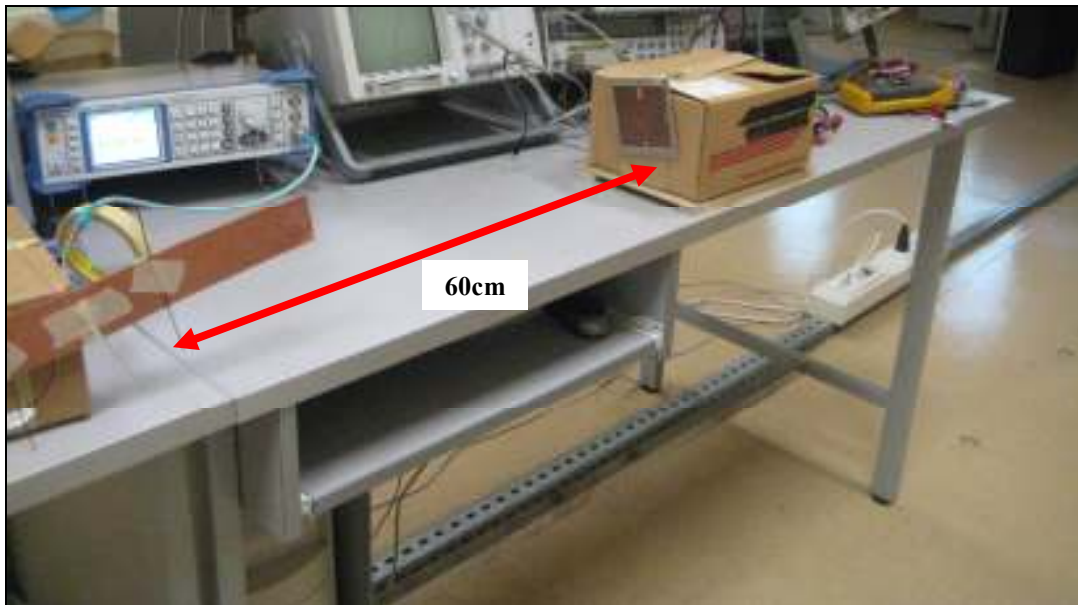


Figure 5.8. Measurement setup when Yagi transmits and designed tag antenna receives

There is separation of 60 cm between Yagi antenna and designed tag antenna. In the measurement, we tried to measure induced voltage on designed tag side. We did measure induced voltage of 13 mV as maximum value when 1 W input power was applied. As it is seen that we achieved to obtain induced voltage which was really small. It is due to fact that there is mismatch factor occurs between designed tag antenna. If this mismatch issue is resolved, it will be able to obtain more induced voltage values.

Since, we were not satisfied the measurement results, we prepared another measurement set-up for Yagi antenna transmitting and dipole antenna receiving. Dipole antenna has real impedance of approximately 70Ω and gain of 2.20 dBi. Measurement set-up when Yagi-Uda transmits and dipole antenna receives can be seen in Figure 5.9;



Figure 5.9. Measurement set-up when Yagi transmits and dipole antenna receives

After preparing the measurement set-up given in Figure 5.9, we set different power levels using power generator and tried to measure the induced voltage on the output of the rectifier circuit connected to dipole antenna. Results which were obtained during measurements after setting different levels of power levels are given on Table 5.6;

Table 5.6. Induced voltage on the output of the rectifier circuit when different levels of power are applied

| Applied Power (dBm) | Induced Voltage (mV) |
|---------------------|----------------------|
| 10 | 1.20 |
| 15 | 1.44 |
| 17 | 5.4 |
| 18 | 12 |
| 20 | 62 |
| 23 | 148 |
| 26 | 264 |
| 29 | 338 |
| 30 | 432 |

The results given on Table 5.6 shows that if the tag antenna is tuned to achieve impedance values similar to dipole since induced voltage values may be higher. This additional power will cause HF tag to have improved read/write ranges. Simulation results confirmed that the proposed method can extend the HF read/write range.

6. CONCLUSIONS

A dual mode, dual band RFID transponder antenna is designed, simulated and measured for HF and UHF bands. The HF antenna is inductively coupled multi-turn loop antenna printed on dielectric substrate and the UHF antenna is a microstrip antenna with U-shape feed and a degenerate ground for gain improvement.

The multi-turn HF antenna inductance is first theoretically calculated in air, and then simulated using 3D EM simulation software. A prototype is built and the simulated inductance value is corroborated with measurements to a reasonable degree of agreement. The multi-turn loop co-exists with the ground of the UHF band antenna. Although the presence of metallic ground at the center of the loop reduces the attainable inductance from the structure, the loop has enough inductance to operate in HF range and has 2.54 μH inductance. Compared to typical inductance values of HF tags which are in the range of 1.5-3 μH , the achieved inductance can be considered good.

Unlike inductive coupling, the UHF band RFID transponder is based on radiated electromagnetic power, which, in turn, provides longer read/write range (5-8 m). However, the transponder antenna gets easily affected from surroundings, especially at or near metallic, high permittivity dielectric materials. To overcome this major disadvantage of UHF band antenna, a low-height, microstrip antenna is designed. Simulations and measurements of the designed structure agree well. The input impedance of the transponder is designed and tuned to a possible capacitive input impedance of transponder IC. The novel structure is also compared to a typical dipole-like UHF antenna for performance metrics and it is observed that the designed antenna is superior to its dipole-like counterparts. Extensive measurements are carried out to characterize its detuning when it is placed near or on metal and dielectric structures. The antenna can be made conformal using elastic substrates, and is cost effective due low PCB manufacturing costs.

Third goal of this study was to increase the read/write range of HF systems. We designed a wireless power transfer scheme at UHF band for the dual mode transponder.

The RF power is rectified and converted to DC with about 63% efficiency. Rectifier circuit optimization is carried out in microwave circuit simulator. Measured data reveals that indeed power transfer works well for the dipole structure but not as efficient as for the designed transponder. We suspect that the Schottky diode model we used in the simulation was not accurate to absorb the inductive energy of the transponder at UHF band. The input rectify circuit, however, can easily be matched to any impedance at our will.

REFERENCES

1. K. Finkenzeller, "*RFID Handbook : Fundamentals and Applications in Contactless Smart Cards and Identification*", 2nd ed., John Wiley and Son LTD, New York, 2003.
2. Basat S. Serkan, Lim Kyutae, Laskar Joy, Tentzeris M. Manos, "*Design and Modeling of Embedded 3.56 MHz RFID Antennas*", Technical Paper, School of ECE, Georgia Institute of Technology, USA, 2005.
3. Clapf C., Missoni A, Pribyl W., Hofer G, Holweg G. and Kargl W., "*Improvements in Operational Distance in passive HF RFID Transponder Systems*", IEEE International Conference on RFID , pp. 250-257, April 16-17 2005, Las Vegas, Veneda, U.S.A.
4. Nikitin P., Roa K.V.S., "*An Overview of Near Field UHF RFID*", IEEE International Conference on RFID, pp. 167-174, March 26-28 2008, Grapevine , TX, U.S.A.
5. Madhuri Bharadwaj Eunni, "*A Novel Planar Microstrip Antenna Design for UHF RFID*", Master Thesis, India, 2004.
6. Rao K.V. Seshagiri, Nikitin V. Pavel, Lam F. Sander, "*Antenna Design for UHF RFID Tags: A Review and a practical application*", IEEE Transc. On Antennas and Propagation, Vol. 53, No 12, 2005.
7. Cho C., Choo H. and Park I, "*Design of planar RFID tag for metallic objects* ", IEEE Transc. On Antennas and Propagation Electronic Letters, vol. 44, no. 3 , 2008.
8. Mo L., Zhang H. and Zhou H., "*Broadband UHF RFID tag antenna with a pair of U slots mountable on metallic objects* ", IEEE Transc. On Antennas and Propagation Electronic Letters, vol. 44, no. 20 , 2008.
9. Choi Wonky, Kim Jeonk-Seong, Bae Jin-Hoon," *RFID Tag Antenna Coupled by Shorted Microstrip Line for Metallic Objects*", ETRI Journal, Vol. 30, pp. 597-599, 2008.

10. Griffin D. and Joshua, Durgin, “*Measurements and Link Budgets for 915 MHz FRID antennas placed on various objects*”, International Workshop on RFID and Wireless Sensors, Texas Wireless Symposium, pp. 15-16, U.S.A, 2005.
11. D. M. Dobkin and S. M. Weigand, “*Environmental Effects on RFID Tag Antennas*,” IEEE International Microwave Symposium, June 2005.
12. Arumugam D., Engel Daniels W., “*Characteristics of Passive UHF RFID Tags on Metal Slabs*”, IEEE Transc. On Antennas and Propagation , pp. 1-4, June 2009.
13. Nikkari M., Bjorninen T., Sydanheimo L, Ukkonen L, Elsherbeni A, Yang F. and Kivikoski M., “*Performance of a Passive UHF RFID Tag in Reflective Environment*”, IEEE Transc. On Antennas and Propagation , pp. 1-4, July 2008.
14. Park K. Y., Lee S. G., Kang J. and Chung C. Y., “*Various UHF RFID Tags for Metallic Object*”, IEEE Transc. On Antennas and Propagation , pp. 2285-2288, June 2007.
15. Leong K. S., Ng L. M. and Cole H. P., “*Dual Frequency Antenna Design for RFID Application*”, Technical Paper, AutoID Lab., School of Electrical and Electronic Engineering, The University of Adelaide.
16. Mayer W. Lukas, Scholtz R. Arpad, “*A Dual-band HF/UHF Antenna for RFID Tags*”, IEEE Transc. On Antennas and Propagation, pp. 1-5, Sep. 2008.
17. Iliev P., Thuck Le P., Luxey C. and Staraj R., “*Dual-band HF-UHF RFID tag antenna*”, IEEE Transc. On Antennas and Propagation , vol. 45, no. 9, 2009.
18. Curty P. J., Declercq M., Dehollain C. and Joehl N., “*Design and Optimization of Passive UHF RFID Systems*”, Springer Science and Business Media, Switzerland, 2007.

19. Garg, R., P. Bhartia, I. Bahl and A. Ittipiboon, "*Microstrip Antenna Design Handbook*", Artech House, Boston-London, 2001.
20. "*HF Antenna Design Notes*", Technical Application Report, Texas Instruments, September 2003.
21. W. L. Stutzman and G. A. Thiele, "*Antenna Theory and Design, 2nd ed.*" Hoboken, NJ, John Wiley and Sons, 1998.
22. Milligan A. T., "*Modern Antenna Design 2nd ed.*", John Wiley and Sons, 2005.
23. Dobkin D., "*RF in RFID: Passive UHF RFID in Practice*", Elsevier Book Aid International, Sabre Foundation, Linacre House, Jordon Hill, Oxford, U.K., 2008.
24. Pozar, D. M., "*Microstrip Antennas*", Proc. of the IEEE, Vol. 80, pp. 79-91, 1992.
25. Balanis, C. A., "*Antenna Theory, Analysis and Design*", John Wiley & Sons Ltd., New York, 1997.
26. Johnson, R. C. and H. Jasik, "*Antenna Engineering Handbook*", Book News, Portland, Or., 1961.